Thèse en cotutelle avec

l'Université de Borås (Suède) et l'Université de Soochow (Chine)

FDM 3D printing of conductive polymer nanocomposites: A novel process for functional and smart textiles

L'Impression 3D de nanocomposites polymères conducteurs: un nouveau procédé pour la fonctionnalisation de surface de smart textiles

Présentée par:
Razieh HASHEMI SANATGAR

Pour obtenir le grade de Docteur de l'Université de Lille

Discipline: Mécanique des solides, des matériaux, des structures et des surfaces

Soutenue le 27/09/2019 devant la commission d' examen

Prof. Jean-François FELLER	Université de Bretagne Sud	Rapporteur
Prof. Anne Schwarz-PFEIFFER	University Hochschule Niederrhein	Rapporteur
Prof. José-Marie LOPEZ-CUESTA	IMT Mines Alès	Examinateur
Dr Karen DELEERSNYDER	Company Copaco Screenweavers	Examinateur
Prof. Jérémy SOULESTIN	IMT Lille Douai	Invité
Prof. Yan CHEN	Soochow University	Invité
Prof. Christine CAMPAGNE	Ecole centrale de Lille	Directeur
Prof. Vincent NIERSTRASZ	University of Borås	Co-directeur
Prof. Guojiang CHEN	Soochow University	Co-directeur
Prof. Jinping GUAN	Soochow University	Co-directeur
Prof. José-Marie LOPEZ-CUESTA	IMT Mines Alès	Président du jury

Abstract

The aim of this study is to get the benefit of functionalities of fused deposition modeling (FDM) 3D printed conductive polymer nanocomposites (CPC) for the development of functional and smart textiles. 3D printing holds strong potential for the formation of a new class of multifunctional nanocomposites. Therefore, development and characterization of 3D printable functional polymers and nanocomposites are needed to apply 3D printing as a novel process for the deposition of functional materials on fabrics. This method will introduce more flexible, resource-efficient and cost-effective textile functionalization processes than conventional printing process like screen and inkjet printing. The goal is to develop an integrated or tailored production process for smart and functional textiles which avoid unnecessary use of water, energy, chemicals and minimize the waste to improve ecological footprint and productivity.

The contribution of this thesis is the creation and characterization of 3D printable CPC filaments, deposition of polymers and nanocomposites on fabrics, and investigation of the performance of the 3D printed CPC layers in terms of functionality. Firstly, the 3D printable CPC filaments were created including multi-walled carbon nanotubes (MWNT) and high-structured carbon black (Ketjenblack) (KB) incorporated into a biobased polymer, polylactic acid (PLA), using a melt mixing process. The morphological, electrical, thermal and mechanical properties of the 3D printer filaments and 3D printed layers were investigated. Secondly, the performance of the 3D printed CPC layers was analyzed under applied tension and compression force. The response for the corresponding resistance change versus applied load was characterized to investigate the performance of the printed layers in terms of functionality. Lastly, the polymers and nanocomposites were deposited on fabrics using 3D printing and the adhesion of the deposited layers onto the fabrics were investigated.

The results showed that PLA-based nanocomposites including MWNT and KB are 3D printable. The changes in morphological, electrical, thermal, and mechanical properties of nanocomposites before and after 3D printing give us a great understanding of the process optimization. Moreover, the results demonstrate PLA/MWNT and PLA/KB as a good piezoresistive feedstock for 3D printing with potential applications in wearable electronics, soft robotics, and prosthetics, where complex design, multi-directionality, and customizability are demanded. Finally, different variables of the 3D printing process showed a significant effect on adhesion force of deposited polymers and nanocomposites onto fabrics which has been presented by the best-fitted model for the specific polymer and fabric.

Keywords: 3D printing, Fused deposition modeling, Adhesion, Deposition, Computer-aided design modeling, Statistical design, Conductive polymer nanocomposite, Multi-walled carbon nanotube, carbon black, Piezoresistive, Pressure/Force sensors

Résumé

Le but de cette étude est d'exploiter les fonctionnalités des nano-Composites Polymères Conducteurs (CPC) imprimés en utilisant la technologie FDM (modélisation par dépôt de monofilament en fusion) pour le développement de textiles fonctionnels et intelligents. L'impression 3D présente un fort potentiel pour la création d'une nouvelle classe de nanocomposites multifonctionnels. Par conséquent, le développement et la caractérisation des polymères et nanocomposites fonctionnels et imprimables en 3D sont nécessaires afin d'utiliser l'impression 3D comme nouveau procédé de dépôt de ces matériaux sur textiles. Cette technique introduira des procédés de fonctionnalisation de textiles plus flexibles, économes en ressources et très rentables, par rapport aux procédés d'impression conventionnels tels que la sérigraphie et le jet d'encre. L'objectif est de développer une méthode de production intégrée et sur mesure pour des textiles intelligents et fonctionnels, afin d'éviter toute utilisation d'eau, d'énergie et de produits chimiques inutiles et de minimiser les déchets dans le but d'améliorer l'empreinte écologique et la productivité.

La contribution apportée par cette thèse consiste en la création et la caractérisation de filaments CPC imprimables en 3D, le dépôt de polymères et de nanocomposites sur des tissus et l'étude des performances en termes de fonctionnalité des couches de CPC imprimées en 3D. Dans un premier temps, nous avons créé des filaments de CPC imprimables en 3D, notamment des nanotubes de carbone à parois multiples (MWNT) et du noir de carbone à haute structure (Ketjenblack) (KB), incorporés dans de l'acide polylactique (PLA) à l'aide d'un procédé de mélange à l'état fondu. Les propriétés morphologiques, électriques, thermiques et mécaniques des filaments et des couches imprimées en 3D ont été étudiées. Deuxièmement, nous avons déposé les polymères et les nanocomposites sur des tissus à l'aide d'une impression 3D et étudié leur adhérence aux tissus. Enfin, les performances des couches de CPC imprimées en 3D ont été analysées sous tension et force de compression appliquées. La variation de la valeur de la résistance correspondant à la charge appliquée permet d'évaluer l'efficacité des couches imprimées en tant que capteur de pression / force.

Les résultats ont montré que les nanocomposites à base de PLA, y compris MWNT et KB, sont imprimables en 3D. Les modifications des propriétés morphologiques, électriques, thermiques et mécaniques des nanocomposites avant et après l'impression 3D nous permettent de mieux comprendre l'optimisation du procédé. De plus, différentes variables du procédé d'impression 3D ont un effet significatif sur la force d'adhérence des polymères et des nanocomposites déposés sur les tissus. Nous avons également développé des modèles statistiques fiables associés à ces résultats valables uniquement pour le polymère et le tissu de l'étude. Enfin, les résultats démontrent que les mélanges PLA/MWNT et PLA/KB sont de bonnes matières

premières piézorésistives pour l'impression 3D. Elles peuvent être potentiellement utilisées dans l'électronique portable, la robotique molle et la fabrication de prothèses, où une conception complexe, multidirectionnelle et personnalisable est nécessaire.

Mots-clés: impression 3D, modélisation par dépôt de filament fondu, adhérence, dépôt, modélisation CAO, conception statistique, nanocomposite en polymère conducteur, nanotube de carbone à parois multiples, noir de carbone Ketjen, piézorésistif, capteurs de pression / force

Abstrakt

Syftet med denna studie är att kunna dra nytta av funktionaliteten hos *fused deposition modeling* (FDM) 3D-skrivna konduktiva polymera nanokompositer (CPC) för utveckling av funktionella och smarta textilier. 3D-skrivare har stor potential, som process, att kunna skapa en ny klass av multifunktionella nanokompositer. Därför behövs utveckling och karakterisering av funktionella polymerer och nanokompositer som går att använda med en 3D-skrivare för att kunna använda 3D-skrivare som en ny process för applicering av funktionella material på textil. Den här metoden introducerar textila funktionaliseringsprocesser som är mer flexibla, resurseffektiva och kostnadseffektiva jämfört med konventionella tryckmetoder som schablontryck och *inkjet*. Målet är att utveckla en integrerad eller skräddarsydd produktionsprocess för smarta och funktionella textilier som undviker onödig användning av vatten, energi och kemikalier samt som minimerar avfall, för förbättrat ekologiskt fotavtryck och produktivitet.

Den här uppsatsen bidrar med skapande och karakterisering av CPC-filament som går att 3D-skriva, applicering av polymerer och nanokompositer på textil och undersökning av de 3D-skrivna CPC-lagrens prestation vad gäller funktionalitet. Först skapades CPC-filament som var avsedda för 3D-skrivare genom att flerväggiga kolnanorör (MWNT) och *high structured carbon black* (Ketjenblack)(KB) inkorporerades i en biobaserad polymer, polymjölksyra (PLA), genom en smältblandningsprocess. De morfologiska, elektriska, termiska och mekaniska egenskaperna hos filamenten och de 3D-skrivna CPC-lagren undersöktes. Därefter analyserades de 3D-skrivna CPC-lagrens prestanda under applicerade spänning- respektive kompressionskrafter. För att utvärdera de utskrivna lagrens effektivitet som tryck-/kraftsensor undersöktes resistansförändringen mot applicerad belastning. Slutligen användes 3D-skrivare för att applicera polymererna och nanokompositerna på textil och lagrens vidhäftningsförmåga på textilen undersöktes.

Resultaten visade att de PLA-baserade nanokompositerna med MWNT och KB går att använda för 3D-skrivare. Förändringarna i de morfologiska, elektriska, termiska och mekaniska egenskaperna hos nanokompositerna till följd av 3D-skrivningen ger oss stor förståelse kring processoptimering. Dessutom visar resultaten att PLA/MWNT- och PLA/KB- kompositer är bra piezoresistiva råmaterial för 3D-skrivare med potentiella tillämpningar inom bärbar elektronik, mjuk robotik och proteser, där det krävs komplex design, anpassningsbarhet och möjlighet till skräddarsydda lösningar. Till sist visades att olika variabler i 3D-skrivarprocessen har signifikant påverkan på polymerernas och nanokompositernas vidhäfningsförmåga på textil, vilket presenteras med den bäst anpassade modellen för den specifika polymeren och textilen.

Nyckelord: 3D-skrivare, *fused deposition modeling*, vidhäftning, applicering, datorstödd designmodellering, statistisk design, konduktiva polymera nanokompositer, flerväggiga kolnanorör, *carbon black*, piezoresistiv, tryck-/kraftsensorer

摘要

此篇博士论文致力于使用熔融沉积成型 3D 打印的导电性高分子纳米复合材料在功能和智能纺织品应用上的优越性的研究。3D 打印在塑造新型多功能纳米复合材料方面极具前景。因此，开发和表征可用于 3D 打印的高分子材料和纳米高分子复合材料对使用 3D 打印在纺织品表面沉积功能材料的新工艺是十分必要的。相较于传统的印刷工艺， 譬如丝网印刷和喷墨打印，使用 3D 打印在纺织品表面沉积功能材料的新工艺将引入更灵活的，高资源能效的和经济有效的纺织品功能化工艺。此论文的目标是致力于整合的或者量身定做的智能化和功能化纺织品的生产流程。此生产流程避免使用不必要的水源，能源和化学品， 减少废料，因此生态足迹和生产效率得到改进。

此博士论文在创造和表征可 3D 打印的导电性高分子纳米复合材料，在纺织品上沉积高分子和高分子纳米复合材料，和在纺织品表面 3D 打印的导电性高分子纳米复合材料器件的功能性研究上具有开创性。首先，通过使用熔融混合法，多壁碳纳米管和高结构炭黑（ketjenblack）被掺入了可 3D 打印的聚乳酸中。聚乳酸是一种基于生物的高分子材料。其次，此论文对 3D 打印机的打印丝以及打印出的高分子层的形貌，电，热和力学性能进行了研究。其次，此论文对 3D 打印的导电性高分子纳米复合材料器件在拉力和压力下的表现进行了分析。器件对应于负载的电阻改变得到表征，可有效用于压力感应器。最后，我们使用 3D 打印在纺织品表面沉积了高分子和导电性高分子纳米复合材料，并研究了沉积材料与纺织品基体之间的表面附着力。

研究结果表明，掺入多壁碳纳米管和高结构炭黑的聚乳酸导电性高分子纳米复合材料可用于 3D 打印。我们可以通过其形貌，电，热以及力学性能在 3D 打印前和 3D 打印后的改变来理解和优化工艺。并且，研究结果表明，用于 3D 打印的聚乳酸/多壁碳纳米管和聚乳酸/高结构炭黑复合材料具有良好的压阻反馈，在可穿戴设备，柔软机器人和假体应用中具有前景，尤其是在设计复杂，多方向，和需要定制的应用上。最后，不同的 3D 打印参数对高分子和高分子纳米复合材料在纺织品上的附着力有重要影响。打印参数对附着力的影响可通过针对不用的高分子和纺织品基体使用最优化模型得到。

关键字：3D 打印；熔融沉积成型； 附着力；沉积法；电脑协助建模；统计学设计；导电性高分子复合材料；多壁碳纳米管；炭黑；压阻；压力传感器

Preface

All the work presented henceforth was conducted in the following laboratories:

Textile Materials Technology, Department of Textile Technology, Faculty of Textiles, Engineering and Business, University of Borås, SE-501 90, Borås, Sweden

GEnie des Matériaux TEXtile (GEMTEX), École Nationale Supérieure des Arts et Industries Textiles (ENSAIT), F-59100, Roubaix, France

College of Textile and Clothing Engineering, Soochow University, Suzhou, Jiangsu, 215006, China

A version of part of Chapter 3 has been published in the Journal of Applied Polymer Science [Sanatgar R.H., Cayla A., Campagne C., and Nierstrasz V. Morphological and electrical characterization of conductive polylactic acid-based nanocomposite before and after FDM 3D printing. J Appl Polym Sci 136(6): 1044-1053, 2019]. I was the main investigator, responsible for planning and conducting the experiments, data analysis, as well as manuscript composition. Nierstrasz V., Campagne C., and Cayla A. were the supervisory authors on this project and were involved throughout the project with guidance and manuscript edits.

A version of Chapter 4 has been submitted in the Smart Materials and Structures [Sanatgar R.H., Cayla A., Guan J., Chen G., Nierstrasz V. and Campagne C. Piezoresistive behavior of 3D printed Polylactic acid (PLA) nanocomposite layers towards pressure sensors.]. I was the main investigator, responsible for planning and conducting the experiments, data analysis, as well as manuscript composition. Campagne C., Cayla A., Nierstrasz V., Guan J., and Chen G. were the supervisory authors on this project and were involved throughout the project with guidance and manuscript edits.

A version of Chapter 5 has been published in the Applied Surface Science [Sanatgar R.H., Campagne C., and Nierstrasz V. Investigation of the adhesion properties of direct 3D printing of polymers and nanocomposites on textiles: Effect of FDM printing process parameters. Appl Surf Sci 403: 551-563, 2017]. I was the main investigator, responsible for planning and conducting the experiments, data analysis, as well as manuscript composition. Nierstrasz V. and Campagne C. were the supervisory authors on this project and were involved throughout the project with guidance and manuscript edits.

Table of content

List of tables

List of figures

List of abbreviations

ABS	Acrylonitrile butadiene styrene
APC	Acetoxypropyl cellulose
AM	Additive manufacturing
ANOVA	Analysis of variance
BET	Brunauer–Emmett–Teller
BCI	Brain-Computer Interfaces
CA	Cellulose acetate
CAD	Computer-aided design
CB	Carbon black
CCVD	Catalytic chemical vapor decomposition
CNT	Carbon nanotube
CPC	Conductive polymer nanocomposite
DLP	Digital light projection
DMA	Dynamic mechanical analysis
DMTA	Dynamic mechanical thermal analysis
DSC	Differential scanning calorimetry
EBA	Ethylene-butyl acrylate
EEG	Electroencephalography
EG	Ethylene glycol
EL	Electroluminescence
EMI SE	Electromagnetic interference shielding efficiency
FDM	Fused deposition modeling
FFF	Fused filament fabrication
FSR	Force-sensing resistor
KB	Ketjenblack
LED	Light-emitting diode

LOM	Laminated object manufacturing
MFI	Melt Flow Index
MWNT	Multi-walled carbon nanotubes
NPC	Negative pressure coefficient
PA	Polyamides
PBT	Polybutylene terephthalate
PEDOT: PSS	Poly(3,4-ethylene dioxythiophene) polystyrene sulfonate
PET	Polyethylene terephthalate
PLA	Polylactic acid
PMMA	Poly(methyl methacrylate)
PPy	Polypyrrole
PVDF	Polyvinylidene fluoride
SE	Silicone elastomer
SEM	Scanning electron microscopy
SHS	Selective heat sintering
SLA	Stereolithography apparatus
SLS	Selective laser sintering
TEM	Transmission electron microscopy
Tg	Glass transition temperature
TPE	Thermoplastic elastomers
UV	Ultraviolet
2W	2-wire ohms measurement
4W	4-wire ohms measurement

Acknowledgments

I would like to express my deepest appreciation to my supervisors Prof. Vincent Nierstrasz, Prof. Christine Campagne, Dr. Aurelie Cayla, Prof. Jinping Guan, and Prof. Guojiang Chen for their patience, understanding, continued support and help during my PhD journey. Special thanks to Prof. Vincent Nierstrasz for all the stimulating discussions, encouragements and continued support in all steps of this thesis. I would like to thank Prof. Mikael Skrifvars, Magnus Bratt, Prof. Xianyi Zeng, Prof. Yan Chen, Dr. Eva Gustafsson, and Marie Hombert for all the support.

I would like to thank my reviewers, Prof. Anne Schwarz-Pfeiffer and Prof. Jean-François Feller for offering valid and valuable comments and insights.

I am thankful to all my friends who made me happy and hopeful during my PhD journey, Sina, May, Felicia, Karin, Veronica, Emanuel, Marzieh, Sweta, Sheenam, Tarun, Vijay, Junchun, Tuser, Prisca, Melkie, Mulat, Molla, Ke Ma, Yannic, Parag, Mellisa, Yuyang, Milad, Neaz. Special thanks to my friends Felicia, Prisca and Junchun for their help in the translation of the abstract.

I would like to express my deepest gratitude to my parents, Aghdas and Reza, and my sisters Mitra, Gita, Zahra, and Marzieh for their unconditional love, support and encouragement.

In the end, I would like to thank my love, Farzad, for his full support.

Gratefully,

Razieh Hashemi Sanatgar

Dedication

To my parents

1 Introduction

Functional and smart textiles are used for different purposes such as healthcare, interior textiles, automobile, protective clothing, communication and entertainment, and are represented by different products like medical shirt, carpet, car sit, firefighters suit and optical fiber display [1]. This project as a part of the European program SMDTex- sustainable management and design for textiles tries to propose a novel process for functional and smart textiles. Applying an inter-disciplinary approach, it addresses the problems of shortage of non-renewable materials and energy sources and points at alternatives, such as new, environmentally acceptable methods of producing source-reduction of the textile chain by designing for less material but more consumer value.

The focus of the thesis is to get the benefit of functionalities of fused deposition modeling (FDM) 3D printed conductive polymer nanocomposites (CPC) for the development of functional and smart textiles. Therefore, here is believed that with 3D printing on textiles, there is more flexible, resource-efficient and cost-efficient functionalization method in comparison with conventional screen and inkjet printing methods to add the desired function to the textiles. The technology will improve the ecological footprint by minimization of textile waste combined with reduced consumption of energy, water, and chemicals. Direct 3D printing on textiles can have effect on energy demand in development of functional and smart textiles by simplification of the supply chain. Supply chain can be improved by functionalization at certain places where needed to the end-user, therefore, the energy consumption will be reduced by shortening the length of the supply chain. Developing new and complex geometrics that would otherwise be problematic, become practical with 3D printing. Therefore, the combination of the supply chain evolution and the product evolution opportunities provided by 3D printing holds the potential to reduce energy consumption [2]. In addition, 3D printing as a more flexible technology can increase productivity by enabling customized production, integrating functions where they are needed, enabling water and solvent-free as well as patterned functionalization that would have not been possible by existing fabrication processes. The possible applications of the technology are in smart bandages, virtual reality gloves, wearables with sensor and heat properties, safety equipment for the defense industry, unique sportswear that manages body temperature, medical equipment, automotive, aviation and aerospace accessories, and more [3]. 3D print technology could have strong potentials in the industrialization of smart and functional textiles.

According to European Committee for Standardization report the definition of functional and smart textiles as well as smart systems are as below [4]:

Functional textile material is “Textile material to which a specific function is added by means of material, composition, construction and/or finishing.” Electrically, thermally and optically conductive textile materials are some examples of functional textile materials which conduct electrical current, heat and light respectively. Optical fibers are applied vastly in communication acting as a waveguide by keeping the light in their core by total internal reflection. Fluorescent textile material is another example which is used in high visible clothing for safety purposes. In this material, the emitted light is of longer wavelength than the absorbed light, which allows e.g. to turn UV radiation into visible light [4].

Smart textile material is “Functional textile material, which interacts actively with its environment, i.e. it responds or adapts to changes in the environment.” Chromic, phase change, auxetic and capacitive textile materials are some examples of smart textile materials. In chromic materials, the absorption, transmission and/or reflection of light changes in response of external stimuli, therefore, a different color impression is resulted. Phase change material (PCM) is capable of storing and releasing large amounts of energy when the material change from solid to liquid and vice versa. Coating or impregnating fibres and fabrics with a polymeric binder containing micro-encapsulated PCMs is the most common method to develop these materials. Auxetic materials have negative Poisson ratio and laterally expand upon elongation which is caused by the macro and micro structure of the material. These material are intended for improved energy absorption and fracture resistance and can be applied for example for blast resistance, window covering and military tents. Capacitive textile materials are able to store electrical charges which can be created by weaving, laminating or printing of multilayers of insulating and conducive materials [4].

Smart textile system is “A textile system which exhibits an intended and exploitable response as a reaction either to changes in its surroundings/environment or to an external signal/input.” Examples of such systems can be in medical applications to monitor the health situation, occupational safety applications such as work wear and protective clothing, leisure and fashion application, underwear based on thermal control by phase change materials (PCM), heated blankets, car seats etc. for comfort or protection [4].

Therefore, smart textiles can be considered as a smart system that due to its behavior sense its environment or external stimuli (passive), sense and respond to it (active) and in very smart category adapt its behavior to the circumstances [5]. Although some drivers such as increase in consumers demands and a desire for higher quality of life exist, there are some barriers to progress of smart textiles which can be of technological, strategic, societal and economic nature [1]. All the three dimension of the barriers are influenced by cost. Generally, big companies plan to achieve a cost leadership in markets with large volumes. Accordingly, they push a

product into the market when the *technology* is able to support *large-scale affordable solutions*. Therefore, one of the most important technological challenge is the scalability of smart textile production. Other main technological barriers to exploit smart textiles are processing and fabrication and their compatibility with existing equipment, interconnection of components into the wearable textile system (including sensors, actuators, data processors, powers, and communicators), standards and the education and knowledge of staff [1].

Integration of the smart function into a textile is another challenging issue in smart textiles. These challenges are the durability, reliability, scalability, and industrialization of the production processes [6]. The awareness and acceptance, being user-friendly and the subsequent added value of smart textiles are also some of the features to consider for contribution to an economic and societal advantage. To fulfill the requirements of a smart textile such as cost, fabric resistance, comfort, flexibility and reliability, an integration of technologies and functionalities, systems and applications is needed to be considered by an inter-disciplinary approach [1]. Therefore, the aim of this thesis is to combine new technologies with new materials and apply them as a novel process for development of functional and smart textiles. The thesis focus is to get the benefit of functionalities of 3D printed conductive polymer nanocomposites (CPCs) for the possible application of the proposed technology in functional and smart textiles.

1.1 Structure of the thesis

The structure of the thesis is as below:

Introduction- This chapter explains the theme and goals of the thesis and contains a thorough review of relevant literature. It presents the goals of the study in form of the research questions and gives the strategy has been used to fulfill them. In addition, the scope and limitations of the study are presented in this chapter.

Materials, methods, and characterization- This chapter presents the materials and detailed methods of production processes and characterization of the materials.

Characterization of CPCs- This chapter presents the morphological, electrical, thermal and dynamic mechanical characterization of the CPCs in different forms of 3D printer filaments, extruded filaments from the 3D printer, 3D printer layers and 3D printed layers on fabric.

Piezoresistive properties of 3D printed layers – This chapter presents the piezoresistivity of 3D printed layers in tension and compression modes.

Direct 3D printing of polymers and nanocomposites on textiles- This chapter discusses the effect of 3D printing process parameters on adhesion force of different polymers and nanocomposites on different fabrics.

Conclusions and future work- This chapter presents the overall analysis and conclusions regarding the goals of the thesis, overall significance, and contribution of the thesis, discussion of potential applications and possible future research directions.

1.2 State of the art

This section presents the background from different disciplines which have been used in this study. The thesis emphasis on using the 3D printing technology for future possible application in development of functionalization and smart textiles. Therefore, 3D printing, 3D printing on textiles, conductive polymer composites (CPCs) and 3D printed sensors are the main parts to be discussed.

1.2.1 Additive manufacturing (AM) (3D printing)

The world of 3D printing holds a wide range of technologies. At the highest level, there are three major categories for production of a 3D part including forming, subtractive or additive manufacturing [7]. In the forming, the material will be reshaped without subtracting or adding material. In subtractive methods, unwanted material will be removed from the 3D object with different methods like cutting or etching. In additive manufacturing, the 3D object will be formed by the layer-by-layer building process by progressive addition of layers of material. AM begins with a 3D model designed with computer-aided design (CAD) software. This model then digitized and sliced into model layers with special software. Accordingly, the AM method prints 2D layers into a 3D build [8]–[14].

In recent years, AM, also known as 3D printing has attracted lots of attention from industry and academia as it holds substantial potentials. Engineers use the technology for rapid prototyping of virtual concepts and digital designs to physical models. The most important advantage of additive manufacturing is the potential for the production of highly complex structures and designs and custom-made products. 3D printing is able to create architected materials that possess both high stiffness and toughness which are often mutually exclusive [15], [16]. Moreover, there is an opportunity of applying different polymers or rigid/soft materials at the same time for the production of an object with AM. It is worth mentioning that with all the benefits of additive manufacturing in 3D objects production, the method is not still industrialized. The main disadvantage is the restricted range and unfamiliar form of feeding materials for industry. The industry knows materials in the form of pellets rather than powder or filaments and their infrastructures are according to a known form of materials. Furthermore, the process speed is slow especially for the production of large parts. Therefore, a lot of effort is still needed for developing new applicable and functional materials and polymers and the growing use of 3D printing in the industry [17].

Figure 1 shows an overview of a different forms of monomer/polymer materials and different production methods for polymer-based additive manufacturing technologies. As it shows in Figure 1, the main difference between the various technologies of additive manufacturing is in

used materials and in the way of layer deposition. The used polymer can be in the form of powder, filament, and film or liquid resin and the patterning or fusing the material can be optical, chemical, mechanical, and thermal procedures [7].

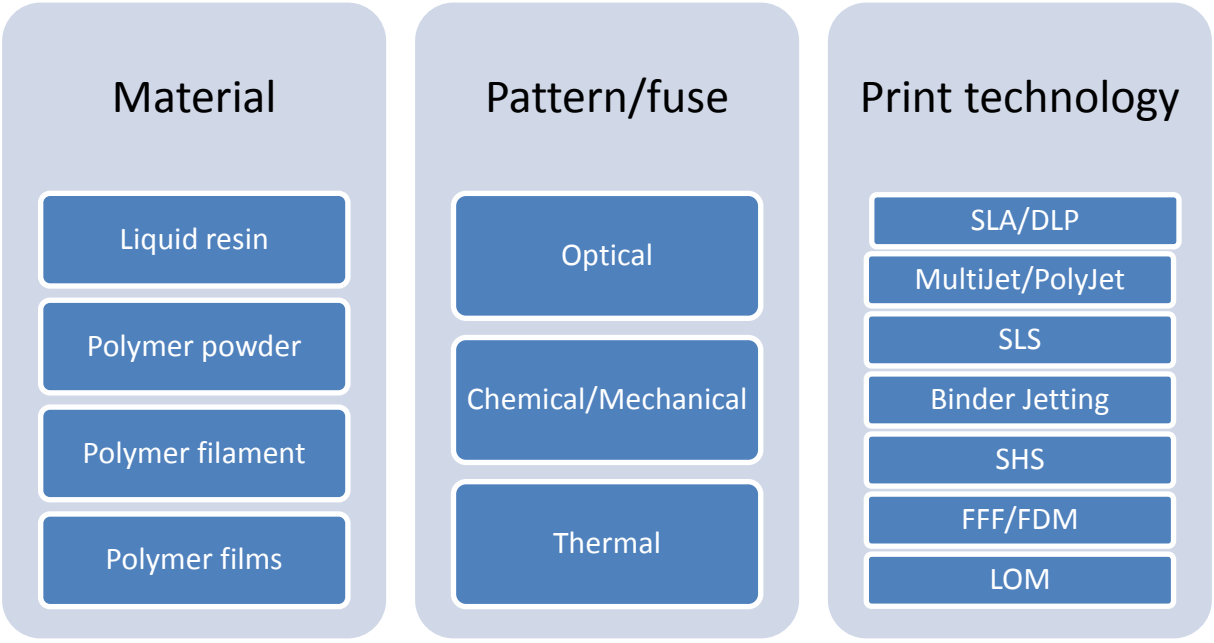

Figure 1 Overview of different monomer/polymer materials used with particular layered building techniques in additive manufacturing (SLA: Stereolithography apparatus, DLP: Digital light projection, SLS: Selective laser sintering, SHS: Selective heat sintering, FFF: Fused filament fabrication, FDM: Fused deposition modelling, LOM: Laminated object manufacturing) [7].

Photopolymerization based approach was the first layered building process when 3D Systems introduced a stereolithography apparatus (SLA). In this method, certain regions of a photosensitive liquid resin are exposed to ultraviolet (UV) laser and undertake localized polymerization. Photopolymerization reactions are mostly chain-growth polymerization and initiated by visible or UV light. The unexposed regions include unreacted monomers can be removed from the 3D build.

MultiJet (or PolyJet) is another UV-cured printing format that can yield smooth parts in highly complex geometries that do not need surface finishing. In this method, heads dispense droplets of liquid (UV-curable polymeric materials) were required for the design and supporting material simultaneously as the printer has multiple heads. The layer-by-layer build is covalently interconnected within a given layer and with the previous layer of the designed shape by

interspersed with photo-curing [18], [19]. Selective laser sintering (SLS) is a method in which a powder is used as the building material. In this approach, powder particles are locally fused by a scanned laser on the surface of a preheated build chamber that is gradually lowered as the process progresses. Therefore, the 3D object is manufactured by compacting and forming a solid mass of powdered material [20].

Fused filament fabrication (FFF) (equivalent to fused deposition modeling-FDM, trademarked by Stratasys) is one of the basic AM methods that use a preformed polymer (filament) as the building material pushed through a heated extrusion nozzle [7]. It is worth to mention that there are already some commercially available pellet printers used for large manufacturing systems, therefore the technology needs to be miniaturized and replicated in a more commercial scale.

In FDM technology, the processing energy input is required in the pre-deposition phase to create a polymer melt material that can be used through a fine print head or nozzle. The deposited patterns follow the design without using molds as it is used in injection molding. As the properties of the 3D printed objects in this method have greater anisotropy because of weaker interlayer bonding than intra-layer, post-print processing is suggested with exposure to gamma radiation to induce crosslink formation within and between layers [21]. As it is mentioned, different methods have been used for AM of 3D objects such as material jetting, powder bed fusion, material extrusion, sheet lamination, directed energy deposition, photopolymerization, and binder jetting. Each method has its advantages and disadvantages. For instance, the SLA approach has high accuracy but limited durability and stability as well as using the liquid photosensitive polymers can be toxic. In SLS method high bandwidth of materials can be applied and high mechanical strength of the 3D printed object is provided, but the 3D printed object has a rough surface, the procedure has high cleaning efforts and the machine cost is high. FDM uses different thermoplastic materials in filament forms such as acrylonitrile butadiene styrene (ABS), polylactic acid (PLA), PA, PLA soft, thermoplastic elastomers, and polyurethanes. The technology is clean and simple-to-use and as it is mentioned above the complex geometrics and cavities that would otherwise be problematic become practical with FDM technology. FDM 3D printing was used in this thesis as it could offer clear advantages in 3D printed objects such as customized geometries, reduced delay between design iterations, single tool production, and increased parts integration.

1.2.2 3D printing (3D polymer deposition) on textiles

Between all the 3D printing methods discussed above, FDM can be applied for deposition of polymers and functional materials directly on fabric, as the method is clean and can be used without liquid resin and supporting material. The method can be an alternative to other techniques like screen printing, inkjet printing, gravure, flexography, and etc. for functionalization and modification of different types of textile substrates without utilizing masks or subsequent etching processes [3].

Screen-printing has been used a lot for the development of functional and smart textiles. In this method, layers with various functions are printed on top of the fabric through a layer-by-layer process. For instance, to obtain sensing functionality polypyrrole (PPy) was screen printed on lycra/cotton fabric to develop resistive fabric strain sensors for detection of human posture [25], [26]. The gauge factor of improved version was about 80 for a strain of 50% but the stability and durability were low [27]. A strain sensor was developed by applying a thermoplastic elastomer/carbon black (CB) nanoparticle composite on a lightweight nylon fabric [28]. One of the most mature fabric pressure sensors has a coating of a composite including carbon black, silicone elastomer (SE), and silicone oil on a single jersey fabric that makes a resistive fabric sensor with acceptable sensitivity and durability [29]. In much research [30]–[35], conductive textiles have been developed by screen printing of conductive silver tracks on textiles with different protective layers which increase durability and conductivity of the silver. Screen printing has some advantages like the use of low-cost patterning process at room temperature, high volume batch fabrication and applicability on any irregular textile surface [36].

Inkjet printing is a conventional direct write deposition tool that in comparison to screen printing has some advantages such as high precision of ink droplet, thin layer deposition capability, short run length as well as tailored/integrated production process. This technology has already been used for different inks such as graphene and graphene-based [37], silver-containing [38], [39] and carbon nanotube (CNT) inks [40]. Inkjet-printed elements such as conductors (antennas), dielectrics (capacitors) and sensors can be developed for wearable electronics applications [41], [42]. Therefore, it is possible to add functionalities onto fabrics by inkjet printing, but the multiple printing is needed to produce the desired functionality with a thin inkjet printed layer on the rough fabric. For this reason, the manufacturing time and cost is increased [41]. A thin based coating or screen printed layer has been used in some researches to decrease the fabric surface roughness for inkjet printing [43], [44].

Mentioned technologies above including screen-printing and inkjet printing are possibly low-cost alternatives to traditional technologies, but there are still many problems to apply them in

industrial scale. For instance, inkjet printers are expensive and the screen printing process has some pollution and waste. At the same time, the needed warehouse for the screens and the downtime for screen-printing increase the manufacturing cost and time. Moreover, fixing the flawed products of these methods is not easy [45].

Accordingly, manufacturing techniques still need to be improved. Additive manufacturing or 3D printing is a technique may solve the problems of existing methods and improve the development of smart and functional textiles by integrated or tailored production processes. This technology can serve the smart and intelligent textiles, as there is still a high demand for innovative, efficient and environmentally friendly processes and products with added value for the end users of smart textiles [46]. To develop smart textiles, conductive materials and components are attached to textile with different methods such as incorporation of conducting yarns into the fabric, mounting electronic components such as sensors and actuators on the surface, or for control, mounting processing units onto a mini printed circuit board on fabric. In all applications, the functional material in modified textile may influence the flexibility and drapability of the fabric [46].

Conductive particles, functional conductive polymers and metal conductors can be printed or integrated into textiles to meet the needs for flexible electronic textiles [46]. As the textiles have porous structures, voids and roughness of the textile substrate can avoid the interconnection of the conducting materials printed in thin layers such as inkjet-printed layers. Therefore, thicker layers of conductive materials are needed to overcome surface discontinuity of the 3D and flexible structure of textile substrates and their absorbency [46]. FDM 3D printing method makes it possible to deposit thermoplastic functional polymers and composites or their blend on textile fabrics to develop functional and smart textiles.

Here is believed there are some potential benefits of the 3D printing on textiles. The technology can be applied where patterned as well as water and solvent-free functionalization is needed. The technology enables to improve the ecological footprint by minimization of textile waste as well as reduced consumption of energy, water and chemicals. The technology is high productive, flexible and cost effective, it has short time to market for textile innovations. It is adaptable to quick changes of customer demands. And it is possible to develop innovative products for functional and smart textiles.

There are lots of unknown aspects of the deposition/3D printing of polymers and composites on textiles which have to be studied such as the adhesion, binding or interaction phenomena in various interfaces. The fact that textiles are made from different materials, structures and architectures make it clear why the understanding of the process is challenging. It is preferred

to apply the process without pretreatments or smoothing coating layers. There are different aspects which have to be considered for effective deposition of polymers onto fabrics: a) the binding and adhesion phenomena of polymer onto fabrics, b) drape-ability of the printed fabric for free movement, c) ability to deform and recover when they are subjected to daily wear forces and d) washability [3], [47], [48].

Over the last few years, along with this thesis, many attempts have been made to print textile structures or to combine 3D printing with textile fabrics. Brinks *et al.* [46] performed deposition of PLA on polyethylene terephthalate (PET) bundles with pressure on the melt immediately after applying the molten polymer onto the fabric to increase penetration and bonding between molten PLA and PET bundle. They modeled their system by considering bonding and penetration of the polymer onto the fabric. In another research, functional parts such as orthopedic braces were printed onto fabrics and their adhesion was investigated [47]. It is believed the flexibility and breathability of the textile provide comfort and the rigid structure of the 3D printed polymer provide support in such orthopedic braces. PLA showed good adhesion and good flexural strength with a high quality of the print.

For the first time, a systematic study was done by Sanatgar *et al.* [3] to investigate the effect of FDM printing process parameters on the adhesion of polymer and composites on textiles. The results showed that different 3D printing processing parameter such as extruder temperature, bed temperature, and printing speed can have a significant effect on adhesion force. According to the introduced model, there is a significant linear effect of extruder temperature and significant quadratic effect of printing speed on the adhesion force of PA6.6/6 on PA6.6 fabric. As far as the bed temperature is lower than the glass transition temperature of the fabric, there is no significant effect of bed temperature on adhesion force. Another research showed that by increasing the printing bed temperature from room temperature to 100˚C for PLA printed on PET fabric, the adhesion force increased but it affects the print quality [49]. The extrusion wide (which determines how wide the lines are) identical to nozzle diameter shows the highest adhesion while increasing the first layer height decrease the adhesion [49].

Low tensile strength which is the main challenge in applying pure 3D printed products in the textile industry encourages Ehrmann *et al.* to combine 3D structures with textiles. Adhesion of the deposited PLA on woven cotton, viscose, wool fabrics was low, just the deposited PLA on net polyester showed a fixed pattern on fabric [50]. The adhesion of 3D printed polymers on knitted and woven fabrics was investigated [51]–[53]. The results showed that the smaller z-distance (the distance between the printing nozzle and printing bed) result in higher adhesion forces because of the higher pressure of the printed polymer on the fabric. In addition, the nozzle diameter influences the dependence of the adhesion forces on the distance between the printing

nozzle and printing bed. The 3D printed auxetic forms on knitted fabrics were also investigated for adjusting permeability and mechanical properties of the textiles [54]. Auxetics may be useful in applications like body armor, knee and elbow pads, filtration and robust shock absorbing materials due to their negative Poisson's ratio, they expand laterally when stretched longitudinally [55]. The results showed that by adjusting the mechanical properties of both partners including 3D printed auxetic forms and knitted fabrics, it is possible to modify the pore sizes and shapes of the final composite. In another research [56], different lamellae with applying soft PLA were 3D printed on knitted fabric which not only it is possible to make new designs, but also it is favorable for technical applications such as transforming a fabric from an air and water vapor permeable state to closed lamellae state to protect from wind and rain and vice versa. 3D printing of Braille on labels in garments and textiles to support blind people during shopping can be another valuable application for 3D printing on textiles [57]. Therefore, a combination of textiles with 3D printed shapes could not only modify the mechanical properties of the textile fabric but also give the opportunity to create new composite materials. Accordingly, understanding and optimizing the adhesion between 3D printed material and textile is high-priority.

Basically, chemical composition (functional groups), molecular organization (branching, molecular weight distribution, cross-linking) and physical state (elastomer, thermoplastic, thermoset, crystalline) of adhesive and adherent can affect the bond performance and its durability [58]. The influence of textile surface properties on the adhesion of 3D printed flexible polymers such as thermoplastic elastomers (TPE) and soft PLA on the textile surface was investigated [59]. Roughened textile substrates showed higher adhesion which is influenced by the form-locking connections of the molten polymer and the textile substrate on the surface. But, as it is mentioned previously, form-locking theory is controversial, as there are some experiments in which the adhesion decreased with increasing roughness. Another important factor that can affect the adhesion force is wettability of the surface which can be controlled with pretreatments of the textile such as washing to remove impurities and plasma treatment to reduce the hydrophobicity of the textile surface. As a result the wettability of the textile surface and therewith the textile surface energy and adhesion force is enhanced [59]. However, it must be mentioned that some pretreatments do not fit into this law. Kozior *et al.* [60] investigated various pretreatment methods for 3D printing of PLA on the cotton woven fabric. The used pretreatment methods were such as glue stick (a typical method to fix PLA or Nylon printed objects on the printing bed), waterproof spray (to create a more hydrophobic textile surface), acetone (a typical lab cleaning agent), NaOH (a base which is used for mercerizing cotton), ironing and so on. Results showed that using the glue stick increases the adhesion force mostly which supports the effectiveness of chemical pretreatment more than physical. Using NaOH

also have a positive effect, however, the other pretreatments resulted in decreased adhesion forces. Ironing and acetone both have a negative impact on the adhesion force. Ironing will decrease the roughness of the surface, causing a decrease in adhesion. For the pretreatment with acetone, the printed PLA surface may have been dissolved by acetone remained in the cotton as acetone can dissolve cotton in high temperatures [60]. Therefore, increasing surface wetting will not always increase the adhesion force.

A method was suggested to improve the adhesion of the 3D printed materials on the textile by previously coating the latter with a polymer layer [61]. PLA on poly(methyl methacrylate) (PMMA) or PLA coatings, as well as ABS on ABS or PLA, showed good results. Recently, Eutionnat-Diffo *et al.* [62] showed that the heat transfer of polyester textiles and their structure also affect the adhesion of 3D printed polymers with textiles.

Recently, an all-cellulose approach was presented for surface tailoring and functionalizing cellulosic fabrics by using 3D printing of two cellulose derivatives, rigid cellulose acetate (CA) and flexible acetoxypropyl cellulose (APC) [63]. The results showed that printed structures of CA with linear structure have excellent adhesion to cellulose molecules in the substrate in comparison with APC with more branched molecular structure. Therefore, the development of new products could be performed in an environmentally friendly fashion by applying renewable and recyclable materials. The impact of 3D printing on garment drape has been investigated by printing different geometrical patterns on textile fabric and concluded that the geometry and the distance of the patterns can influence the fabric drape [64].

Recently, some attempts have been done to apply 3D printed objects for development of electronic structures on textiles. 3D printed conductive PLA used as contacts between textile or textile-integrated circuit paths and small electronic components like light emitting diodes (LED) have basically shown the suitability of the method for electrical and mechanical connections [65]. Tadesse *et al.* [66] tried to develop a flexible and lightweight electroluminescence (EL) device by coating poly(3,4-ethylene dioxythiophene):poly(styrene sulfonic acid) (PEDOT:PSS) with ethylene glycol (EG), 3D printing of Ninjaflex (a specially formulated thermoplastic polyurethane (TPU) with high flexibility and good dielectric properties), coating phosphor paste, and 3D printing BendLay filaments layer by layer on polyester fabric. NinjaFlex showed sufficient adhesion to coated polyester with PEDOT: PSS and no weight loss was recorded following three washing cycles. The prototype emitted light with an AC voltage as low as 12 V in a dark environment.

It is clear that the deposition of the polymers on textiles depends on the combination of the textile material and printed polymer and it may need specific processes to get the best

efficiency. This area of research needs a profound knowledge regarding not only new but also existing materials, polymer-textile adhesion and deposition/extrusion technology. The technology can give potential benefits for fabrication of smart, functional and innovative textiles such as flexibility, durability, surface tailoring and customization with minimized material usage and simple processes.

1.2.3 Adhesion

Adhesion is the bonding of one material to another called adhesive to substrate (adherent) caused by different possible interaction at the adhesive-substrate surface interface [22]. Cohesion is defined as the internal strength of an adhesive due to different interactions within the adhesive. The adhesion force between two materials depends on their interactions and the surface area which the two materials are in contact, therefore, different factors can have effect on the adhesion force.

1.2.3.1 Contact angle and surface tension

Wetting is the ability of a liquid to form an interface with a solid surface which can be determined by the contact angle θ formed between the liquid and the solid surface. Contact angle is affected by the surface tension of the liquid as well as the surface properties of the substrate. Lower surface tension of the liquid and smaller contact angles cause higher degree of wetting. When the wetting property of the materials is high, they tend to have a larger contact area. Wetting depends on the relative surface energy of the adhesive and substrate and high surface energy materials show higher adhesion forces while bonding together [22]. Therefore, adhesive liquid should be able to wet the surface of the substrate for better adhesion which can be affected by different factors such as the surface properties of substrate like pores and roughness and adhesive properties.

1.2.3.2 Chemical adhesion

Chemical adhesion occurs when the surface atoms of an adhesive and adherent form ionic, covalent, or hydrogen bonding which result in high strength bonding. However, surfaces with the potential for chemical bonding should be brought very close together as the chemical bond lengths are short. The surfaces need to be remained close for the chemical bonds to be stable. Hydrogen bonds are about an order of magnitude weaker than the covalent and ionic bonds [22].

1.2.3.3 Dispersive adhesion

The effective force for dispersive adhesion or physisorption is van der Waals that are the attractive forces between two molecules. Each molecule has a region of small positive and negative charge such that the molecules are polar with respect to the average charge density of the molecule. London forces which are caused by the random electron motion within the molecules are particularly effective in adhesion because they occur without the need for either the adhesive or the substrate surface to have any permanent polarity. In surface science, adhesion generally refers to dispersive adhesion. The van der Waals forces have longer bond lengths than those of other molecular forces but they are still short (0.45 nm), therefore, they act over very small distances. The nature of the interfacial bonds is brittle, therefore, when a crack is initiated, it extended along the interface and, as a result, different contact surface areas often provide small difference in the measured adhesion [22].

1.2.3.4 Diffusive adhesion

Diffusion is a theory that explains the adhesion of polymers to each other by the diffusion of chainlike molecules that leads to the formation of a strong bond between adhesive and adherent. Polymer diffusion has a major effect on properties of the layers of polymers across the interface and is the function of temperature, composition, compatibility, molecular weight, orientation and molecular structure of polymers [23]. Diffusion improves the adhesion between the two layers of the polymer and makes the interface stable.

1.2.3.5 Mechanical interlocking

Mechanical interlocking states that an adhesive will adhere to a rough substrate stronger than to smooth surface. The reason is that the adhesive can penetrate into the pores of the rough surface and lock mechanically to the substrate. However, the theory is controversial as there are some experiments showed increasing roughness causes the adhesion decrease [24].

1.2.4 Nanomaterials-based additive manufacturing (3D printing)

Nanocomposites attract lots of attention from researchers and industry because of the combination of properties provided from both nanomaterials and host matrix in different areas such as aerospace, automotive, semiconductor, plastics, and chemicals. However, applying nanocomposites has been still faced some challenges such as processing, cost, consistency, and reliability in volume production and high lead time. Campbell *et al.* in 2013 [8] argued the potentials offered by nanomaterials-based additive manufacturing as a new paradigm for nanocomposite functionality. It is possible to develop complex 3D objects of nanomaterials

layer by layer with greater control over material properties across part dimensions by additive manufacturing. Therefore, the marriage of nanomaterials and 3D printing can give new opportunities in nanocomposites by the manipulation of basic host material properties through nanomaterials and by tailored/customized geometries, the reduced delay between design repetitions, single and simple tool production, and increased part integration through 3D printing.

There are two different methods to incorporate nanomaterials into the 3D printing process. The first method is to 3D print the host matrix material with periodic stoppage of the printing process and the introduction of nanomaterials manually or automatically, and the second method is to mix the nanomaterials into the host matrix and 3D print the nanocomposite subsequently. However, to be able to control the 3D printed nanocomposite material properties, the 3D printing process parameters are required to be controlled. But, there are still many fundamental questions before nanocomposites can be commonly processed by additive manufacturing like what nanomaterials can be applied in what additive manufacturing processes and what measurement methods and standards can be applied for characterization the properties [8].

1.2.5 Conductive polymer composites (CPC)

Conductive polymer composites (CPCs) are insulating polymer matrices with conductive fillers - like carbon or metallic particles that can be zero, one or two-dimensional such as fullerene, carbon nanotube and graphene, respectively (Figure 2) [67].

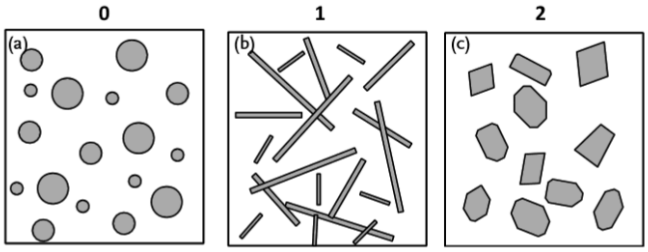

Figure 2 Schematic of zero, one and two-dimensional fillers in the polymer matrix [67]

The sudden increase of conductivity of thermoplastic polymer composites (from insulator to a conductor) at a critical volume content of a conductive filler is a phenomenon often called percolation (P_c) [68], [69]. This phenomenon is usually explained with the help of percolation theory which examines the formation of conductive pathways inside the polymer matrix in the form of continues agglomerates or clusters of connected fillers (Figure 3) [67].

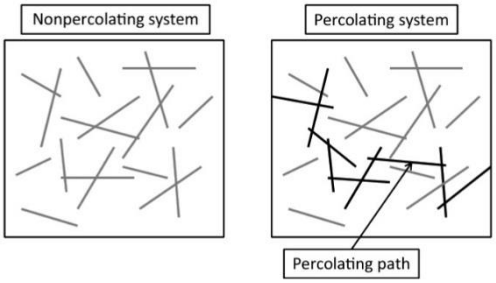

Figure 3 Schematic of the formation of conductive pathways in the polymer matrix according to percolation theory [67]

Equation 1 based on percolation theory is given as below:

$$\sigma_c = \sigma_0(\varphi_f - \varphi_c)^t \quad (1)$$

where σ_c is the composite electrical conductivity (S/cm); σ_0, filler electrical conductivity (S/cm); φ_f, the fraction of conductive filler (v/v or wt. %); φ_c, percolation threshold (v/v or wt. %); t, critical exponent as a fitting parameter. The percolation threshold value is usually calculated by plotting the electrical conductivity of the composite versus reduced filler mass fraction and fitting with a power law function [70]. After percolation threshold the conductivity increases exponentially with the amount of filler and finally the saturation of the electrical conductivity is observed (Figure 4) [67].

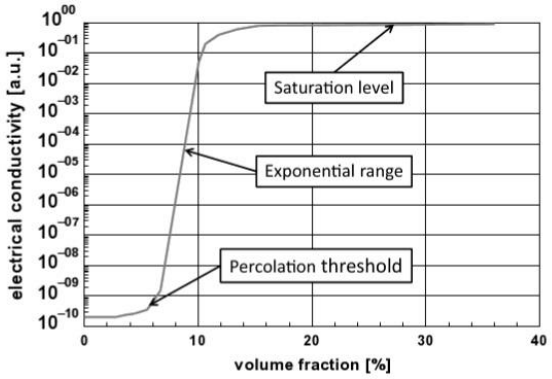

Figure 4 The typical diagram of electrical conductivity of conductive polymer nanocomposites as a function of the filler volume fraction [67]

Distinct advantages of high aspect ratio (length/diameter) fillers based on carbon allotropes like carbon nanotubes in comparison with more traditional fillers like carbon black originate from their sheer size [71]. Since carbon black is still a desirable filler in polymers which is generally UV absorbent, heat and chemical resistant, has a low density and low thermal expansion, and

acts as an anti-abrasive [72], a nanosize carbon black with the high structure is favorable. A nanosize or high-structured CB is made by fusion of the primary particles into an extended three-dimensional structure which the final dimension and density depend on the preparation method [73]. Moreover, the conductivity of CB allows it to be applied in radiation shielding and static dissipative applications [74].

Although a lot of development is going on in the field of conductive polymer nanocomposites by different preparation methods such as melt blending, in situ polymerization, and solution mixing, still, the primary challenge is to control the morphology of nanocomposites like size, shape, and distribution. By controlling the morphology of nanocomposites, the properties of nanocomposites can be controlled to reach up to our desired application [75].

Recently, some research has been done for combining the FDM technology and CPCs materials to get the benefit of specific functions of 3D printed conductive composites. Dorigato *et al.* [76] studied the electrical, thermal and mechanical properties of compression mold and 3D printed MWNT/ABS composites. They found out that the 3D printing direction can affect the mechanical and electrical properties of 3D printed objects. Lebedev *et al.* [77] showed that PLA conductive composites containing single-walled carbon nanotubes and powder of natural graphite are suitable for processing by injection molding or fused deposition modeling for fabricating 3D biodegradable scaffolds and heat sinks. The biocompatibility of nanocomposites containing single-walled carbon nanotubes has already proved [78]. Gnanasekaran *et al.* [79] did 3D printing of a non-conventional conductive structure, CNT- and graphene-based PBT. The results showed that 3D printed PBT/CNT objects have better conductive and mechanical properties as well as performance in comparison with 3D printed PBT/graphene structures and the CPC has the potential to print conductive structures like electrodes within a 3D-printed insulating matrix. 3D printed PLA/graphene nanocomposites also has been proposed to use as lightweight EMI shielding materials with the mechanism of reflection rather than absorption in the X-band frequency region with the electromagnetic interference shielding efficiency (EMI SE) of 16 dB [80].

1.2.6 3D printed sensors

In recent years, a lot of research has focused on the application of 3D printing for sensor manufacturing. The fabrication of 3D printed sensor can be conducted by either embedding a sensor into 3D printed structures or printing the entire sensor consistently [81]. Several important technologies such as printing technology combined with electronic device design in printed electronics. Electronic devices manufactured by different printing processes for

customized substrates are the key components and most important trends of 3D printed sensors [82]. Using 3D printing technology offers a new approach for the fabrication of sensors that are both geometrically and functionally complex. Recently, significant researches have been done on the fabrication of 3D printed sensors such as force [83], motion [84], optic [85], hearing [86], etc. by various 3D printing technologies with different transduction mechanism, application and printing materials.

3D printing enables the creation of complex geometric designs and combining of selected functional components into any configuration, therefore providing a new approach for the development of multifunctional end-use devices that can potentially merge optical, chemical, electronic, electromagnetic, fluidic, thermal and acoustic characteristics [12].

Saari *et al.* [87] created a capacitive force sensor using FDM method and ABS-based materials consists of a 3D printed rigid frame with embedded wires in a spiral pattern imitates a flat plate capacitor and a thermoplastic elastomer dielectric spacer that compresses under the applied force. An ear prosthesis fabricated by 3D printing of polyvinylidene fluoride (PVDF) [88] showed reliable responses under different conditions of pressure (0 to 16350 Pa) and temperature (2 to 90 °C) regarding the pyroelectric and piezoelectric properties. Krachunov [89] presented a method using 3D printing of ABS and PLA (with the silver paint coating after 3D printing) for the design and manufacture of customized dry electrodes for electroencephalography (EEG) which is a procedure that records brain activity in a non-invasive manner. The performance of the proposed electrodes is suitable for Brain-Computer Interfaces (BCI) applications, despite the presence of additional noise.

The electrical conductivity CPCs under stress, thermal variation, UV radiation, moisture or chemicals varies and can be observed and used as a measuring parameter [90]–[92]. Much research [90], [93]–[95] has been done to make a functional CPC by introducing CNT with high electrical conductivity and large aspect ratio to PLA. PLA/CNT composites have been examined as sensing materials for different stimuli such as liquid [96], degradation [94] and vapor [95]. Generally, the basic mechanism is that the introduced external stimuli cause a deformation of the CNT percolation network (as it can be seen in Figure 3), and consequently, the electrical conductivity of the composite will change.

Some researchers have combined the FDM technology and CPCs materials to develop 3D printed sensors. For example, a simple conductive thermoplastic composite called ‘carbomorph’ (carbon black in a matrix of polycaprolactone) has been used for 3D printing of functional elements such as electronic sensors able to sense mechanical flexing and capacitance changes [97]. Christ *et al.* [98] developed a flexible thermoplastic-based strain sensor by 3D

printing of TPU/MWNT. The results demonstrated TPU/MWNT as an excellent piezoresistive feedstock for 3D printing with the piezoresistivity gauge factors of as high as 176 under applied strains of as large as 100% for 3D printed strain sensors. The sensor showed a highly repeatable resistance-strain response under cyclic loadings capable of potential applications in wearable electronics, soft robotics, and prosthetics. Kim *et al.* [99] 3D printed TPU and TPU/MWNT (a structural part and a sensing part, respectively) to fabricate 3D multiaxial force sensor which could detect the submillimetre scale deflection and its corresponding force on each axis. FDM 3D printed objects of PVDF/MWNT showed chemiresistive properties in response to volatile organic compounds [100]. Decreasing the MWNT loading generated larger responses in manufactured chemical sensors. Printing in different geometries expand the utility of 3D printed sensors in wearable forms and make researchers closer to the desire of applying 3D printing for functional and smart textiles [3].

1.2.7 Strain and pressure sensors

Sensors have been vastly investigated in electronic textiles as they have promising applications such as healthcare, personal protection, intelligent control and early warning [36], [101]. Along with temperature [102]–[105], chemical [106]–[110] and humidity sensors [111], [112], strain and pressure sensors have been also extensively investigated in electronic textiles.

There are different types of electronic textiles which respond to mechanical stimuli such as strain and pressure with different sensing mechanism called resistive, capacitive, inductive and self-powering (piezoelectric) [113][114].

1.2.7.1 Piezoresistive sensors

In piezoresistive sensors, the electrical resistance changes with the deformation of the geometry in accordance with the application of strain and stress. There are two different strategies to develop electronic textiles with piezoresistive sensing functionality. The first one is to integrate the fiber sensors into textiles [115]–[119] and the second method is to deposit the functional materials onto fabrics [25]–[27], [91], [120]. Various conductive materials such as conducting polymers (e.g. polypyrrole, poly(3,4-ethylene dioxythiophene) polystyrene sulfonate (PEDOT: PSS)), carbon materials and metallic fillers are used as conductive layers and different polymer fibers like polyamide 6 (PA6), polyolefin and polyurethane used as elastic substrates. Different factors are involved in a resistance change of the piezoresistive sensor such as deformation change of the fiber/textile and change in contact resistance of the conductive components. There are different methods for deposition of the conductive materials onto polymer fibers to form a

conductive layer such as solution dipping, in situ polymerization and chemical vapor deposition [121]–[123]. To improve the stretching mismatch between the conductive layer and polymer fiber substrate, composite fibers were developed instead of coating procedures. Different composite fibers like polyurethane and PEDOT: PSS, as well as styrene-butadiene-styrene and silver nanowires, showed high efficiency as strain sensors which could be woven into textiles and fabrics [124][125][126]. To improve the stability, CNTs have been vastly investigated because of their high mechanical and electrical properties which introduce into strain sensors [127][128].

1.2.7.2 Capacitive sensors

In capacitive sensors which composed of a dielectric layer and two conductive layers, the capacitance of the dielectric layer change with the variation in the layer thickness caused by mechanical stimuli. High sensitivity and low consumption of energy are two advantages of the capacitive sensors [113]. Incorporation of conducting polymers, metallic or carbon fillers can make conductive fibers and fabrics [113][129], on the other side elastic polymers such as polydimethylsiloxane and polyurethane can act as a dielectric elastomer to develop fiber-shaped capacitive sensors [130][131]. Sandwiched configuration and weaving the coated fibers with conductive and dielectric materials are the other methods which have been investigated to develop capacitive sensors [131][132]. The fabric capacitive sensors can be applied as wearable keyboards.

1.2.7.3 Inductive sensors

Inductive sensors can be developed by introducing the conductive yarns or wires into the fabric structure to form helical strips [114]. The inductance, which is the tendency of an electrical conductor to oppose a change in the electric current through it, changes in response to applied strain. Changing the current induces a reverse electromotive force. Applying this mechanism, stainless steel yarns [133] and copper wires [134] were knitted into fabrics to monitor respiration and angular movements of the body joints.

1.2.7.4 Piezoelectric sensors

Piezoelectric textile sensors provide electronic signals with mechanical stimuli without applying external power source and as a consequence of a change in the distance between dipoles. PVDF is one of the most interesting polymers which have been investigated in piezoelectric fiber sensors as it has high flexibility and good processability in comparison to inorganic materials like ZnO. The nonwoven mats of PVDF by electrospinning process can be a good candidate for piezoelectric sensors [135]–[137].

1.3 Objectives

The aim of this study is to get the benefit of functionalities of 3D printed conductive polymer nanocomposites (CPCs) deposited on textiles for the development of functional and smart textiles. Therefore, appropriate knowledge is needed to be achieved regarding used CPC and its behavior before and after 3D printing. This is important to find out the change in different properties of CPCs such as morphological, electrical, thermal, and mechanical before the 3D printing process (in form of filaments) and after the process (in form of 3D printed layers). The performance of the 3D printed layers in terms of functionality should be addressed. In the end, direct deposition of polymers and nanocomposites on textiles should be investigated systematically.

The following research questions were set as guidelines to fulfill the goals.

1) what are the characteristics of conductive polymer nanocomposites before and after FDM 3D printing?
2) what is the performance of the CPC FDM 3D printed layers in terms of functionality?
3) what is the effect of FDM 3D printing process parameters on the adhesion properties of deposited polymer and nanocomposites on textile fabric?

1.4 Research strategy

The thesis combined 3D printing with nanocomposites on textiles to investigate the performance and functionality of the proposed technology for further applications in functional and smart textiles (Figure 5).

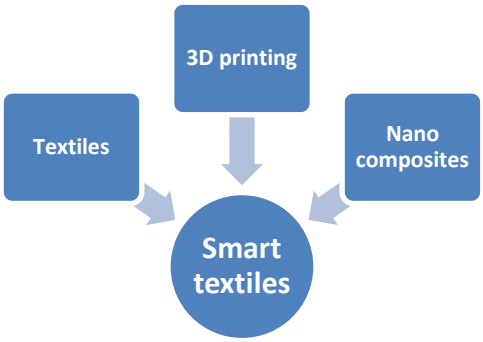

Figure 5 Union of 3D printing, nanocomposites, and textiles for smart and functional textile applications

To answer the research questions and fulfill the objective of the study, a research strategy is presented below:

Step 1. At the first step, CPC filaments were required to be feed into the 3D printer. Therefore, two different fillers including multi-walled carbon nanotube (MWNT) and high-structured carbon black (KB) in the matrix of polylactic acid (PLA) were used to compound and extruded as 3D printer filaments.

Step 2. The morphology, electrical, thermal and dynamic mechanical thermal properties of the developed 3D printer filaments were investigated to have essential knowledge about the feeding material to the 3D printer.

Step 3. The developed filaments were fed to the 3D printer to print tracks and layers of conductive polymer nanocomposites.

Step 4. The morphology and electrical properties of the monofilaments come out of 3D printer was investigated. In addition, the morphology, electrical, thermal and dynamic mechanical thermal properties of the 3D printed layers were investigated. The DMTA of the 3D printed layers on the fabric was also done.

Step 5. To find out the functionality of the 3D printed layers, their piezoresistive behavior under (cyclic) applied load was evaluated.

Step 6. The polymers and CPCs were deposited on fabrics and one of the main important aspects of printed material on fabrics or films, which is the adhesion, was investigated. The effect of FDM 3D printing process on adhesion was studied.

1.5 Scope

In this thesis, fused deposition modeling (FDM) was used as an additive manufacturing technique. Other 3D printing techniques were not in the scope of this project. The polymer applied as a matrix of the nanocomposite was PLA as a 3D printable and well-behaved polymer through 3D printing to be able to analyze the changes of the nanocomposite properties before and after 3D printing. To investigate the adhesion properties of the polymers and nanocomposites onto fabrics and propose the relevant model, the effect of FDM process parameters were analyzed. Therefore, the effect of fabric properties on the adhesion was not in the scope of this thesis.

2 Materials, methods, and characterization

In this thesis, it has been tried to use the well-known polymers for 3D printing such as PLA (also as a matrix for CPC 3D printer filaments) and PA to get an overview on the effect of 3D printing process on their different properties. For deposition of polymers and nanocomposites onto textiles, the fabrics were also selected from the same material as 3D printed polymer (such as PLA onto PLA, PA onto PA, PLA CPCs onto PLA) to propose more pure approaches for sustainable development of smart and functional textiles. A one-dimensional and a two-dimensional nano-sized fillers were selected to develop conductive 3D printer filaments and investigate their 3D printed layers properties and effectiveness towards development of functional and smart textiles. Multi-wall carbon nanotubes and high-structured carbon black were selected because they are carbonaceous fillers, more stable than metal fillers and intrinsically conductive polymer (in molten processes). In addition, these two nanofillers have large specific surface area as well as high aspect ratio, allowing to expect lower percolation thresholds.

2.1 Materials

Conductive filaments were formulated using two different nanofillers in a polylactide acid (PLA) matrix. The used polymer is a semi-crystalline thermoplastic PLA under the reference NatureWorks®-6202 D from NatureWorks (M_n = 58300 g/mol; D-Isomer = 1.3%). Pellets were dried at 60°C for 12 hours before compounding and extrusion. Multi-wall carbon nanotubes (MWNTs) with purity of 90% were supplied by Nanocyl (Belgium) under the reference Nanocyl®-7000. The main characteristics are the diameter of about 10 nm and lengths of 0.1-10 µm (aspect ratio about 157) with a surface area of 250 m^2/g that synthesized via catalytic chemical vapor decomposition (CCVD). The carbon black (KB) was supplied by AKZO NOBEL (Amersfoort, the Netherlands) under the reference Ketjenblack® EC-600JD. The main characteristics according to the supplier was the aggregate size of 10-50 nm, the apparent bulk density of 1-1.2 g/cm^3 and BET (Brunauer–Emmett–Teller) surface area of 1400 m^2/g.

A natural white copolymer of polyamide (Taulman 3D- Nylon 618) (PA6.6/6) and orange PLA (ECO-PLA) printing filaments were also purchased from Creative Tools AB with the diameter of 1.75 mm and used as received.

Three different weave structures of PLA fabric (plain, twill and panama) prepared in Swedish School of Textiles and two PA6.6 fabrics with different number of threads per centimeter in

warp and weft with different yarn count (type (1) 50×30 / 78×180 dtex, type (2) 39×27 / 180 ×180 dtex) purchased from FOV fabrics AB (Borås, Sweden) were applied.

2.2 Manufacturing of CPC filaments for FDM feedstock

The masterbatch technique improves the dispersion and distribution of nanofillers into matrix, therefore, a two-step extrusion was applied. In the first step, fillers (MWNT and KB separately) were incorporated into PLA with a weight percentage of 10% (this is the maximum percentage which is applicable to extrude) and dispersed using a Thermo Haake co-rotating, an intermeshing twin-screw extruder (L/D=25) (Figure 6). To facilitate the dispersion of nanofillers in a polymer, the applied shear stress to the molten polymer was optimized, because of the residence time within the barrel. However, the screw rotational speed was fixed at 100 rpm (the pressure is about 20 bar). The applied extruder subtends five heating zones in which the temperature was independently fixed at 160, 175, 175, 170 and 160° C.

In the second step, the pelletized masterbatch (dried at 60°C for 12 hours) was diluted with PLA pellets to obtain contents of 0.5 to 5 wt.% of MWNT and 1 to 7% of KB in PLA to define the percolation thresholds. To cool down the produced filaments more efficiently, a cooling bath (YVROUD, France) with a closed circulation of water in room temperature was applied. The produced rods were collected with the speed of 1m/min and used directly for electrical measurements. These monofilaments can be introduced to the 3D printer.

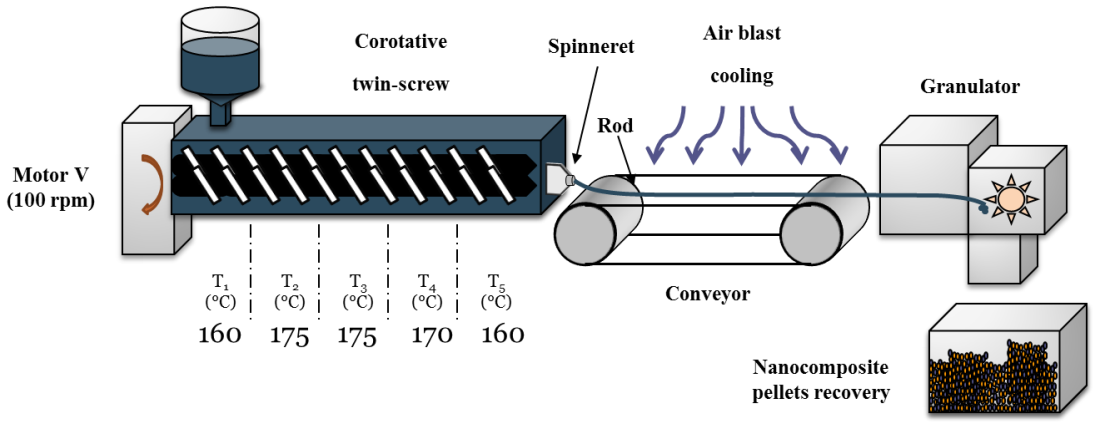

Figure 6 First step of the preparation of the CPC 3D printer filaments: preparation of the pelletized masterbatch

2.3 Melt Flow Index (MFI) Measurements

The Melt Flow Tester from Thermo Haake was used for MFI measurements to analyze the fluidity of the molten nanocomposites. The test was done under the standard test method ISO 1133 with 2.16 Kg at 230°C for nanocomposites and 180°C for raw PLA.

2.4 Scanning electron microscopy (SEM)

After gold sputtering, a scanning electron microscope (JEOL JSM-6301F) was used to characterize the surface morphology of the rods. The used voltage was 6kV.

2.5 Transmission electron microscopy (TEM)

A cryo-microtome (Leica Ultracut UCT microtome) with a Diatome diamond knife was used to obtain sections of samples with a nominal thickness of 90 nm at room temperature. Sections were transferred to Cu grids of 250 meshes. Rods before 3D printing and filaments come out of 3D printer were embedded into epoxy resin and were ultramicrotomed following filament direction and in cross-section. Bright-field TEM images of composites were obtained at 200 kV under low dose conditions with an FEI TECNAI G2 20 electron microscope, using a Gatan CCD Orius camera. Low magnification and high magnification images were taken to ensure representative analysis.

2.6 3D printing

The 3D printer used was a two-head WANHAO Duplicator 4/4x purchased from Creative Tools AB (Halmstad, Sweden) (Figure 7). The maximum printing size was 22.5x14.5x15 cm (length, width, and height respectively) with a nozzle diameter of 0.4mm.

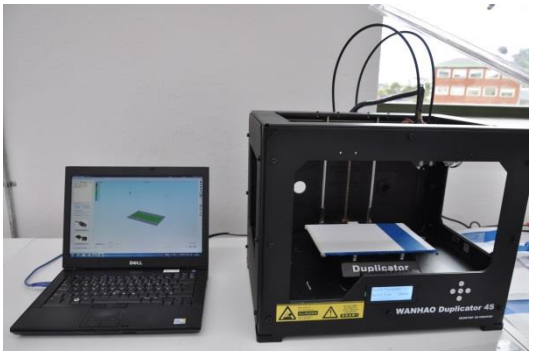

Figure 7 A two-head WANHAO 3D printer

CAD designs were drawn and visualized in Rhinoceros software and transferred to 3D printable format using the Simplify3D software supplied by Creative Tools AB (Halmstad, Sweden). For printing tracks in the different cross-sectional area and 3D printed layers in different geometries, the infill was set to 100% and the angle of printing was set at 0°. The default printing speed was 3000 mm/min and the first layer speed was 50%. Filled PLA tracks (5% KB and 2% MWNT) were 3D printed at 240°C. Different geometries including rectangular for electrical resistance measurement (1× 12.75 × 60 mm^3) and tension tests (1×6.33×38.5 mm^3), as well as circular for compression (1 mm thickness and 40 mm diameter), were 3D printed at 240°C (Figure 8). It is recommended to remove filaments from the nozzle quickly after printing to avoid extruder blockage. Filaments were dried at 50°C for 12 hours before 3D printing.

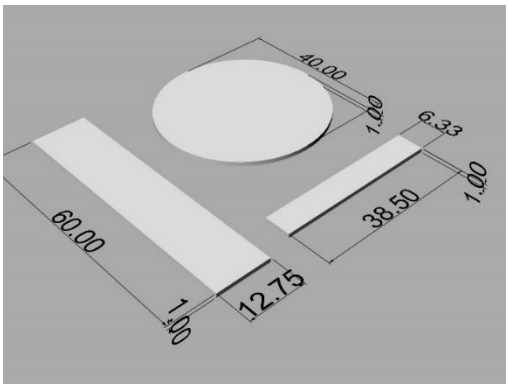

Figure 8 Schematic of 3D printed layers of PLA/MWNT and PLA/KB nanocomposites in various geometries (the dimensions are in millimeter)

2.7 Differential scanning calorimetry (DSC)

The DSC analysis was done on a DSC Q2000 supplied by TA Instruments, New Castle, DE, USA. The 3D printer filament and 3D printed layer specimens were heated under a nitrogen gas flow at a rate of 10°C/min from 25°C to 250°C and from -20°C to 220°C, respectively. The percentage crystallinity (X_{DSC}) of 3D printer filaments and 3D printed layers of PLA nanocomposites was calculated using Equation 2:

$$X_{DSC}\% = \frac{\Delta H_f - \Delta H_{cc}}{\Delta H_f^0} \times \frac{100}{w} \quad (2)$$

Where ΔH_f^0= 93 J.g^{-1} for 100% crystalline PLA [138], ΔH_f (J.g^{-1}) is the enthalpy of melting, ΔH_{cc} (J.g^{-1}) is the cold crystallization enthalpy, and w (wt.%) is the weight fraction of PLA in the composite.

2.8 Dynamic mechanical thermal analysis (DMTA)

Dynamic mechanical thermal analysis (DMA) let us relate molecular structure, processing conditions and product properties of the material to describe the material behavior. In DMA, the sample is subjected to periodic stress in one of several different modes of deformation like shear, bending, tension and compression. Additionally, DMTA is used to determine the mechanical performance of solid material with significant application-related properties, for example, brittleness, stiffness, impact resistance, or damping. The rheological parameters such as loss modulus (E″), storage modulus (E′), and the loss or damping factor (tan δ) are obtained from DMTA.

Tension and bending (dual cantilever) tests were operated with a dynamic mechanical analyzer (Q800, TA Instruments) to investigate the dynamic mechanical properties of the 3D printer filaments and 3D printed layers (as well as 3D printed layers on fabric), respectively. DMA multi-frequency strain with a temperature ramp method was used for the tests. The test temperature ranged from 25˚C up to 120˚C at a heating rate of 3˚C min^{-1} and 1% strain for scattering frequencies of 1 Hz. The sample in the dual cantilever test is shown in Figure 9.

Figure 9 Dual cantilever test for nanocomposite 3D printed layers

2.9 Electrical resistance measurement

Electrical properties were measured using two different methods including two-point measurement or 2-wire ohms measurement (2w) and four-point measurement or 4-wire ohms measurement (4w).

The electrical conductivity (σ) of all samples including 3D printer filaments, extruded filaments from the 3D printer, 3D printed tracks and 3D printed layers were calculated using Equation 3.

$$R = \frac{V}{I} \qquad R = \frac{\rho L}{A} \ \ and \ \ \sigma = \frac{1}{\rho} \qquad \sigma = {}^{L}/_{R.A} \tag{3}$$

Where, R is the electrical resistance of the material (Ω), V is the voltage (V), I is the current (A), ρ is the resistivity (Ω.m), L is the length (m), A is the cross sectional area of the sample (m^2), and σ is the electrical conductivity $(\Omega.m)^{-1}$ or Siemens per meter (S/m).

The percolation threshold values were calculated by plotting the electrical conductivity of the composites versus reduced filler mass fraction and fitting with a power law function according to Equation 1.

2.9.1 The two-wire resistance measurement method

In this method, a Keithley 617 electrometer was connected with alligator clips to rods with the measurement length of 1 cm as shown in Figure 10 (according to different tests which have been done in GEMTEX, there is no significant difference between conductivity of rods in different measurement lengths of 1, 5 and 10 cm, as the rods conductivity is homogeneous). The electrometer was also connected to a computer to record the data using VEE Pro-Keith617 IEEE program. By DC voltage, the current intensity was measured according to the given voltage (tension) which was varied from -0.5 to 15 V with an automatic increment of 0.5 V. The I/V curve was plotted for each CPC sample which 1/R was the slope of the linear part of the curve. 10 measurements per CPC were carried out.

The electrical resistance of 3D printed layers was measured using a two-point measurement method by a digital multimeter connected with alligator clips to rectangular 3D printed layers with thickness, width, and length of 1× 12.75 × 60 mm^3, respectively. 3 measurements per CPC formulations ((PLA/2, 3, 4, 5, 7 wt.% KB) and (PLA/0.5, 1, 1.5, 3, 5 wt.% MWNT) were carried out.

The main measurement issue with the two-wire method, especially for low resistance measurement, is that the voltage drop across the resistor being measured is sensed internal to the electrometer. Therefore, test lead resistance is also measured. Due to the limitations of the

two-wire method, four- wire measurement as follow was used to eliminate the voltage drop in the test leads as described below.

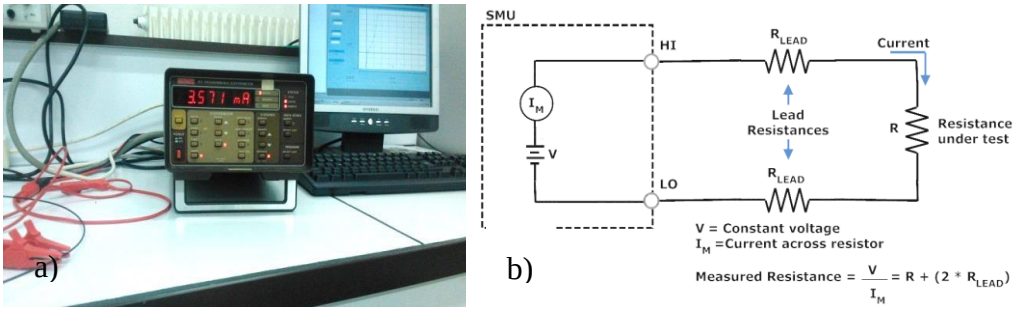

Figure 10 (a) Two-wire resistance measurement method (b) Schematic of connections in source measurement unit instrument (SMU) and the circuit applied for electrical characterization of filaments [17]

2.9.2 The four-wire resistance measurement method

The home-made four-point measurement set up as is shown in Figure 11a was used. Basically, the setup has two parts including an Agilent 34401A multimeter and a sample holder. It has eight identical tubes to support the test object that could be a single thread, rod or track of conductive materials. The tubes were made of brass with a diameter of 30 mm and length of 80 mm. For resistance measurement, four tubes were placed in the plexiglass holder and sample was placed on tubes, then the other four tubes were placed on the samples. The multimeter was set on 4 wire ohms function and the test current flows from the input HI terminal and then through the resistor being measured. The two pairs of outer tubes were connected into input terminals and the two pairs of inner tubes were connected into sense terminals (Figure 11b) [139]. With this configuration, the test current (I) is forced through the test resistance (R) via one set of test leads, while the voltage (V_M) is measured through the second set of leads (sense leads). Therefore, with the separate sense connections with no current flow, the resistance in the sense leads does not give a measurement error and the voltage measured by the meter (V_M) is essentially the same as the voltage (V_R) across the resistance (R). As a result, the resistance value can be determined much more accurately than with the two-wire method. The contact resistance also is automatically reduced using this method [140]. 10 measurements per CPC were carried out. The measurement length was 6 cm, the distance between two pairs of inner tubes.

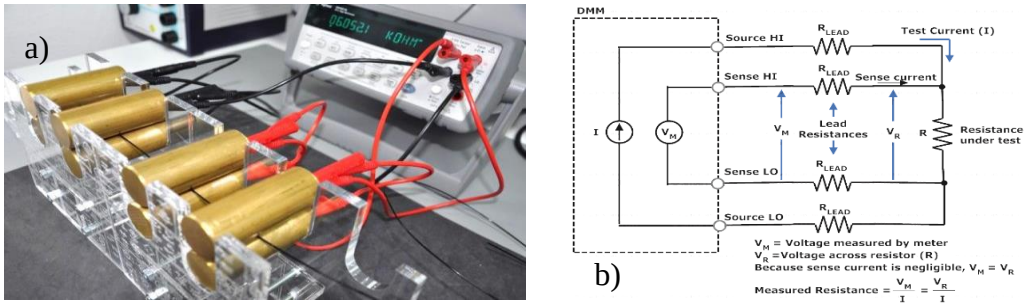

Figure 11 (a) Four wire resistance measurement setup (b) Schematic of connections in digital multimeter (DMM) and the circuit applied for electrical characterization of filaments [17]

2.10 Tension and compression measurement for piezoresistive properties

Compression and tension tests were operated with a dynamic mechanical analyzer (Q800, TA Instruments) in controlled force mode with stress/strain method to investigate the piezoresistive properties of the 3D printed layers (Figure 12).

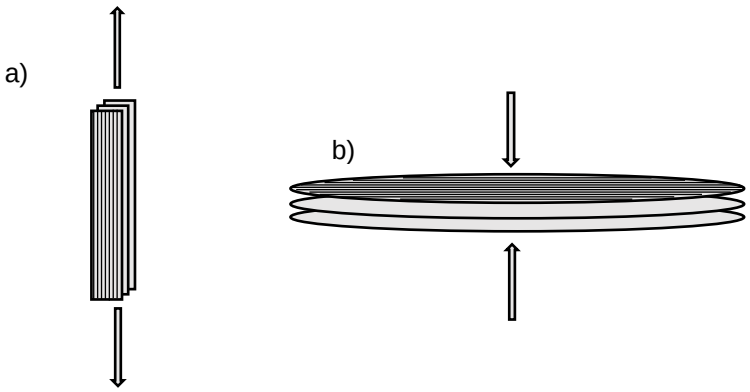

Figure 12 Schematic of 3D printed layers under (a) tension and (b) compression test

In tension mode, the sample was placed in a tension between a fixed and moveable clamp using a film tension cantilever. Tensile loading was applied during the test at a stress rate of 3 N/min up to 18 N.

The piezoresistive properties of the 3D printed samples under compression were measured by

compression clamp (15 mm diameter) consisting in DMA Q800 and a multimeter/system switch (Keithley 3706A) controlled by the instrument web interface. The experimental setup used to investigate the piezoresistive properties is described in Figure 13. 3D printed layers with the thickness of 1 mm and a diameter of 40 mm were clamped between two copper plates of 30 mm diameter as electrodes to investigate the piezoresistive behavior. Copper plates were connected to a multimeter to measure the nanocomposite layers resistance. The samples and electrodes were clamped between a fixed part and the moving part providing the force. An initial preload of 2 N was applied to the sample in order to ensure the full contact between the loading clamps and the sample surfaces. Compressive stress was then applied to the sample in the direction of resistance's measurement. The geometry of the sample changes continuously due to the applied stress. Compressive loading was applied during the test at two different force rates (1 and 18 N/min) up to 18 N. The pressure applied on the specimen was provided by DMA compression clamps and increased on the electrodes, yielding responses under the form of resistance. The relative difference of resistance amplitude or piezoresistive response (A_R) of sensors was calculated according to Equation 4 [141]:

$$A_r = \frac{\Delta R}{R_0} = \frac{R - R_0}{R_0} \qquad (4)$$

where R represents the resistance of the composite under an applied pressure and R_0 is the static resistance.

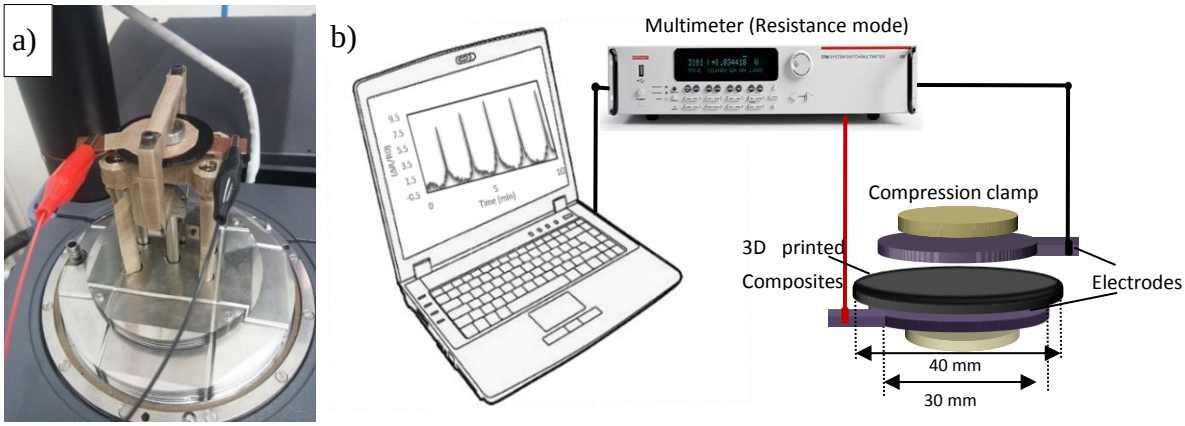

Figure 13(a) Sample setup used to study the piezoresistive properties in compression of 3D printed nanocomposite layers; (b) Schematic diagram of clamps and electrodes in which the sample is positioned.

2.11 3D printing on textiles

Fabrics were placed on 3D printer platform longitudinally in the warp direction. CAD designs were drawn and visualized in Rhinoceros software and transferred to 3D printable format using the Simplify3D software. Then, the polymers and CPCs were 3D printed on textiles (Figure 14) according to different series of experimental design which will be explained below.

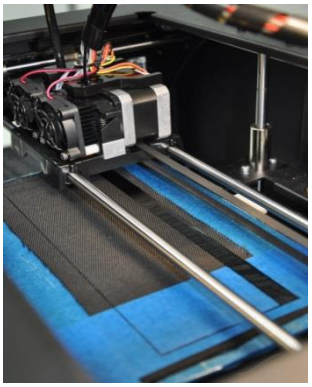

Figure 14 FDM printing of PLA/ 2 wt.% MWNT filament on PLA fabric [3]

2.11.1 Statistical design of experiments for adhesion properties

To investigate the adhesion force of deposited polymers on fabrics by 3D printing, different series of experimental design was done. There are three aspects of the process that were analyzed by a designed experiment [142]: (a) treatment factors or inputs to the process. In this case, the controllable factors were 3D printing process parameters like extruder temperature, platform temperature, and printing speed. Fabric type and filler type could also be considered as factors of the process. (b) levels or settings of each factor. Examples included the temperature and speed settings of the 3D printer and a particular type of filler and fabric chosen for evaluation. (c) response or output of the experiment. Adhesion force which was measurable by the tensile device and potentially influenced by the factors and their levels was the output of the experiment. The factors and levels considered for 3D printing onto fabrics are shown in Table 1. Treatment factors were labeled F1, F2, F3, F4, F5, F6 and levels were labeled 1,2,... . Since each experiment (PA6.6/6 on PA, PLA on PA, PLA on PLA and nanocomposites (PLA/KB and PLA/MWNT) on PLA) involved more than one treatment factor, every adhesion force measurement was on some combination of levels of the various treatment factors (Table 2 and 3). For example, if there were three treatment factors (extruder temperature, platform temperature, and printing speed), whenever a measurement was taken at a certain extruder temperature, it must necessarily be taken at some platform temperature and printing speed and

vice versa. Suppose there were three levels of extruder temperature coded 1,2,3 and two levels of platform temperature coded 1,2. Then there were six combinations of levels coded 11, 12,..., 32, where the first digit of each pair refers to the level of extruder temperature and the second digit to the level of platform temperature.

Table 1 Factors and levels and the coding applied in different series of experiments [3]

Factor (code)	Level (code)
Extruder temperature (ºC) (**F1**)	190, 210, 230, 235, 240, 250, 260 (**1,2,3,4,5,6,7**)
Platform temperature (ºC) (**F2**)	23, 50,70 (**1,2,3**)
Printing speed (mm/ min) (**F3**)	18, 50, 83 (**1,2,3**)
PA6.6 fabric type (**F4**)*	warp 50 × weft 30 with 78×180 dtex yarn count (**1**), warp 39 × weft 27 with 180 ×180 dtex yarn count (**2**)
PLA fabric type (**F5**)	Panama, Twill (**1,2**)
Filler type (**F6**) **	2% MWNT, 5% KB (**1,2**)

* PA fabric type 2 has higher yarn count in warp per centimeter

** The selected 3D printer filament has almost the same conductivity of 0.04 S/cm

The combinations of the levels were called treatments combinations and an experiment involving two or more treatment factors was called a factorial experiment. The term treatment will be used to mean a level of a treatment factor in a single factor experiment or to mean a treatment combination in a factorial experiment [142]. Adhesion force which was the output of the experiment is shown in Table 2 and 3 for each treatment. Each treatment was done with three replications.

Table 2 Statistical design of different series of adhesion tests [3]

Experiment	Type	Material	Considered Factor (Considered level)	Number of the treatment combination	Treatment combination	Sample coding	Average of F adhesion (N/100 mm width)
1	Factorial experiment	PA6.6/6 on PA6.6	F1(4,6,7) F2(1,2) F3(1,2,3)	18	411	S1	41.3
					412	S2	60
					413	S3	50.7
					611	S4	68
					612	S5	93.3
					613	S6	90.7
					711	S7	66.7
					712	S8	112
					713	S9	108
					421	S10	44
					422	S11	50.7
					423	S12	37.3
					621	S13	49.3
					622	S14	78.7
					623	S15	58.7
					721	S16	100
					722	S17	118.7
					723	S18	104
2*	Single factor	PLA on PA6.6	F1(1,2,3)	3	1	S19	5.3
					2	S20	8
					3	S21	12
3**	Factorial experiment	PLA on PA6.6	F2(1,2,3) F4(1,2)	6	11	S21***	12
					21	S22	28
					31	S23	41.3
					12	S24	30.7
					22	S25	57.3
					32	S26	69.3

*in constant printing speed of 83 mm/min and platform temperature of 23 °C

**in constant printing speed of 83 mm/min and extruder temperature of 230 °C

***Sample 21 was used for both experiments 2 and 3

Table 3 Continuation of statistical design of different series of adhesion tests [3]

Experiment	Type	Material	Considered Factor (Considered level)	Number of the treatment combination	Treatment combination	Sample coding	Average of fabric tear strength (N/100 mm width)	Average of deposited layer break strength (N/100 mm width)
4	Factorial experiment	PLA on PLA	F1(1,2,3) F2(1,2) F3(1,2,3)	18	111	S27	21	-
					112	S28	15.3	-
					113	S29	-	5.7
					211	S30	11.7	-
					212	S31	14.5	-
					213	S32	13.7	-
					311	S33	-	15
					312	S34	-	10.7
					313	S35	12.3	-
					121	S36	15	-
					122	S37	14	-
					123	S38	-	5
					221	S39	14	-
					222	S40	12.3	-
					223	S41	12.3	-
					321	S42	-	9.7
					322	S43	-	16
					323	S44	12.7	-
5	Factorial experiment	PLA nanocomposites (PLA/KB, PLA/MWNT) on PLA	F1(5,7) F2(1,2) F5(1,2) F6(1,2)	16	5111	S45	-	222
					5121	S46	318	-
					7111	S47	-	110
					7121	S48	358	-
					5211	S49	-	220
					5221	S50	492	-
					7211	S51	-	146
					7221	S52	-	38
					5112	S53	-	30
					5122	S54	-	104
					7112	S55	-	98
					7122	S56	-	46
					5212	S57	-	116
					5222	S58	-	36
					7212	S59	-	22
					7222	S60	-	41.5

2.11.2 Adhesion test

Adhesion tests were done according to standard test method SS-EN ISO 11339:2010 (T-peel test for flexible-to-flexible bonded assemblies) using a Zwick/Z010 tensile tester. Rectangular shape deposited layers on fabric with 200 mm length, 25mm width and 0.1 mm thickness were tested with the separation rate of 100 mm/min. The steps which applied for preparation and test the samples are shown in Figure 15. Firstly a double-sided tape was used for installing fabric on a construction platform. Then, a tape was placed on one side of the sample to avoid deposition of polymer on fabric while printing. The positioned tape in one side was separated from the fabric after 3D printing to position the samples in the test frame of tensile tester for peeling test.

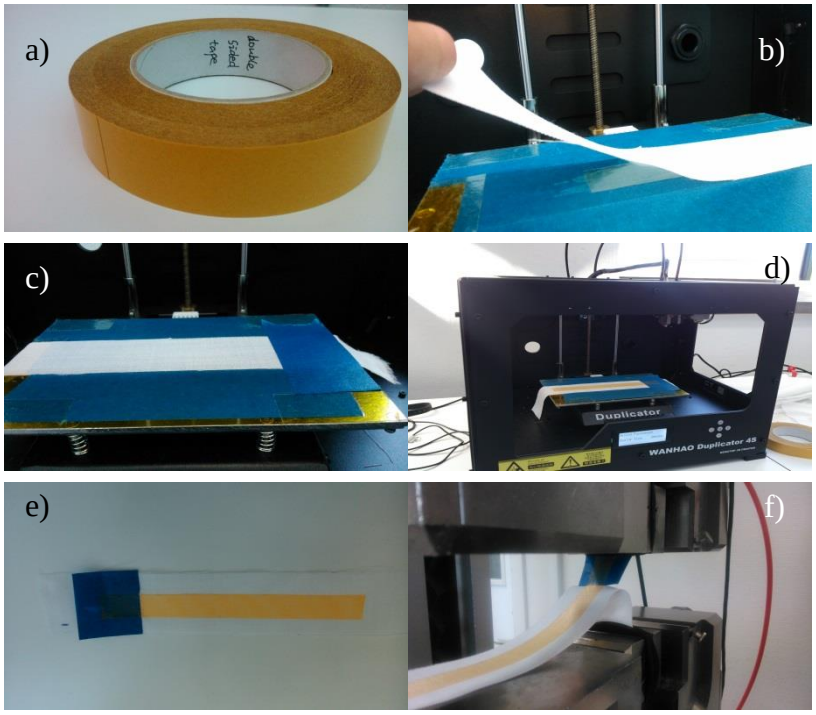

Figure 15 Steps of preparing a sample for measuring adhesion force for polymer deposited fabrics [3]

3 Characterization of CPCs

This section explores to characterize morphological, electrical, thermal and mechanical properties of CPCs in the form of 3D printer filaments, extruded monofilaments from the 3D printer, 3D printed layers and 3D printed layers on fabrics. Conductive PLA/MWNT and PLA/KB filaments were developed to allow us to 3D print electrically conductive components. The conductive filaments do not only find their application in 3D printed circuitry and sensors, but they can also be applied in EMI and RF shielding applications for industries like aerospace and automotive, medical devices and hospital equipment to block the electromagnetic field and radio frequency electromagnetic radiation within a space.

3.1 Morphological and electrical properties

3.1.1 3D printer filaments

Figure 16a shows one of the produced rods (PLA/ 2 wt.% MWNT) as a 3D printer filament and figure 16b reveals that the filament surface is rough and irregular. This may be attributed to the MWNTs aggregation in the PLA matrix, which leads to the formation of clusters on the surface of the filament. This indicates that the MWNTs are not uniformly dispersed in the PLA matrix. It is believed that the MWNT aggregates in a PLA matrix are caused by the Van der Waals interaction among MWNTs as well as the poor compatibility of MWNT with the PLA matrix [143]. The resulting rods displayed sufficiently circular cross-sectional profiles (Figure 16c) and MWNTs appear as white particles in the cross section (Figure 16d).

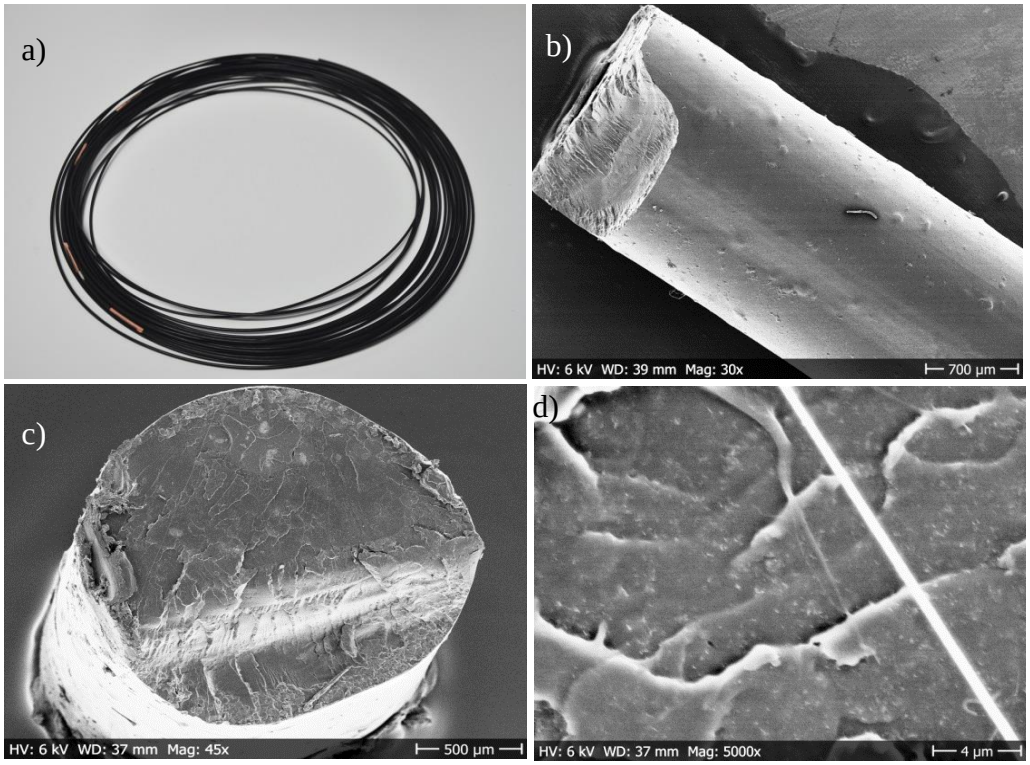

Figure 16(a) PLA/ 2 wt.% MWNT 3D printer filament (b,c,d) SEM images in three magnifications [17]

Figure 17 shows the diameter of the extruded rods as a function of the filler content for MWNT and KB. The production was done using circular extruder die with 2.0 mm diameter. It was evident that there was no dependence of rod diameter on the MWNT loading, instead, the diameter was dependent on the KB loading and increased with increasing the filler amount. The result of the independence of rods diameter on the MWNT loading corroborates similar observations for melt-spun filaments in Ref. [144]. Finding explanation, MFI test was done to investigate the difference between the fluidity of the different nanocomposites including MWNT and KB. The MFI test is a single point measurement test that indicates the fluidity of the materials at one temperature.

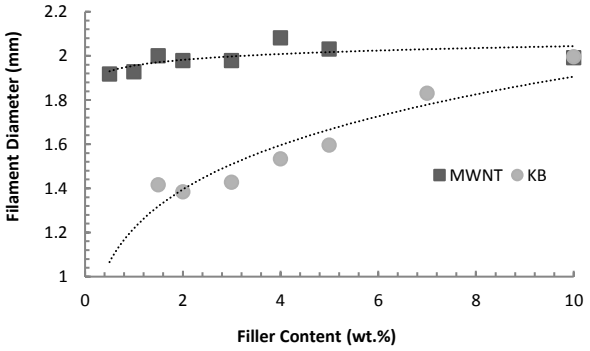

Figure 17 Diameter dependence of nanocomposite 3D printer filaments on the filler content [17]

Figure 18 shows the MFI results of different nanocomposites depending on filler content. As it is obvious the MFI difference of KB composites is larger than MWNT composites with the same filler content. For example, the MFI for PLA composites containing 1.5 and 3 wt.% filler content is 66.8 and 36 for KB as well as 20.4 and 4.9 for MWNT, respectively. Therefore, the MFI difference of KB composites is almost twice in comparison to MWNT composites with the same filler content of 1.5 and 3 wt.%. Extruding KB composites with more different viscosities may cause the increasing of the rod diameter with increasing the filler content. KB composites with lower viscosities may be more stretched while collecting. But, the good secondary agglomerate network of MWNT may cause no dependence of filament diameter on filler content.

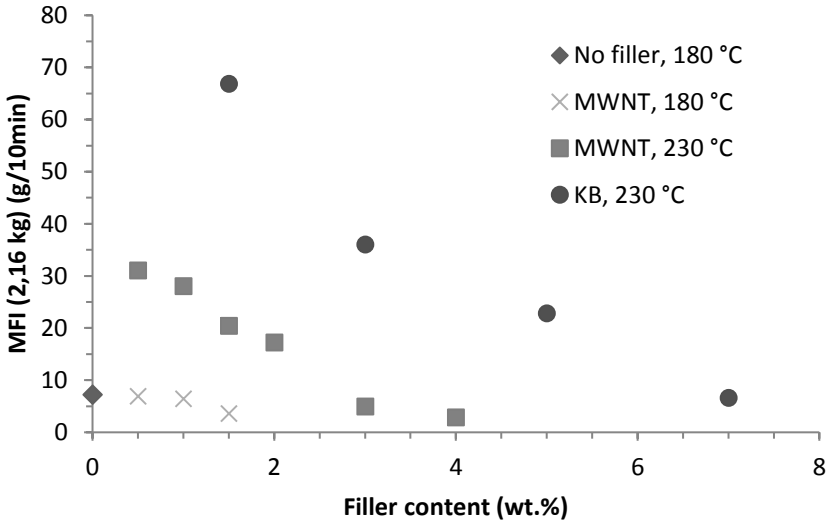

Figure 18 Melt Flow Index depending on the filler content in PLA [17]

As shown in Figure 19, the MWNT and KB composites conductivity measured with 4W agrees better than the 2W method with the percolation behavior given in Equation 1. The percolation threshold value was calculated by plotting the electrical conductivity of the composite versus reduced filler mass fraction and fitting with a power law function. The straight line in Figure 19a with m_c=0.54 % (m_c is percolation threshold mass fraction) gives an excellent fit to the data with a correlation factor of 0.988, indicating a low percolation threshold at 0.54 wt.% MWNT loading in 4W method (in comparison with the straight line in Figure 19b with m_c=1.09 % with a correlation factor of 0.977 in 2W method). Regarding KB composites (Figure 19c, 19d), the straight line with m_c=1.7 % with a correlation factor of 0.985 in the 4W method, indicates a lower percolation threshold in comparison with the line with m_c=2.6 % with a correlation factor of 0.979. Presenting the lower percolation thresholds and more precise results can be attributed to eliminating the effect of contact resistance by 4W measuring system [140]. As compared with that of two-point measurement, four-point measurement is not only favorable for the irrelevance of the contact resistance but also has no assumptions about the contact shape and size [145]. Also, KBs as spherical particles (zero-dimensional) have the higher percolation threshold in comparison with MWNTs (one-dimensional), as the percolation threshold is proportional to the ratio of the average particle diameter over its mean length [69].

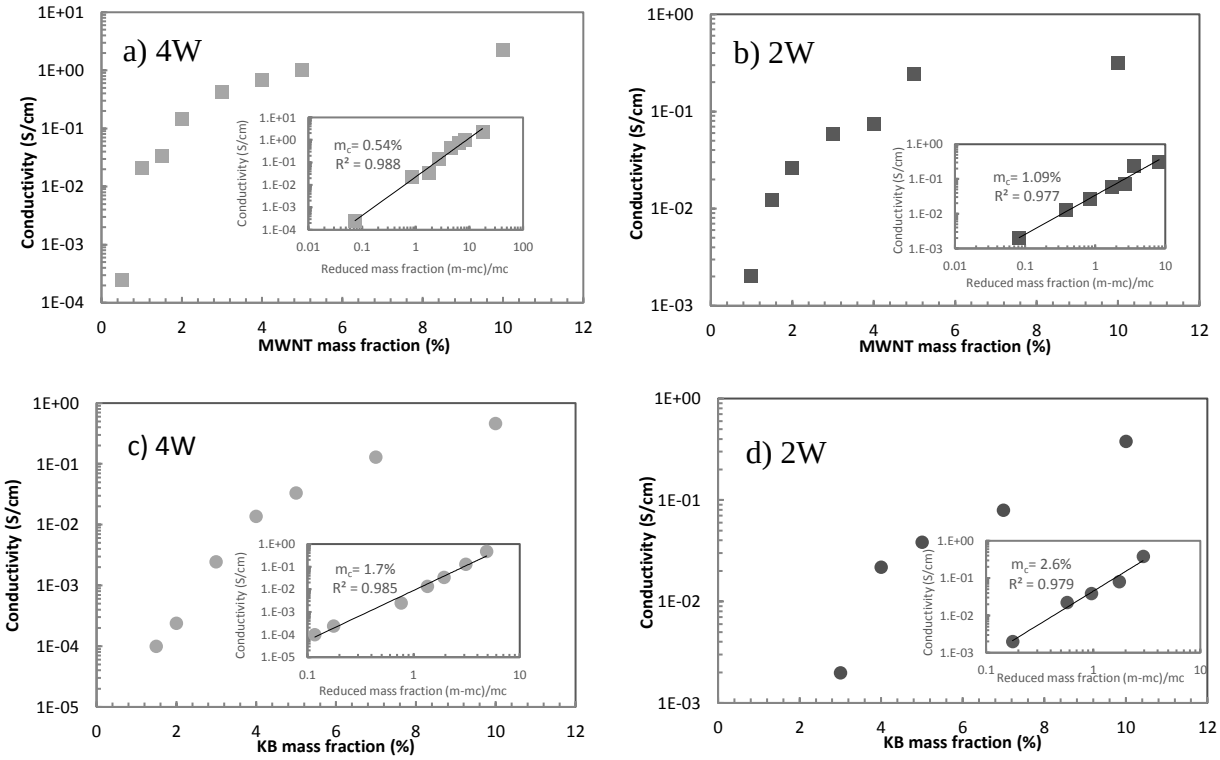

Figure 19 Electrical conductivity as a function of the filler mass fraction and calculation of the percolation threshold by application of power law (eqn [2]) to experimental data for composites containing MWNT and KB by two different resistance measurement method (a) MWNT 4W (b) MWNT 2W (c) KB 4W (d) KB 2W [17]

Figure 19 shows that in both methods of 2W and 4W, after the percolation threshold, the conductivity increases exponentially with the amount of filler. For MWNT composites finally the saturation of the electrical conductivity is observed, but in KB composites in the range of investigated concentration (1.5 to 10 wt.%), saturation is not observed. The conductivity of MWNT nanocomposites is higher than the conductivity of KB nanocomposites with the same filler content. The needle-like structure of MWNT and consequently, more effective contact of fillers in comparison with the more spherical structures like conventional carbon black, cause higher conductivity values. In fact, CNTs make a 3D electrically conductive network in the polymer matrix; accordingly, electrons can pass over from one particle to another and as a result overcome the high electrical resistivity of the polymeric matrix [70].

Figure 20 shows the TEM images of KB powder. The pore structure of KB is the key reason that allows it to perform superior to that of other types of carbon blacks. KB is a highly structured carbon black that refers to systems made by fusion of the primary particles into an extended three-dimensional structure. The final dimensions and density of the chain or cluster-like structure depend on the preparation method of the CB [73]. Oxfall *et al.* [71] showed that the substantially higher percolation threshold of a low structured carbon black (12.1 vol.%) compared to the highly structured carbon black (2.1 vol.%) in a poly(ethylene-butyl acrylate) copolymer (EBA) is likely associated with the much lower BET surface area of the former particles. The percolation threshold of 1.7 wt.% for KB in comparison with other types of CBs (even with low percolation threshold of 2.74 vol.% with a DBP value of 380 cm^3 /100 g [146]) showed the effectiveness as the promising filler to enhance the conductivity of PLA filaments.

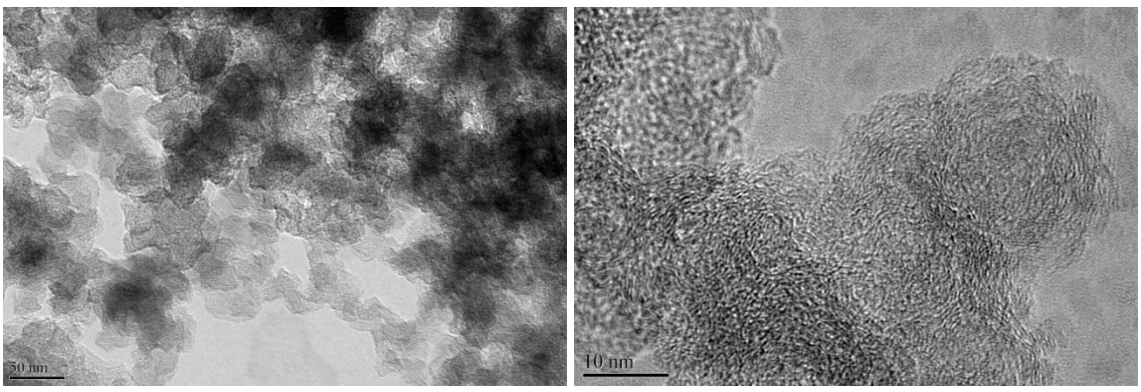

Figure 20 Transmission electron microscopic images of KB (Ketjenblack® EC-600JD) [17]

It is interesting to note that the corresponding curves in Figure 19 of the KB composites (19c, 19d), except for the onsets, almost match in 4W and 2W systems. Differently, the MWNT composites curves (Figure 19a, 19b) do not match. The conductivity corresponding to the

plateau value approached at higher MWNT contents was about one order of magnitude higher for the 4W method than for those measuring by 2W. The difference can be attributed to the anisotropic electrical conductivity of MWNT composite filaments and the 1D structure of the filler. Gong *et al.* [147] showed that the anisotropic electrical property of aligned CNT/polymer composites is mostly affected by the anisotropic average conductive pathway density, which differs with the CNT alignment state in the polymer matrix. Using a four-point measurement method may also cause a higher average density of anisotropic conductive pathways to be taken into account. Therefore, using a four-point measurement method for MWNT composites could present higher electrical conductivities as is shown above.

Figure 21 shows the TEM images of the composites in one lower and one higher concentration of their percolation thresholds. It is obvious that MWNTs and carbon blacks in produced 3D printer filaments are not homogeneously distributed in the matrix and form so-called secondary agglomerates. In reality, there are weak attractive interactions between most nano-objects which cause agglomeration [148]. Therefore, several mechanisms have been used to explain the nature of the contacts between conductive agglomerations in a conductor-insulator composite. In percolation theory, it is assumed that the formation of an infinite percolation network occurs via physical contact between the conductive aggregates. However, charge carriers are allowed to tunnel from one cluster to another without any physical contact in real composite systems (tunneling effect). Therefore, tunneling conduction which has been reported in KB and MWNT nanocomposites can explain the nature of the contacts as a dominant mechanism [148]–[150].

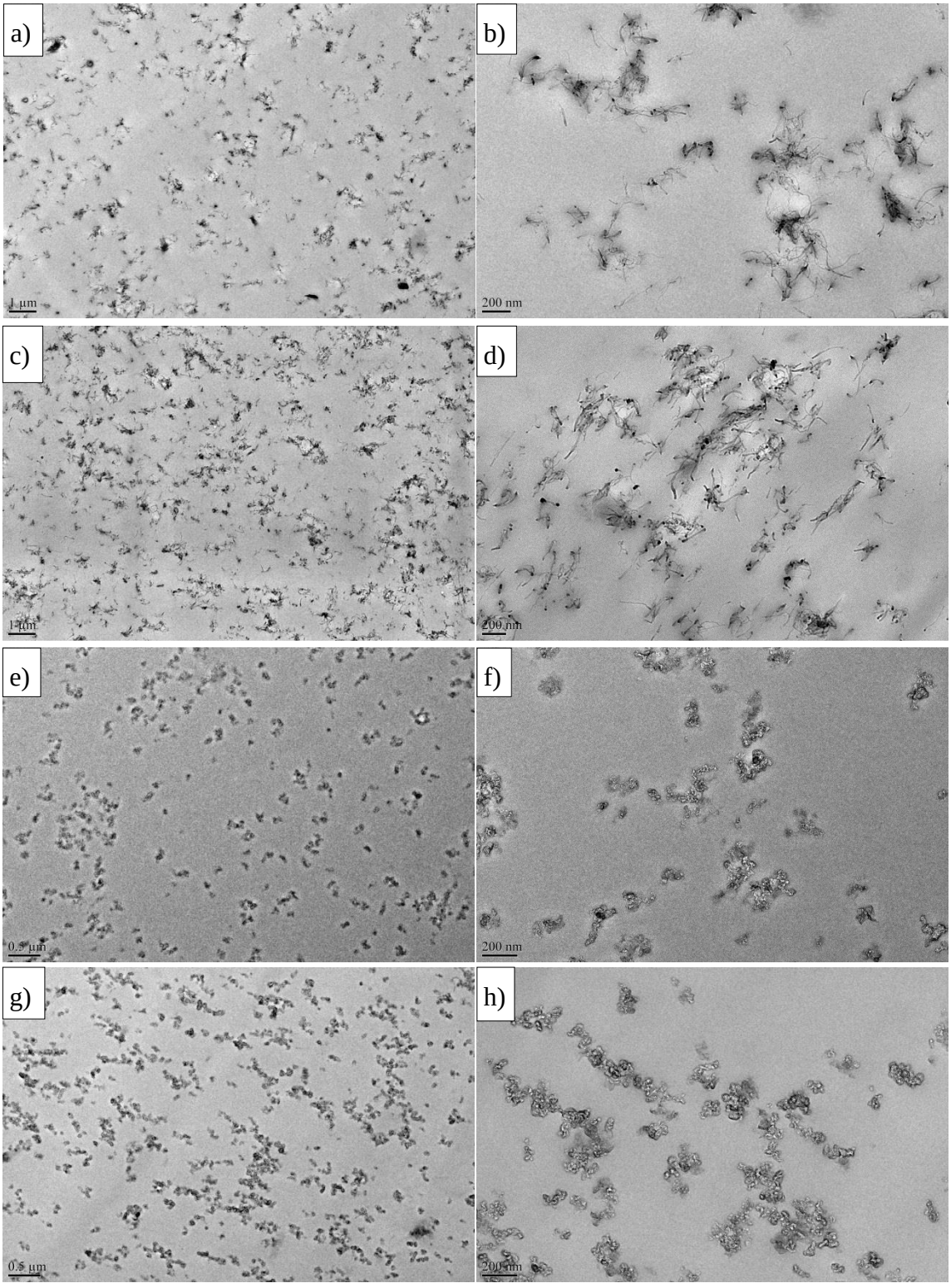

Figure 21 TEM images of cross section of the PLA nanocomposite filaments (before impression) in two magnifications containing (a,b) 0.5% MWNT (c,d) 1% MWNT (e,f) 1.5% KB (g,h) 3% KB [17]

3.1.2 Extruded filaments from the 3D printer

To investigate the composite morphological and electrical properties after 3D printing, the extruded filaments from the nozzle were collected. The extruder speed of 240 mm/min at 230ºC was used for preparing all the samples to have consistent flow of molten nanocomposites coming out of the nozzle.

Figure 22 shows the diameter and the conductivity of the extruded filaments from the 3D printer as a function of filler content in comparison with loaded extruded filaments. It is obvious that the diameter trend is in agreement with previous results. There is no dependence of filament diameter on the MWNT loading and dependency on the KB loading (Figure 22a). It is worth to mention that the four-point measurement system was applied for measuring the conductivity of extruded filaments from 3D printer which decreases up to several orders of magnitude in comparison with loaded filaments in both conductivity curves of MWNT and KB composites (Figure 22b). Electrical conductivity decreases because of the change of the filler network pathways during 3D printing process due to the diameter difference of the loaded filaments and the extruded filaments from the 3D printer in all filler contents (die diameter of the extruder (2 mm) and the 3D printer nozzle diameter (0.4 mm)).

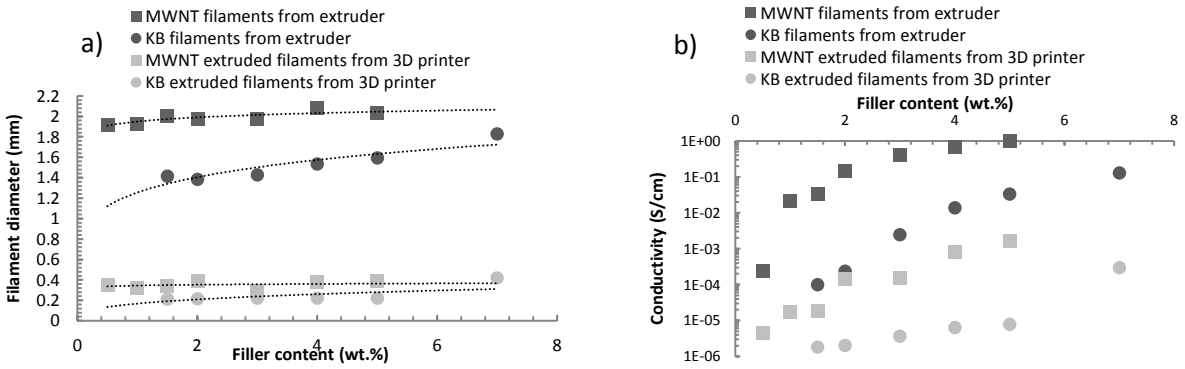

Figure 22 (a) Filament diameter and (b) Electrical conductivity as a function of the filler content for filaments containing MWNT and KB before and after 3D printing [17]

The effect of 3D printer extruder temperature on the conductivity of produced monofilaments was investigated. Minitab software was used to do a regression analysis. As it is shown in Figure 23, interestingly, in low filler contents close to percolation thresholds (0.5 and 1 % for MWNT, 1.5 and 2 % for KB), the conductivity versus extruder temperature has linear regression model and the conductivity of filaments decreases with increasing extruder temperature. In mentioned

contents, P-value (a small p-value (typically ≤ 0.05) indicates strong evidence against the null hypothesis, so the null hypothesis will be rejected [142]) is less than 0.05 that means there is a significant linear effect of the factor extruder temperature on conductivity. Nevertheless, in higher filler contents there is no effect of extruder temperature on the conductivity of the extruded filaments by the 3D printer.

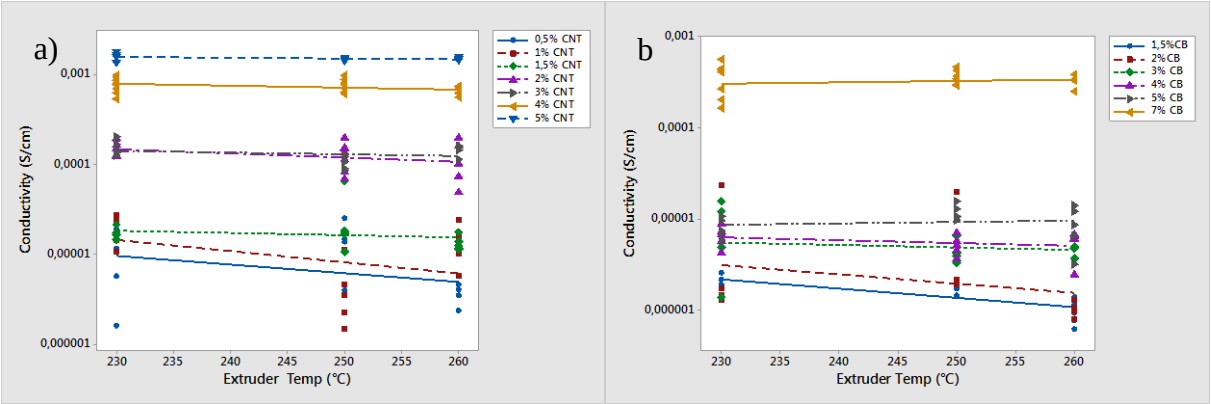

Figure 23 Scatterplot of electrical conductivity as the function of printing extruder temperature with regression for extruded monofilaments by 3D printer containing (a) MWNT (b) KB [17]

As discussed above and can be seen in TEM images (Figure 21), there are secondary agglomerates of fillers in produced 3D printer composite filaments and they are not well and homogeneously distributed. However, for the well-dispersed fillers including nanotubes and carbon blacks, the measured electrical conductivity of the composites is in the order of the conductivity of the neat polymer [148]. By formation of secondary agglomerations of fillers and a conductive network of interconnected agglomerates, the conductivity of the composite can be increased by several orders of magnitude.

3D printing of a nanocomposite filament into a fine filament can be considered as a process like melt spinning (but not with the same draw ratio) which involves two types of fluid flow: one is shear flow before the extrusion i.e. flow through the nozzle and the other is elongation flow. However, differently, instead of gathering the filaments on a collector, produced filaments are deposited on a substrate or movable platform layer by layer following a pre-designed computer layout.

Moreover, shear flow through the nozzle can both generate and destroy secondary agglomerates. Although agglomerate formation is accelerated by shear flow, however, the loose

building blocks of secondary agglomerations or clusters can be easily destroyed by shear flow. Therefore, the competition between construction and destruction of secondary agglomerates can be considered as a principal mechanism to find out the dependence of the final electrical conductivity of extruded filaments on the processing factors like extruder temperature of a 3D printer. As shown in Figure 23, there is no dependence of electrical conductivity of extruded filaments from the 3D printer on extruder temperature in higher filler contents than percolation thresholds for both fillers. Normally, there are more and bigger agglomerates in higher loadings of the fillers [148]. Therefore, it is assumed that at higher loadings even in higher extruder temperatures (lower viscosity) agglomerate networks are able to recover their conductivity through the flow condition. In percolation thresholds, the destruction of the secondary agglomerations happen through the shear flow by increasing the extruder temperature (decreasing the viscosity) and there is less time to recover the conductivity of the filament by remaining agglomerates networks. Therefore, there is a significant effect of extruder temperature on the electrical conductivity of filaments in the percolation threshold. Figure 24 shows the TEM images of extruded filament from 3D printer at 230 ºC containing 1% MWNT in cross section and longitudinal (flow parallel) section. As it is obvious, there are less secondary agglomerates in comparison with TEM images of the filament before 3D printing at the same filler content in Figure 21.

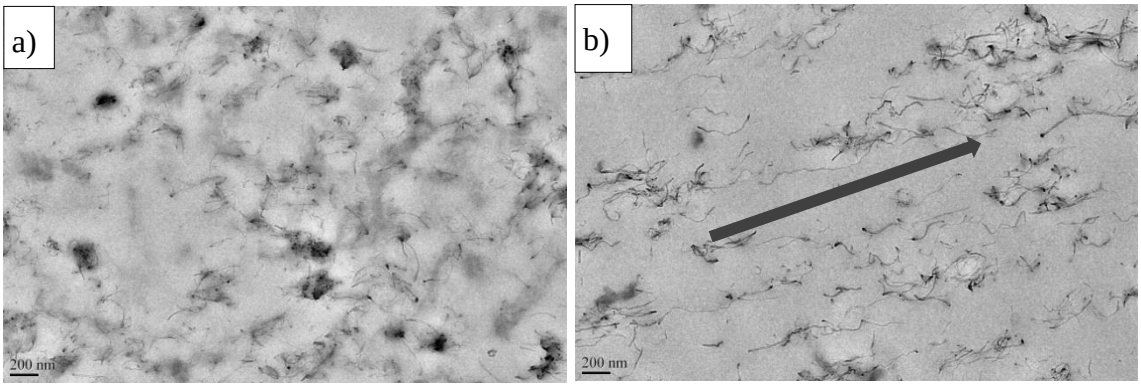

Figure 24 TEM image of (a) cross section (b) longitudinal (flow parallel) section of the PLA nanocomposite extruded filament from the 3D printer containing 1% MWNT (arrow shows the MWNT orientation) [17]

3.1.3 3D printed tracks

To investigate the conductivity of 3D printed nanocomposites for possible interconnection applications, two 3D printer filaments containing 5% KB and 2% MWNT with almost the same conductivity were chosen to print tracks (Figure 25).

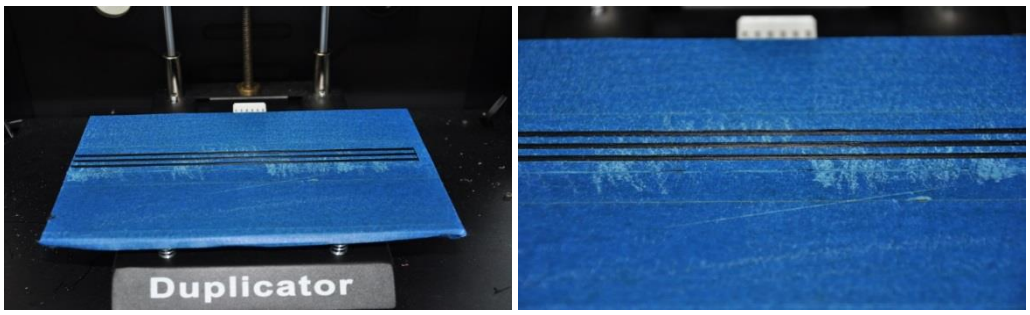

Figure 25 3D printed conductive tracks [17]

The electrical properties of tracks were investigated by four-point measurement method. Each layer of conductive tracks consists of some fine filaments (Figure 26a). Figure 26b shows the exponential decay of the resistance with a cross-sectional area of 3D printed tracks. As expected, the resistance decreases exponentially with the increase of the cross-sectional area of tracks in agreement with Equation 3.

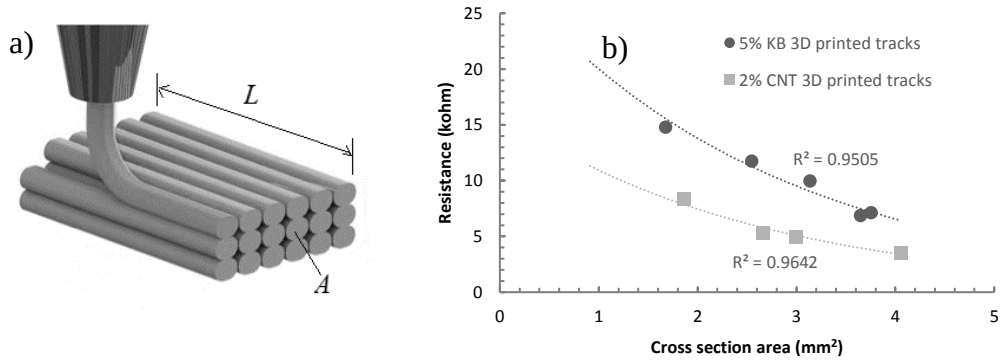

Figure 26 (a) Schematic of 3D printed tracks (b) Resistance (kΩ) as a function of the cross-section area (mm^2) of 3D printed tracks containing 2% MWNT and 5% KB [17]

3.1.4 3D printed layers

In 3D printed layers, the sudden transition from insulator to conductor which is the indication of percolation threshold happened in PLA/4 wt.% KB and PLA/1 wt.% MWNT. 3D printed layers containing 2 and 3 wt.% KB as well as 0.5 wt.% MWNT does not show any conductivity by two point measurement method (Figure 27).

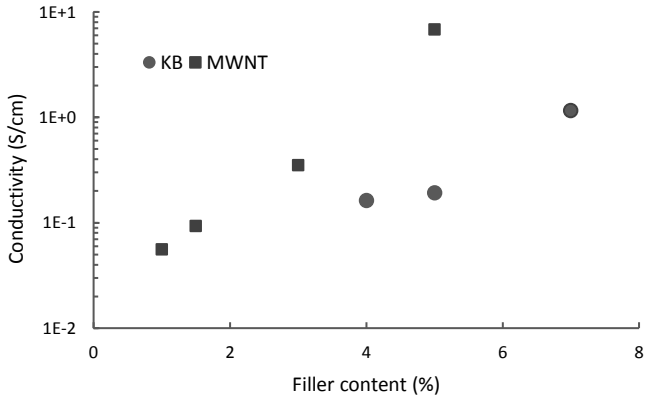

Figure 27 Electrical conductivity as a function of the filler content for 3D printed layers of PLA nanocomposites containing MWNT and KB

3.2 Thermal properties

3.2.1 3D printer filament

The DSC heating thermograms of 3D printer filaments are shown in Figure 28a and b. The glass transition temperature (T_g), cold crystallization temperature (T_{cc}), melting temperature (T_m), cold crystallization enthalpy (ΔH_{cc}), and melting enthalpy (ΔH_m) obtained from the DSC studies are summarized in Table 4. The data indicate that the T_g and T_m of the PLA nanocomposites is not affected with the addition of both nanofillers MWNTs and KBs to the PLA matrix (decreased less than 2 ˚C), however, the ΔH_{cc} and T_{cc} of the PLA composites decreased significantly in the presence of nanofillers which is more notable in the case of MWNTs. These results suggest that MWNT and KB significantly affect the crystallization properties of the PLA matrix. The increase in crystallinity is more significant in MWNTs composite filaments. Two main factors control the crystallization of polymeric composite systems [151]. The first is the nucleating effect of filler which results in the decrease in the crystallization temperature and has a positive effect on the crystallization degree. The second

is when the filler disturbs the formation of nuclei and delayed overall crystallization, resulting in the crystallization temperature elevation and has a negative effect on crystallization. In manufactured 3D printer PLA filaments, the addition of KB and MWNT significantly lowered the crystallization temperature values (up to about 20 for KB and to 35 ˚C for MWNT) which signify that both fillers have the positive effect on crystallization and acted as a nucleating agent and accelerated overall crystallization. In the case of KB, with increasing the filler content to 5 and 7, the crystallinity slightly decreased in comparison with lower filler contents. These results are in corroboration with the reference [151].

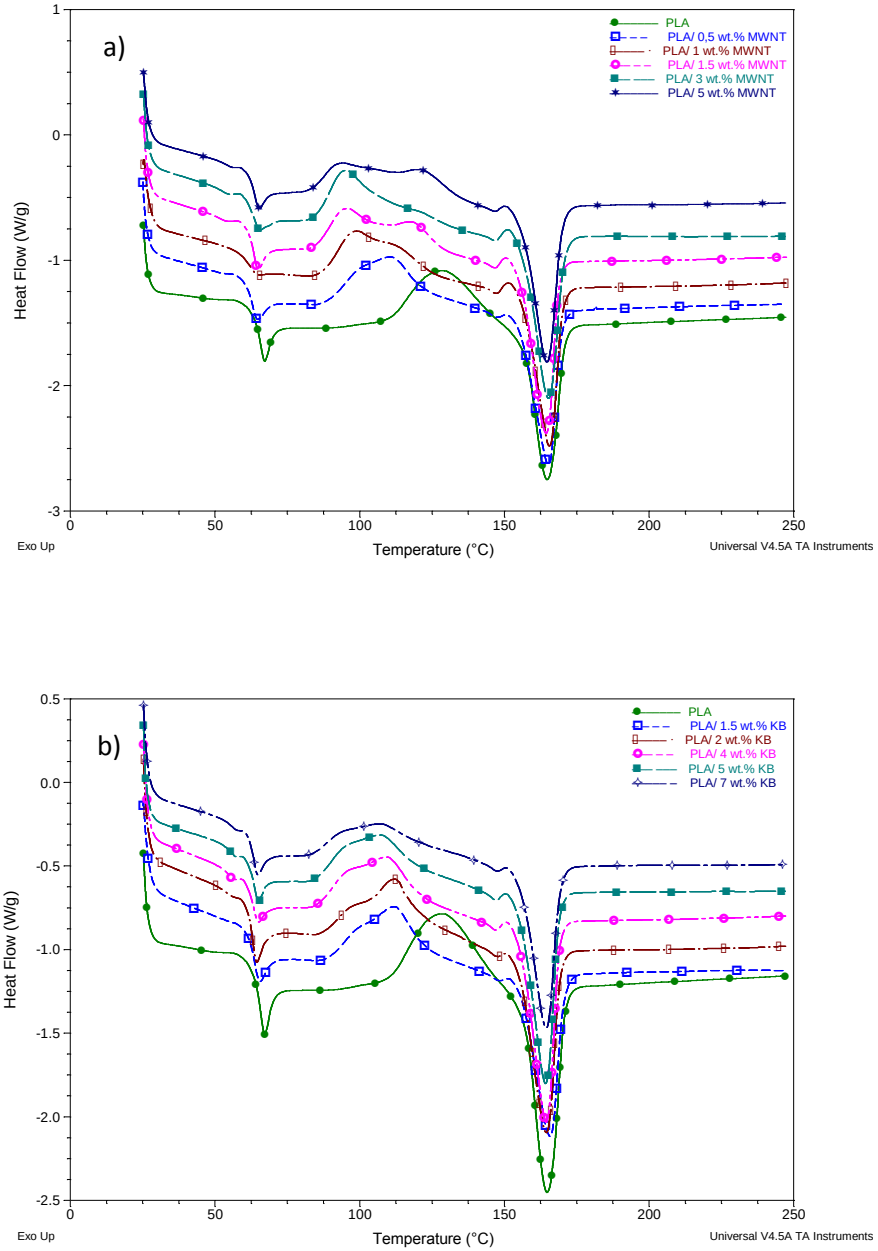

Figure 28 DSC heating thermograms for manufactured 3D printer filaments (a) PLA/MWNT (b) PLA/KB.

Table 4 Calorimetric data for PLA 3D printer filaments for the first heating run (10 °C/min)

Sample	T_g[a] (°C)	T_{cc}[b] (°C)	T_m (°C)	ΔH_{cc}[c] (J/g)	ΔH_m[d] (J/g)	X_{DSC} (%)
PLA	64.7	128	164.6	32.4	35.9	3.8
PLA/ o.5 wt.% MWNT	63.1	110.7	165.1	27.1	38.8	12.6
PLA/ 1 wt.% MWNT	62.1	98.7	165.4	25.1	40.2	16.3
PLA/ 1.5 wt.% MWNT	63.8	95.1	164.5	25.4	43.8	20.1
PLA/ 3 wt.% MWNT	63.7	94.1	165	23.4	45.6	24.4
PLA/ 5 wt. % MWNT	63.5	94	164.4	22	44.4	25.3
PLA/ 1.5 wt. % KB	63.9	111.8	165.5	20.5	34.5	15.2
PLA/ 2 wt. % KB	63	111.9	164.2	20	38.5	20.3
PLA/ 4 wt. % KB	63.4	109.3	164.2	22.1	37.9	17.6
PLA/ 5 wt. % KB	63.9	107.2	164	21.9	35.1	14.9
PLA/ 7 wt. % KB	63.3	107.1	164.4	16.5	29.7	15.3

[a] Glass transition temperature
[b] T_{cc} is the peak temperature of cold crystallization.
[c] ΔH_{cc} is cold crystallization enthalpy.
[d] ΔH_m is enthalpy of melting.

3.2.2 3D printed layers

The DSC heating thermograms of 3D printed layers are shown in Figure 29a and b. The glass transition temperature (T_g), cold crystallization temperature (T_{cc}), melting temperature (T_m), cold crystallization enthalpy (ΔH_{cc}), and melting enthalpy (ΔH_m) obtained from the DSC thermograms are summarized in Table 5. The comparison of crystallization behavior of 3D printer filaments and 3D printed layers are shown in Figure 30. The data in Table 5 and Figure 28 indicate the T_g and T_m of the 3D printed nanocomposite layers in comparison with the 3D printer filaments has not been changed significantly (T_g decreased about 3˚C and T_m increased about 3˚C).

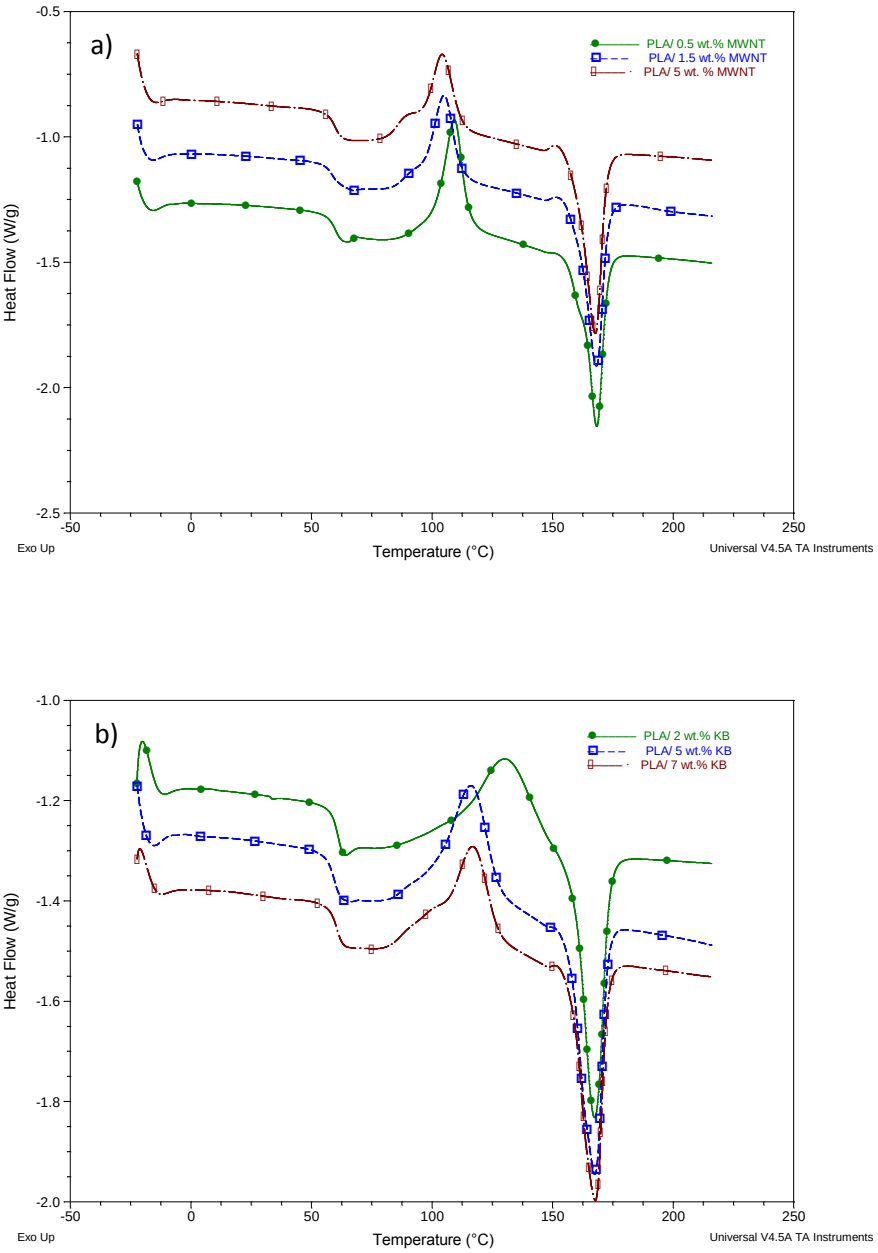

Figure 29 DSC heating thermograms for 3D printed layers (a) PLA/MWNT (b) PLA/KB.

Table 5 Calorimetric data for PLA 3D printed layers for the first heating run (10 °C/min)

Sample	T_g[a] (°C)	T_{cc}[b] (°C)	T_m (°C)	ΔH_{cc}[c] (J/g)	ΔH_m[d] (J/g)	X_{DSC} (%)
PLA/ o.5 wt.% MWNT	59.8	109.1	168.1	33.8	42.8	9.8
PLA/ 1.5 wt.% MWNT	58.4	104.8	168	29.3	40.8	12.6
Annealed PLA/ 1.5 wt.% MWNT	61.9	105	167.5	28.7	44.9	17.7
PLA/ 5 wt. % MWNT	59.5	104.1	167.5	32.4	42.9	11.9
PLA/ 2 wt. % KB	60.8	129.9	167.2	30.3	31.9	1.7
PLA/ 5 wt. % KB	59.5	116	167.2	27.6	37.1	10.7
Annealed PLA/ 5 wt. % KB	62.2	116.7	167.6	26.1	40.1	15.8
PLA/ 7 wt. % KB	60.4	116.7	167.5	26.1	32.5	7.4

As it is shown in Figure 30, the T_{cc} and ΔH_{cc} of the 3D printed layers increased significantly in comparison with the 3D printer filaments. Subsequently, the crystallinity percent remarkably decreased. As it is discussed above, the competition between construction and destruction of secondary agglomerates can be considered as a principal mechanism to find out the decrease of crystallinity percent in 3D printed layers in comparison with 3D printer filaments. It seems there are less recovery and construction after the destruction of the secondary agglomerations to happen through the shear flow through the 3D printing process. So, the nucleating effect of nanofillers decreased while cold crystallization process and it begins at the higher temperatures (T_{cc}) which needs higher energy (ΔH_{cc}) to grow polymer crystals in the composites.

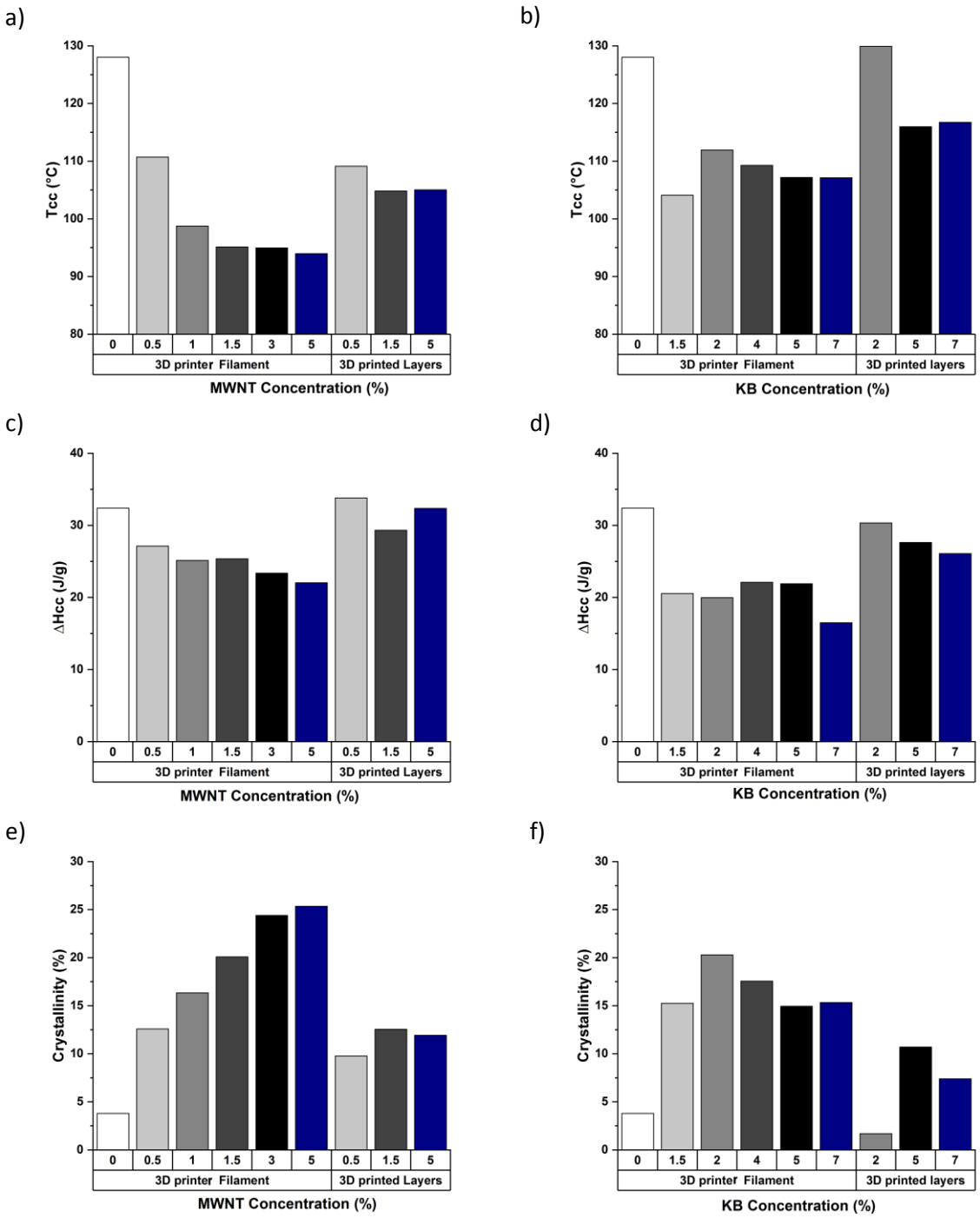

Figure 30 The comparison of crystallization properties of PLA/MWNT and PLA/KB composites in form of 3D printer filaments and 3D printed layers with different filler contents (a, b) cold crystallization temperature (Tcc) (c, d) cold crystallisation enthalpy (ΔHcc) and (e, f) Crystallinity (%)

3.2.2.1 Annealing effect

The annealing effect is to generate chains relaxation that would increase lamellae thickness in the crystalline phase of PLA. Generally, as discussed above, nanofillers can have a nucleating effect on polymers in nanocomposites [152]. The effect of annealing on PLA microstructure has been studied by Yu *et al.* [153]. They found out that annealing above Tg increased crystallinity because of polymer chain relaxation, which resulted in an increase in both strength and toughness. In our study, PLA/1.5 wt.% MWNT and PLA/5 wt.% KB 3D printed layers were kept at 60 ˚C for 12 h. The DSC thermograms of the annealed samples are shown in Figure 31 and Table 5. It is clear from the results that annealing affects the 3D printed samples by increasing the T_g about 3˚C and increasing the crystallinity percent about 5 percent. Annealing causes the thickening of PLA nanocrystals into larger lamellae making a decreased free volume and confinement of CNT, which increase both glass transition (Tg) and melting (Tm) temperatures [153][154]. An increase has not been observed in melting point of annealed samples, but the T_g and crystallinity degree.

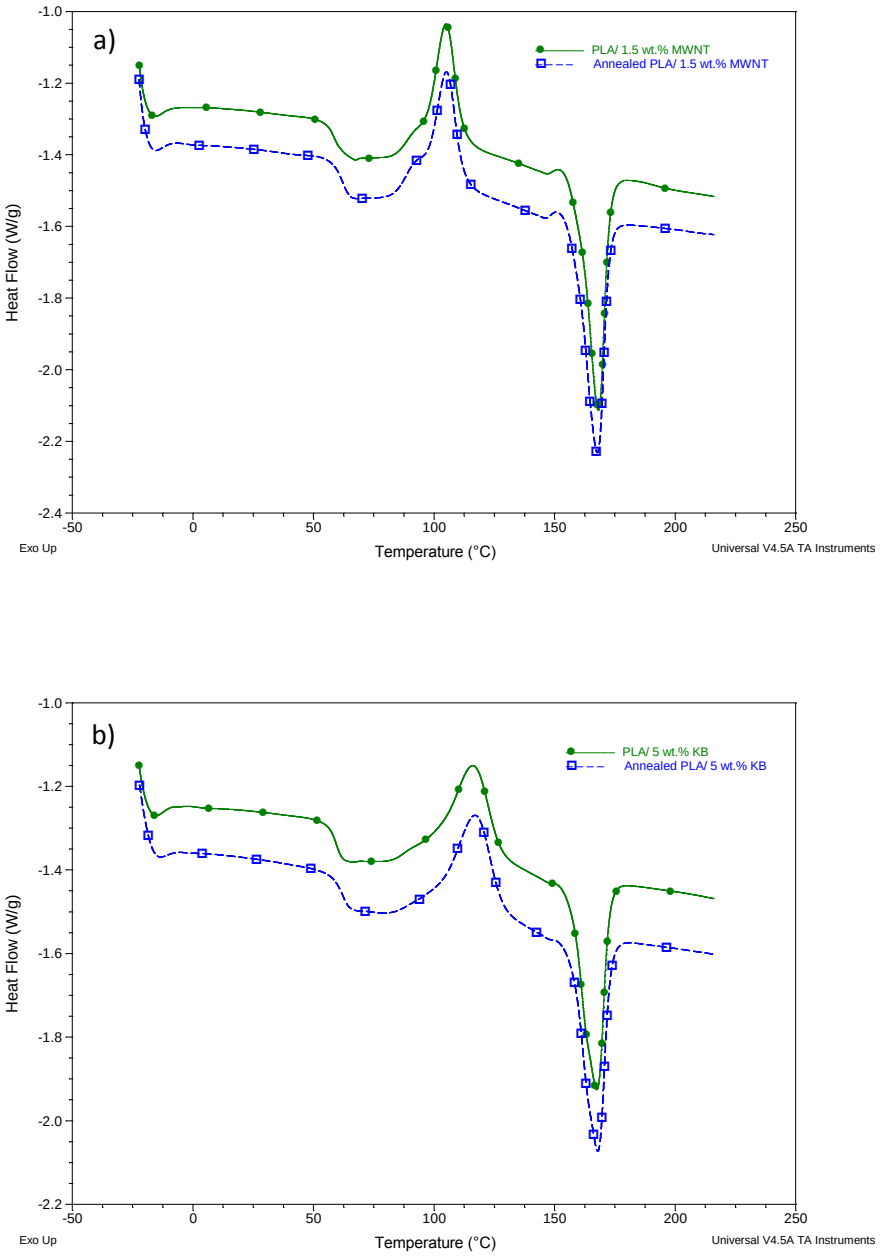

Figure 31 DSC heating thermograms for annealed 3D printed layers (a) PLA/MWNT (b) PLA/KB.

3.3 Dynamic mechanical thermal properties

3.3.1 3D printer filament

The mechanical behavior of the 3D printer filaments studied by DMTA under tension mode, a technique in which the storage modulus (E′) and loss modulus (E″) of the samples were monitored under oscillating load. The diagrams can be reported against time, temperature or frequency of oscillation [155]. The ratio E″/ E′ is called tan δ or loss factor which the maximum is commonly taken as the glass transition temperature. As it is shown in Figure 32 and 33, the storage modulus of the PLA and nanocomposites decreases rapidly whereas the tan δ go through a maximum when the polymer is heated through the glass transition temperature.

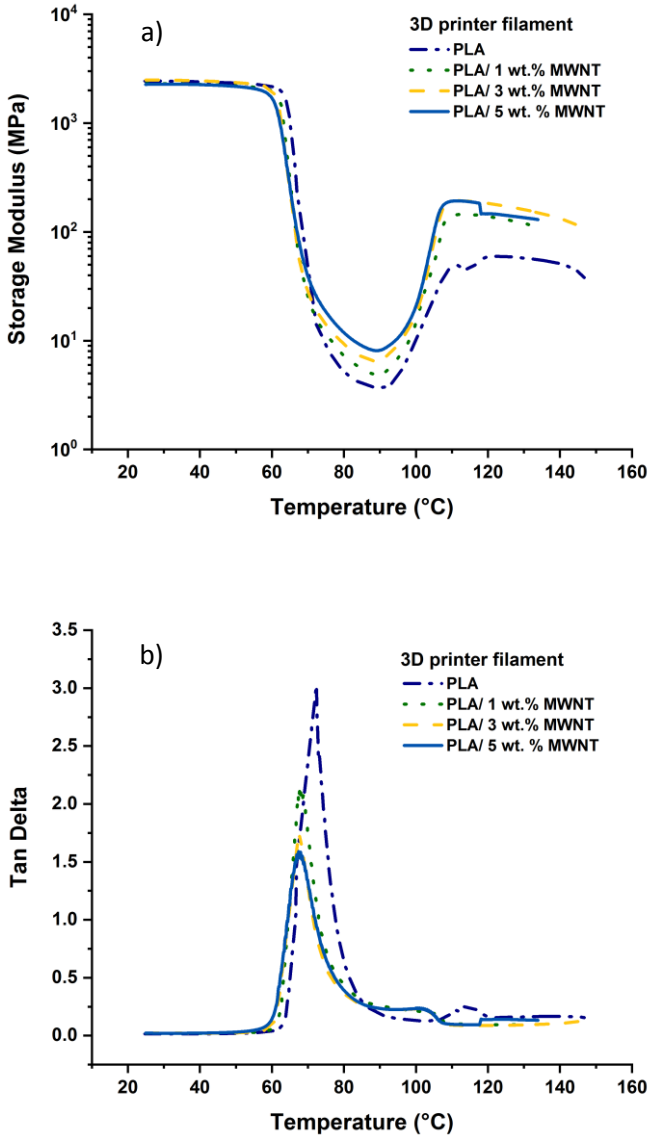

Figure 32 DMTA analysis of manufactured 3D printer filaments of PLA/MWNTs (a) Storage modulus vs. Temperature; and (b) tan δ curves.

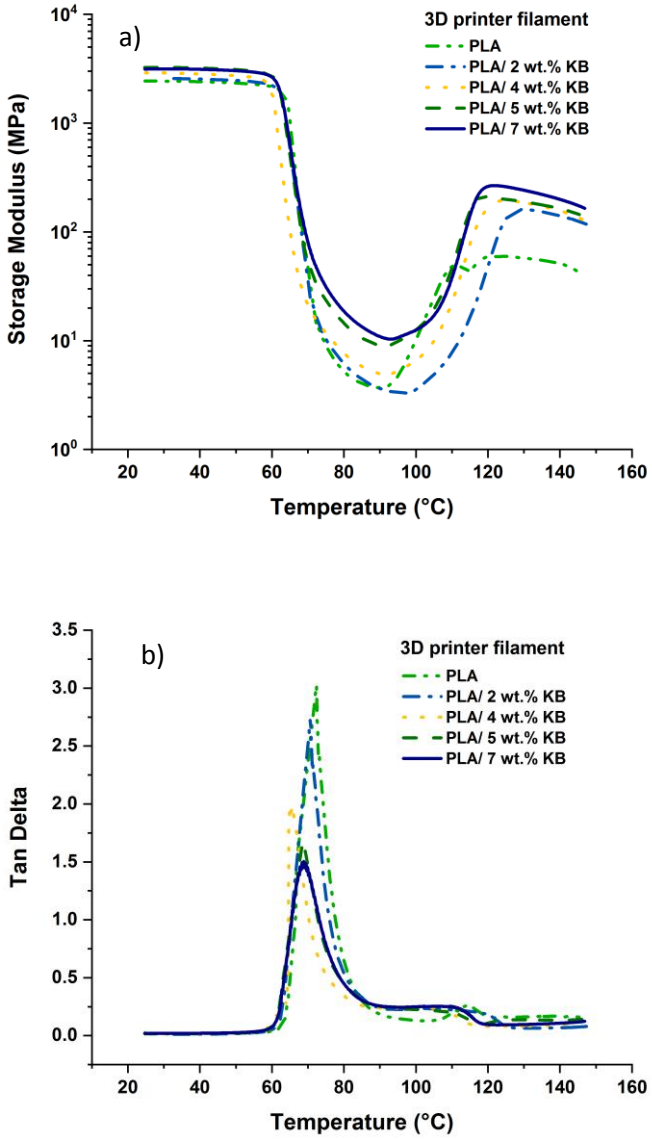

Figure 33 DMTA analysis of manufactured 3D printer filaments of PLA/KBs (a) Storage modulus vs. Temperature; and (b) tan δ curves.

The T_g values, starting and ending softening temperatures [T_{soft}(S) and T_{soft}(E), respectively] of PLA 3D printer filaments with MWNT and KB fillers at different filler contents during heating from room temperature were obtained from DMA curves in Figure 32 and 33 and are presented in Table 6. The procedures for estimating T_{soft}(S) and T_{soft}(E) are shown in Figure 34. That is, T_{soft}(S) and T_{soft}(E) are the intersection temperatures of the baselines for lower and higher temperature ranges and the tangent line for the curve. The softening temperatures of the 3D printer filaments can provide knowledge regarding the behavior of the filament through the 3D printing process. If the softening temperature is too low or too high, it may cause the stocking of the filament before melting through the 3D printer nozzle. As seen in Table 6, the T_g values,

T_{soft}(S) and T_{soft}(E) of PLA nanocomposites with the fillers were slightly lower than that of pure PLA filaments, revealing that the chain mobility of PLA was enhanced by the presence of MWNT and KB fillers. Tsuji *et al.* [151] also reported the reduction in T_g for PLA composite films with carbon fillers except for fullerene C60 and carbon nanoballoon (CNB) at 5 wt.%. Moreover, there is no significant difference in the T_g values, T_{soft}(S) and T_{soft}(E) of PLA nanocomposites 3D printer filaments with increasing the filler content. It is worth to mention that DMA is more sensitive to the changes and the T_g values obtained are higher than the values obtained from DSC tests.

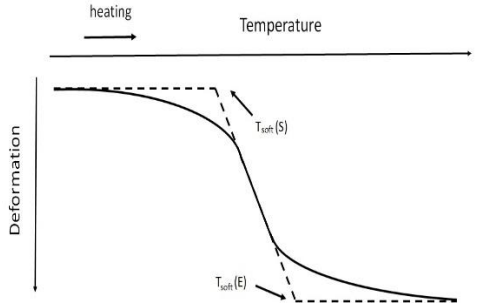

Figure 34 Procedures for estimating the starting and ending softening temperatures [T_{soft}(S) and T_{soft}(E), respectively][151]

According to the Table 6, there is no significant difference in storage modulus of PLA nanocomposite 3D printer filaments by increasing filler content at 40°C (below T_g), but the stiffening effect of the fillers especially nanotubes is specifically significant at higher temperatures like 90°C. Therefore, the presence of fillers enables the filament to sustain a higher modulus value to higher temperature. The storage modulus increase is due to the uniform mixing of fillers by applying shear stress during melt mixing that leads to the formation of filler/matrix chain network that acts as reinforcement. The ratio of modulus at 90°C to that at 40°C is about 0.0015 for PLA, but about 0.0045 for the nanocomposites containing 5 wt.% MWNT (about 3 times higher) and 0.0035 for the nanocomposites containing 7 wt.% KB (Figure 35). 3D printing of the nanocomposites with the higher storage modulus will need slower speeds or a higher nozzle temperature [156]. But, if the residence time of the polymer is too long at slower printing speed in the hot end or the printing temperature is too high, polymer degradation may occur, generally resulting in voids in the 3D printed structure [157].

Table 6 The glass transition temperature, tan δ, the storage modulus and the starting and ending temperature of softening of PLA 3D printer filament with different fillers.

Sample	$T_{g,DMA}$[a] (°C)	tan δ at $T_{g,DMA}$	T_{soft} (S)[b] (°C)	T_{soft} (E)[b] (°C)	E´(40 °C) (MPa)	E´(90 °C) (MPa)
PLA	72.3	3	63.9	74.6	2398	3.7
PLA/ 1 wt.% MWNT	67.7	2.1	62.1	72.8	2270	5.2
PLA/ 3 wt.% MWNT	67.6	1.7	61.2	71	2446	6.5
PLA/ 5 wt. % MWNT	67.4	1.6	61.2	72.1	2258	9.6
PLA/ 2 wt. % KB	70.7	2.7	62.6	74	2536	3.6
PLA/ 4 wt. % KB	66.7	2	59.6	70.2	2829	5
PLA/ 5 wt. % KB	68.6	1.6	61.6	72.5	3206	9
PLA/ 7 wt. % KB	68.8	1.5	62	73	3125	10.9

[a] Glass transition temperature

[b] T_{soft} (S) and T_{soft} (E) are the starting and ending temperatures of softening, respectively.

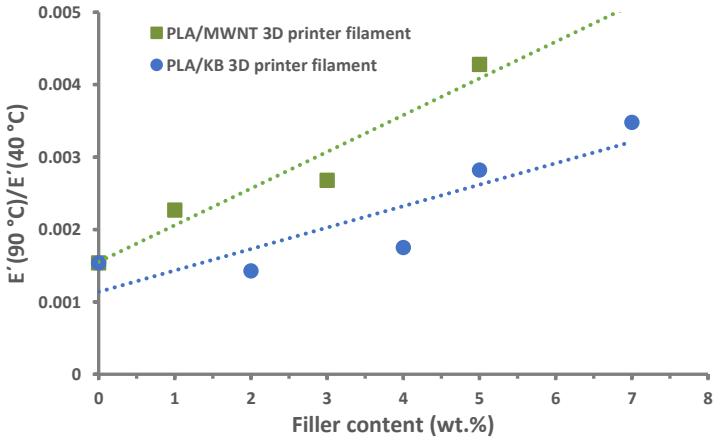

Figure 35 The ratio of the storage modulus at 90°C to 40°C in PLA/MWNT and PLA/KB 3D printer filaments with different filler contents

3.3.2 3D printed layers

The viscoelastic properties of 3D printed composite layers were characterized by dual cantilever DMTA as a function of nanofillers content from 2 to 7 wt.% KB and 0.5 to 5 wt.% MWNT. The test was done by recording the evolution of the storage modulus during a temperature sweep from 25˚C up to 120˚C. Overall, according to Figure 36 and 37 below the glass transition temperature (T_g), the storage modulus of 3D printed nanocomposites decreased and then increased. To find out more, a 2% KB 3D printed sample was annealed at 60˚C for 8 hours. The

comparison of the storage modulus evolution with temperature of annealed and unannealed samples is shown in Figure 38.

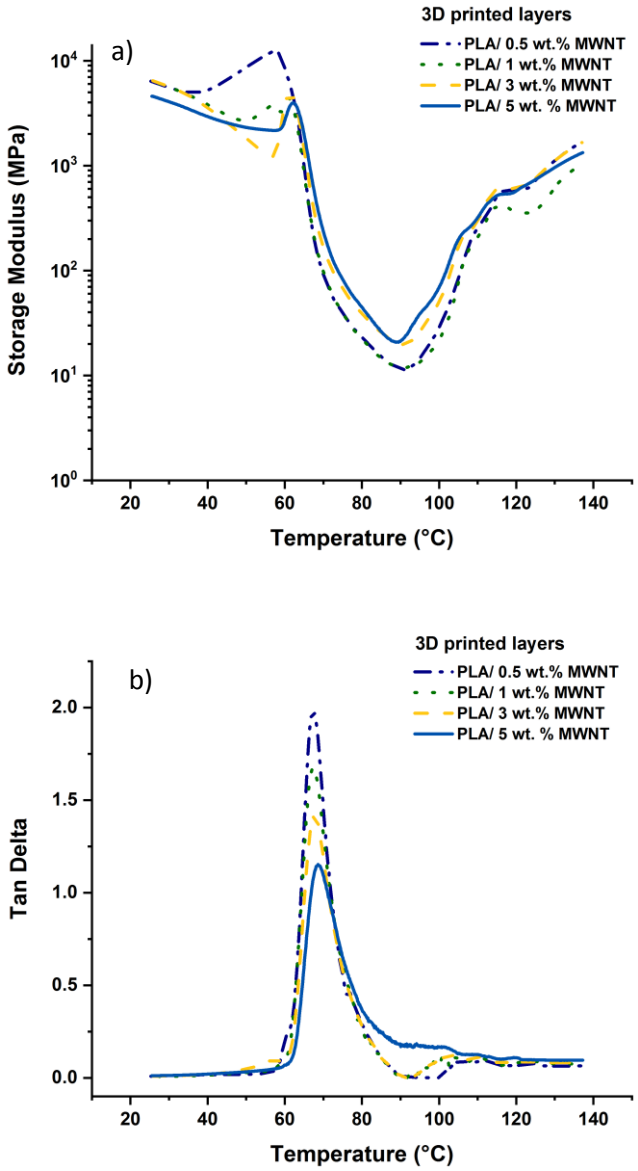

Figure 36 DMTA analysis of 3D printed layers of PLA/MWNTs (a) Storage modulus vs. Temperature, and (b) tan δ curves.

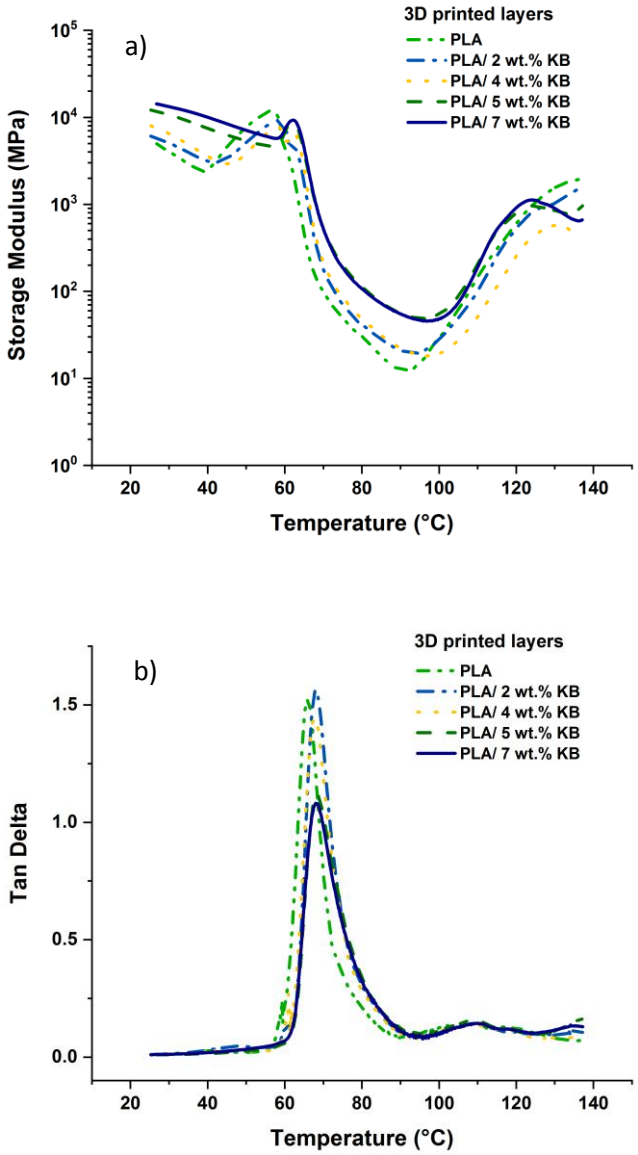

Figure 37 DMTA analysis of 3D printed layers of PLA/KBs (a) Storage modulus vs. Temperature, and (b) tan δ curves.

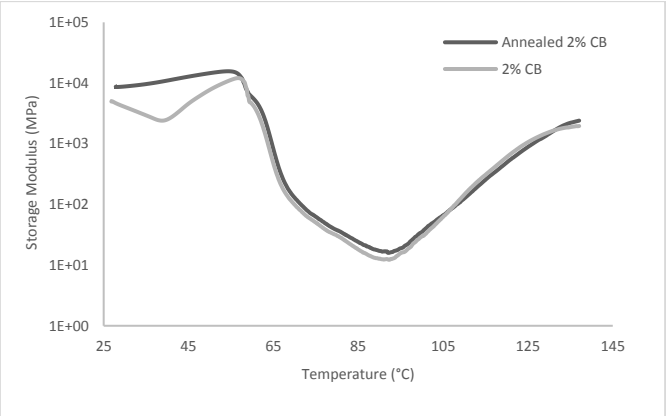

Figure 38 The effect of annealing process on the storage modulus curves of 3D printed layers of PLA/ 2 wt.% KB

It is evident that after annealing, there is no decrease in storage modulus below the glass transition temperature (T_g). During the FDM 3D printing process, the molten filament is attached on the surface of the solid layer, resulting in poor entanglement of polymer molecular [158]. At the same time, the arrangement of round filaments in the FDM process cannot avoid the gaps between filaments, resulting in voids in printed objects. Annealing can promote the entanglement of molten filaments with filling the gaps, avoiding storage modulus decrease with increasing temperature up to the glass transition. An increase in crystallinity degree after annealing also could increase the mechanical properties. After, storage modulus decreased abruptly where the region was contributed to the glass transition around 60–80°C, and then it started to increase after Tg due to the cold crystallization of PLA.

The trend of storage modulus of 3D printed layers is interesting to be noted (Figure 36, 37 and Table 7). The storage modulus of the 3D printed nanocomposites of KB (below and over T_g) was found to substantially increase with the KB content in the PLA matrix which corroborates the results in Ref. [159]. This positive synergy is evidencing a good dispersion of nanofillers within PLA suggesting an interface of good quality between KB nanofillers and PLA macromolecules which results in good stress transfer from KB to the PLA matrix.

Table 7 The glass transition temperature, tan δ and the storage modulus of PLA 3D printed layers with different fillers

Sample	$T_{g,DMA}$[a] (°C)	tan δ at $T_{g,DMA}$	E´(40 °C) (MPa)	E´(90 °C) (MPa)
PLA	65.8	1.5	2532	12.8
PLA/ 0.5 wt.% MWNT	67.6	2	5256	11.5
PLA/ 1 wt.% MWNT	67.5	1.7	3803	11.8
PLA/ 3 wt.% MWNT	67.6	1.4	3532	19.9
PLA/ 5 wt. % MWNT	68.6	1.1	2922	21.3
PLA/ 2 wt. % KB	67.8	1.5	3130	21
PLA/ 4 wt. % KB	67.8	1.4	3569	22.2
PLA/ 5 wt. % KB	68	1.1	7504	55.3
PLA/ 7 wt. % KB	68.3	1	10000	54.9

By adding 0.5 wt.% MWNT to PLA matrix, the storage modulus of 3D printed layers at 40°C increased. However, with increasing the filler content to 5 wt. %, the storage modulus at 40°C (below Tg) decreased. It seems the positive synergy effect of MWNTs decreases with increasing the MWNT content, which is evidencing a better dispersion of fillers within PLA in lower content of MWNT. The stiffening effect of the MWNT is specifically significant at higher temperatures like 90°C, therefore, the presence of fillers enables the 3D printed layers to sustain a higher modulus value to higher temperature.

The dampening (loss factor), or tan δ, is the ratio between the loss modulus and the storage modulus and gives information about the internal friction of the material [138]. There is a common trend of the data in Figure 36b and 37b, reduced tan δ values with higher KB and MWNT contents as it has been shown by other researchers for PLA nanocomposites [80], [146], [160], [161]. For a nanocomposite with lower filler content, the polymer chains are relatively free to move. Increasing the filler content decrease the mobility of the polymer chains and consequently reduce the loss factor which it means the energy is more recovered than lost [162]. The glass transition temperature is often recorded at the peak of tan δ in the region where the material changes from a glass to a rubbery state. Applying this method, the T_g does not show a significant difference in all nanocomposite 3D printed layers.

3.3.3 3D printed layers on the fabric

To investigate the viscoelastic properties of 3D printed layers on fabric, 3D printed layers with the same dimension as above were deposited on PLA fabric. The storage modulus and tan δ of PLA/MWNT and PLA/KB 3D printed layers on fabric are shown in Figure 39 and 40. The T_g, tan δ, E′(40˚C) and E′(90˚) according to the figures are shown in Table 8.

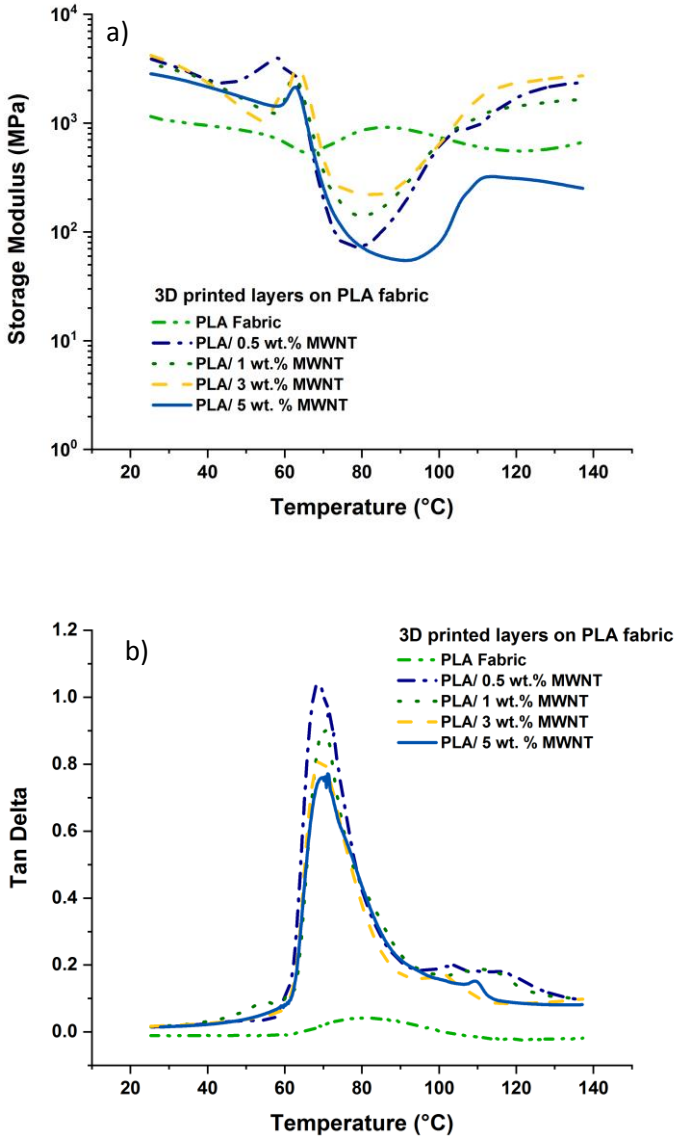

Figure 39 DMTA analysis of 3D printed layers of PLA/MWNTs on PLA fabric (a) Storage modulus vs. Temperature, and (b) tan δ curve.

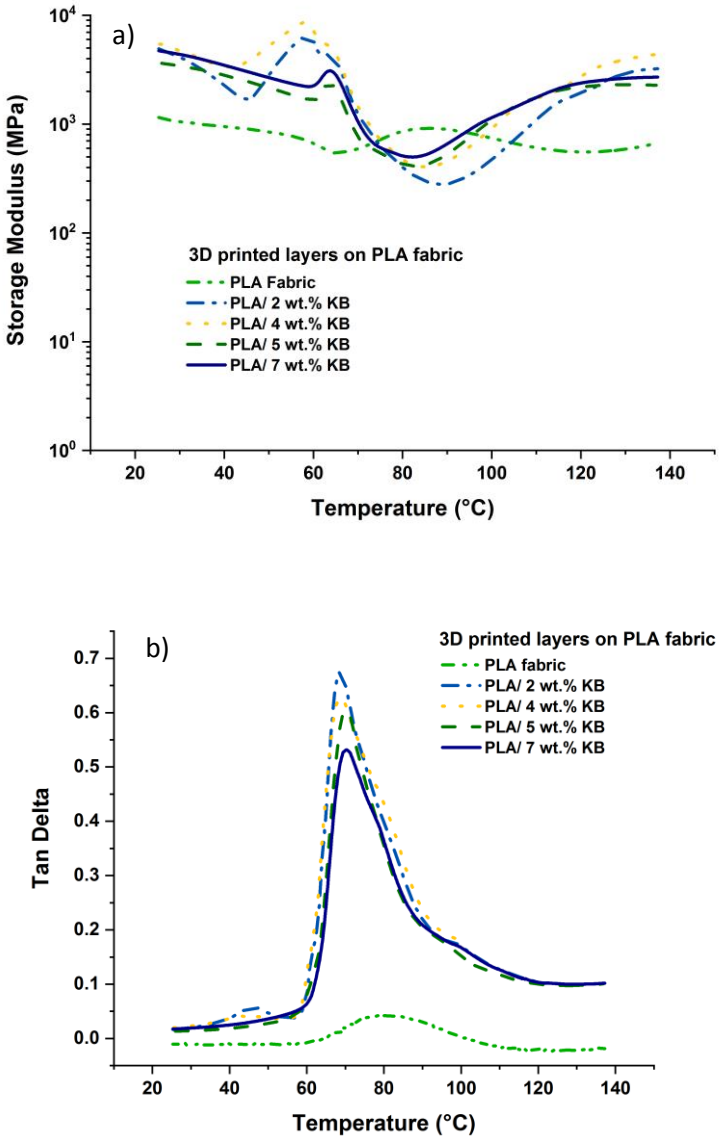

Figure 40 DMTA analysis of 3D printed layers of PLA/KBs on PLA fabric (a) Storage modulus vs. Temperature, and (b) tan δ curves.

Table 8 The glass transition temperature, tan δ and the storage modulus of PLA 3D printed layers on fabric with different fillers

Sample	**$T_{g,DMA}$[a] (°C)**	**tan δ at $T_{g,DMA}$**	**E´(40 °C) (MPa)**	**E´(90 °C) (MPa)**
PLA fabric	81.2	0.04	949	892
PLA/ 0.5 wt.% MWNT	68.5	1	2494	162
PLA/ 1 wt.% MWNT	71	0.7	2425	240
PLA/ 3 wt.% MWNT	70	0.9	2345	267
PLA/ 5 wt. % MWNT	69.2	0.8	2150	54
PLA/ 2 wt. % KB	68.7	0.6	2263	283
PLA/ 4 wt. % KB	68.4	0.6	3382	455
PLA/ 5 wt. % KB	70.2	0.6	2803	533
PLA/ 7 wt. % KB	70.2	0.5	3466	658

To make a more clear comparison between 3D printed layers and 3D printed layers on fabric, a series of column diagrams is shown in Figures 41-44. It is clear that the T_g of the 3D printed layers on fabric is to some extent higher than T_g of the 3D printed layers because of high T_g of PLA fabric. The interesting part is that the 3D printed layers on the fabric have a lower storage modulus at 40˚C in comparison with the 3D printed layers. It means the 3D printed layers on fabric are less stiff and more flexible which is a positive effect for applying 3D printed nanocomposites on fabrics for functional and smart applications. At the same time, 3D printed layers on the fabric have the higher storage modulus at 90˚C in comparison with 3D printed layers which again is the positive effect as the storage modulus of the 3D printed layers of PLA nanocomposites is too low in high temperatures like 90˚C. In addition, tan δ of the 3D printed layers on fabric is lower than the 3D printed layers which means the energy dissipation potential of the layers printed on fabrics is lower, resulting in more elastic response of the layers.

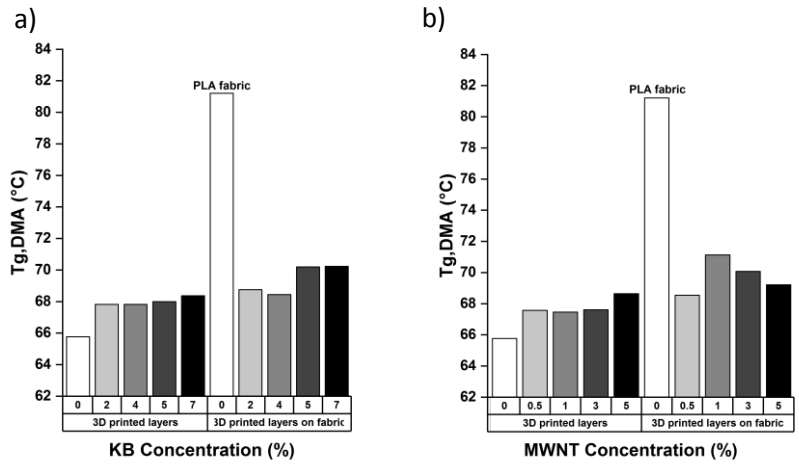

Figure 41 The comparison of glass transition temperature (T_g) of (a) PLA/KB (b) PLA/MWNT nanocomposites in 3D printed layers and 3D printed layers on the fabric

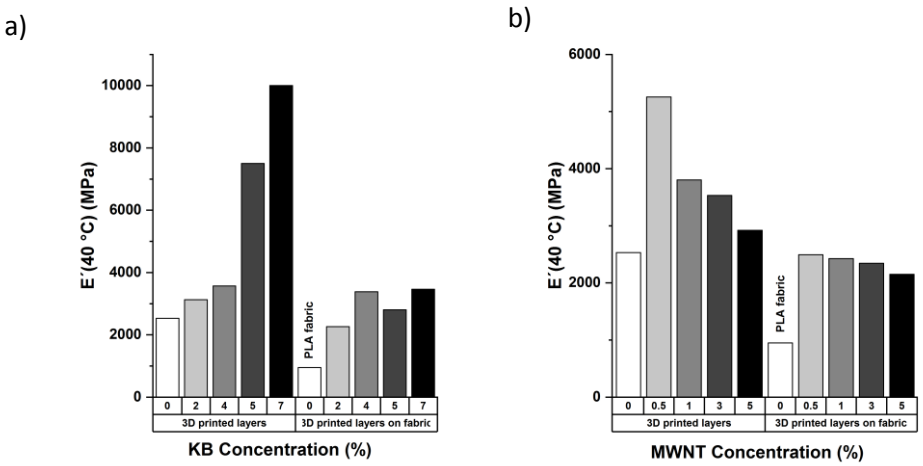

Figure 42 The comparison of storage modulus of (a) PLA/KB (b) PLA/MWNT nanocomposites at 40˚C in 3D printed layers and 3D printed layers on the fabric

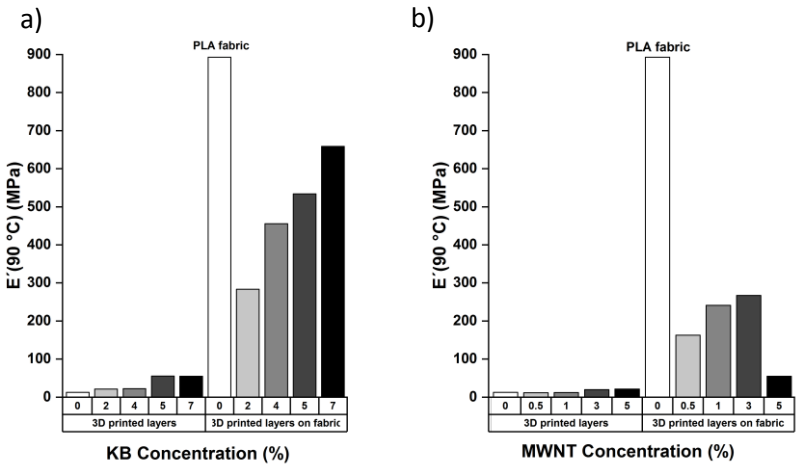

Figure 43 The comparison of storage modulus of (a) PLA/KB (b) PLA/MWNT nanocomposites at 90˚C in 3D printed layers and 3D printed layers on the fabric

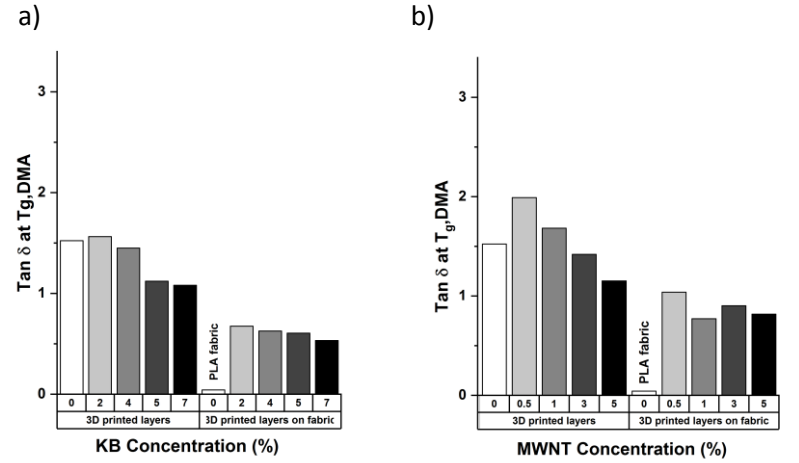

Figure 44 The comparison of tan δ of (a) PLA/KB (b) PLA/MWNT nanocomposites in 3D printed layers and 3D printed layers on the fabric

3.4 Conclusion

In this part of the thesis, the PLA-based conductive 3D printer filaments were developed using a melt mixing process containing two types of nanofillers including MWNT and KB. The focus was on the morphological, electrical, thermal and mechanical properties of CPCs in different forms before and after 3D printing. The results showed that there was no dependence of developed rod diameter on the MWNT loading, instead, the diameter was dependent on the KB loading and increased with increasing the filler amount.

Electrical properties were measured using two different systems including two-point measurement (2w) and four-point measurement (4w). A 4w method in comparison with 2w showed lower percolation thresholds and higher conductivity especially in the case of anisotropic nanocomposite filament containing nanotubes, therefore 4w method is proposed to apply if precise results are needed. Presenting the lower percolation thresholds and more precise results can be attributed to eliminating the effect of contact resistance by 4W measuring system.

KBs as spherical particles showed the higher percolation threshold in comparison with MWNTs, as the percolation threshold is proportional to the ratio of the average particle diameter over its mean length. However, the percolation threshold of 1.7 wt.% for KB in comparison with other types of CBs showed the effectiveness as the promising filler to enhance the conductivity of PLA filaments.

The conductivity of the extruded filaments from 3D printer decreases up to several orders of magnitude in comparison with loaded filaments in both conductivity curves of MWNT and KB composites. The effect of extruder temperature on the conductivity of monofilaments extruded from the 3D printer was investigated. The conductivity of filaments in low filler contents decreases with increasing extruder temperature, yet in higher filler contents there is no effect of extruder temperature on conductivity. More, two CPC including 2% MWNT and 5% KB were applied to 3D print tracks with different cross-sectional areas. Results show that the resistance decreases exponentially with the increase of the cross-sectional area of 3D printed tracks. In 3D printed layers, the sudden transition from insulator to conductor which is the indication of percolation threshold happened in PLA/4 wt.% KB and PLA/1 wt.% MWNT.

In manufactured 3D printer PLA filaments, the addition of KB and MWNT significantly lowered the crystallization temperature values (up to about 20 for KB and to 35 ˚C for MWNT) which signify that both fillers have the positive effect on crystallization and acted as a nucleating agent and accelerated overall crystallization. However, crystallinity percent of 3D printed layers remarkably decreased in comparison with the 3D printer filaments. The annealing process could affect the 3D printed samples by increasing the crystallinity percent.

DMTA curves showed that there is no significant difference in storage modulus of various composites of PLA 3D printer filaments at 40°C (below Tg), but the stiffening effect of the fillers especially nanotubes is specifically significant at higher temperatures like 90°C. The storage modulus of the 3D printed nanocomposites of KB (below and over T_g) was found to substantially increase with the KB content in the PLA matrix. By adding 0.5 wt.% MWNT to PLA matrix, the storage modulus of 3D printed layers increased. However, with increasing the filler content to 5 wt. %, the storage modulus at 40°C decreased significantly. The stiffening effect of the MWNT is specifically significant at higher temperatures like 90°C, therefore, the presence of fillers enables the 3D printer filaments and 3D printed layers to sustain a higher modulus value to higher temperature.

Finally, the 3D printed layers on fabric showed lower storage modulus at 40˚C in comparison with the 3D printed layers which means more flexibility. However, the 3D printed layers on the fabric have the higher storage modulus at 90˚C in comparison with 3D printed layers which again shows the positive effect of printing on fabric as the storage modulus of the 3D printed layers of PLA nanocomposites is too low in high temperatures like 90˚C. Accordingly, 3D printing of nanocomposites on fabrics gives rise to the flexibility of these nanocomposites for different applications in smart and functional textiles.

4 Piezoresistive properties of 3D printed layers

In this part, the potentiality of CPC FDM 3D printed layers with piezoresistive properties was investigated for the design of the force-sensing resistor (FSR) or a pressure sensor. Conductive filaments including MWNT and KB in a PLA matrix were 3D printed and the piezoresistive behavior (tension and compression) of 3D printed components were investigated. Next, the piezoresistive behavior of 3D printed layers was studied under compression in a cyclic mode in terms of filler type, filler content, and loading force rate.

4.1 Piezoresistive properties in tension and compression mode

The piezoresistive behavior of 1% MWNT 3D printed nanocomposite layers were investigated when subjected to tensile and compression load ranging from 0.5 to 18 N. Figure 45 shows the evolution of piezoresistive source signals and the related stress-strain diagrams. It is evident that in tensile mode there is no significant change in piezoresistive responses with tensile stress, as the maximum strain up to 18N load is about 0.2%. But, in compression mode, the 1 wt.% MWNT 3D printed composite layer is found to exhibit a negative pressure coefficient (NPC) characterized by a decrease of piezoresistive responses with increasing compressive loadings up to 18 N with the maximum strain up to about 16%. Piezoresistive pressure sensors undergo a change in resistance under applied pressure that is assumed to be caused by the different compressibility of filler and polymeric matrix under an applied force. Fillers either separate or approach by the applied compression and cause a positive or negative relationship between pressure and resistance depending on filler geometry and magnitude of the pressure [163]. The 3D printed layers approach by the applied compression leading to better connections between conducting nanofillers with decreasing the average inter-fillers distance and hence lower relative resistance, which explains the NPC effect observed in the 3D printed nanocomposites. The layer-by-layer structure of 3D printed nanocomposites acts as a spacer able to increase the inter-fillers gap and make the conductive nanocomposite less dense and more sensitive to compression.

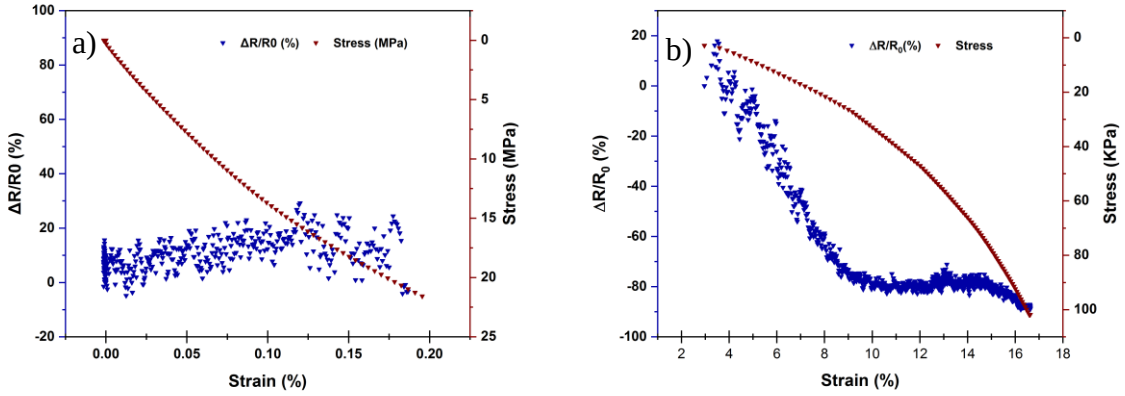

Figure 45 Piezoresistive responses of 1% MWNT nanocomposite 3D printed layers under (a) tensile (b) compressive loading

4.2 Piezoresistive behavior in cyclic compression mode

4.2.1 Effect of filler type and concentration

The nanocomposite 3D printed layers resistance variation has been monitored under cyclic loadings increasing from 2 to 18 N. The maximum force provided by DMA is 18 N, resulting in a normal pressure stress up to 100 kPa. The minimum force of 2 N was applied enabling the efficient contact of cupper electrodes with samples in between. The pressure sensor with the sensitivity in medium range from 10 to 100 kPa can be applied, for example, to fabricate sensor gloves to monitor hand stress during manual activity and object manipulation [164][165]. The existing pressure sensors with high sensitivity in the medium to high pressure range [166][167], can not be easily integrated in the garments without hindering the manual motion. The pressure produced by the foot due to the body weight and the force applied by athletes using tools such as tennis racket with repetitive motions are other examples of the medium pressure ranges [164]. Therefore, in this part of the thesis, it has been tried to investigate the behavior of nanocomposite 3D printed layers under cyclic load in the medium pressure range. Four cycles were performed to check the reproducibility of the sample response with different filler contents (a sample in percolation threshold and a sample with higher contents of filler) in low force speed of 1 N/min and a 15 mm diameter compression clamp. Figure 46 shows the sensors responses with applied stress and related strain.

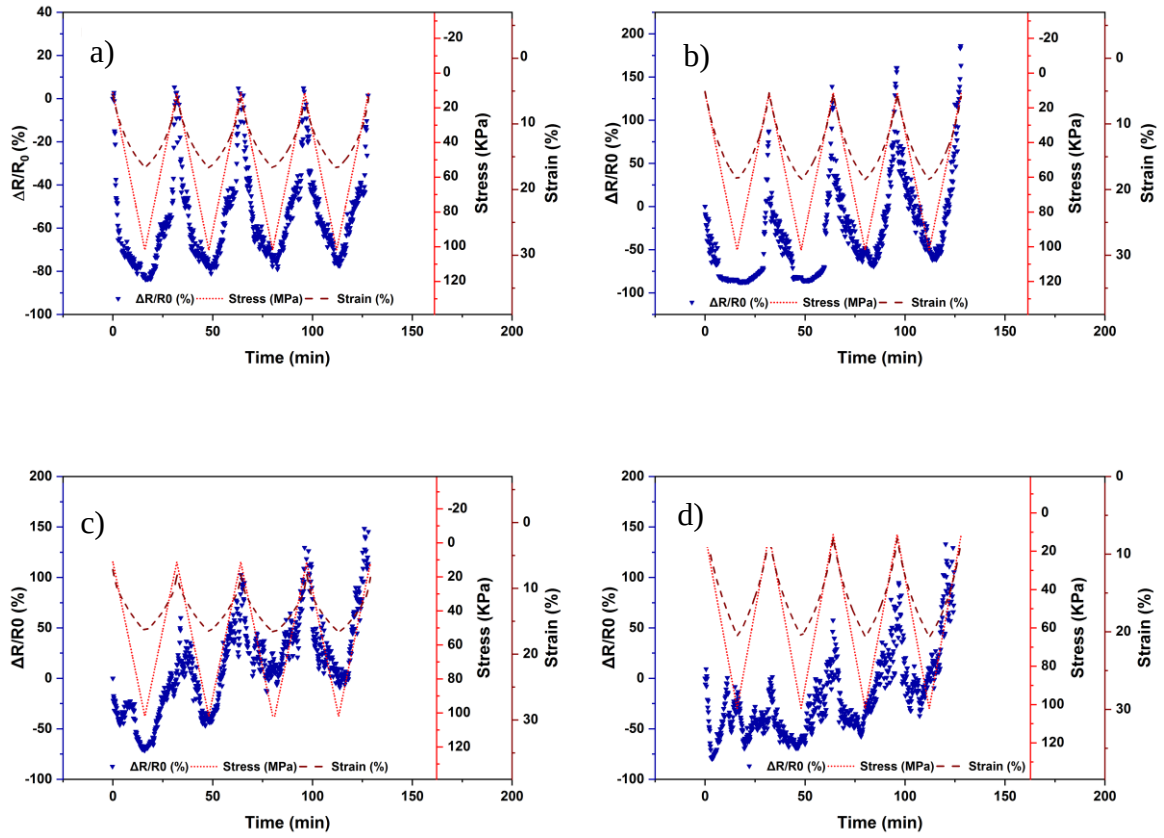

Figure 46 Comparison of nanocomposites piezoresistive responses (a) PLA/1 wt.% MWNT, (b) PLA/ 5 wt.% MWNT, (c) PLA/4 wt.% KB and (d) PLA/ 7 wt.% KB

As shown in Figure 46, PLA/ 1 wt.% MWNT responses $A_r = \frac{\Delta R}{R_0}$ (Equation 4) are synchronic with strain and stress and the variation of resistance follows the deformation which returns to its original value after unloading. But, the sensor responses of samples including 5 wt.% MWNT, 4 and 7 wt.% KB are not synchronic with the applied stress and strain. Figure 47 shows the resistance change in the start and end of each cycle for all samples.

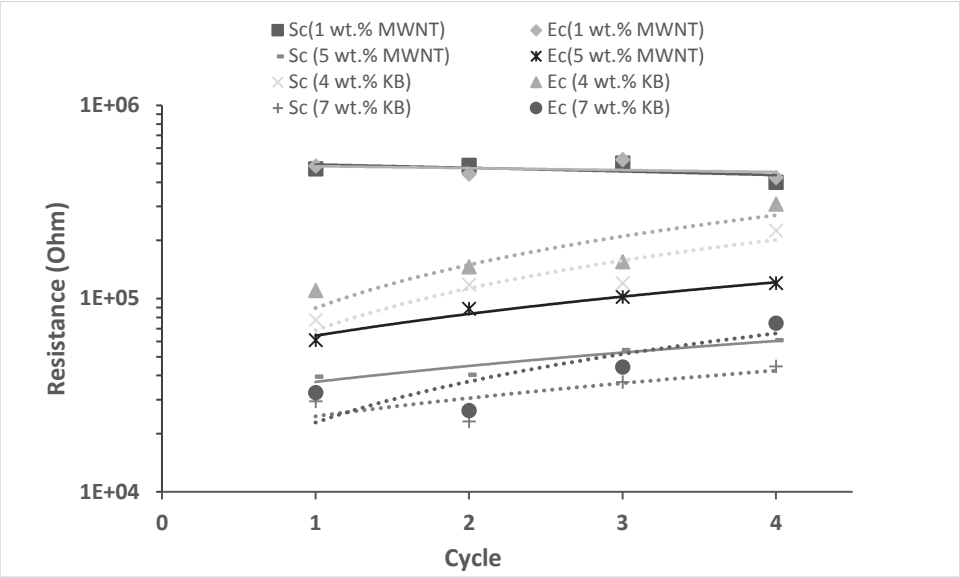

Figure 47 Resistance change in the start and end of each compression cycle for different samples (Sc is the start of the cycle and Ec is the end of the cycle. The solid and dot linear trend lines represented MWNT and KB composites respectively.

It is clear that except PLA/ 1 wt.% MWNT, other 3D printed layers shows significant hysteresis behavior, which is because of the residual strain of 3D printed layer composites after the compression. The same behavior has been reported in studies about compression test of porous structures including carbon nanotubes [168][169]. 3D printing of nanocomposites with high filler content in comparison to percolation threshold may cause structures that are more porous. As the melt flow index of composites in 5 wt.% MWNT and 7 wt.% KB is low [17], it is required to 3D print at a lower speed or using higher nozzle temperature [156]. However, it causes higher porous 3D printed structures and eventually larger hysteresis behavior under compression cycles. Moreover, in higher nanofillers contents than percolation threshold, the dominant mechanism of conduction is percolation [170], therefore the destruction of effective conductive paths in successive loading/unloading cycles is the dominant mechanism especially when the related strain also is high (low force speed). So, by successive loading/unloading cycles in higher filler contents, the increase of minimum and maximum sensitivity is observed. The same behavior is observed in PLA/ 4 wt.% KB which the content is close to the percolation threshold. The compression can lead to the changes in effective conductive paths of carbon black in three different following ways [171]: 1) change in gap size in existing effective conductive paths, 2) formation of new effective conductive paths and 3) destruction of the conductive effective pass. Luheng *et al.* [171] showed that the relation between the number of effective conductive path(s) and uniaxial pressure presents monotonically increasing, non-

monotonical, and monotonically decreasing depending on different carbon black content in silicone rubber composite. 4% KB is most probably higher than real percolation threshold of the printed composites (as the electrical resistance of 3D printed layers in this study were measured using a two-point measurement method and according to our recent study [17] the resistance value can be determined much more accurately with the four-point measurement method). So, with successive load/unloading cycles with low force speed and high strain rates, the destruction of conductive ways overcome the formation of new ways and contributes to the increasing tendency of the composite resistance.

The hysteresis behavior of PLA/ 1 wt.% MWNT layers is clearer in Figure 48 that evidence after a large hysteresis in the first cycle, the traces of the three consecutive cycles of loading/unloading are almost imposable with a small deviation observed between the second and the fourth loops. This behavior is similar to findings of Slobodian and Saha [172] which accordingly in MWNT network a ratcheting strain appears after the first compression cycle due to the initial deformation of the porous structure and blocked reverse motion of nanotubes inside the compact networks. During consecutive cycles of loading and unloading the nanotubes rearrangement becomes steady and MWNT network reaches a stable stress-strain hysteresis loop form. It implies that the entangled carbon nanotube network can be used as a sensing element of compressive stress, mainly when the network is well deformed in advance. In Figure 48a, it can also be observed that the signal is linear with a slope difference below and over 30 kPa. Figure 48b depicts a schematic representation of 1 wt.% MWNT 3D printed layer sandwiched between two copper electrodes. Dashed lines between MWNT individual particles and clusters represent quantum tunneling bridges which accordingly charge carriers are allowed to tunnel from one cluster to another without any physical contact in composite systems.

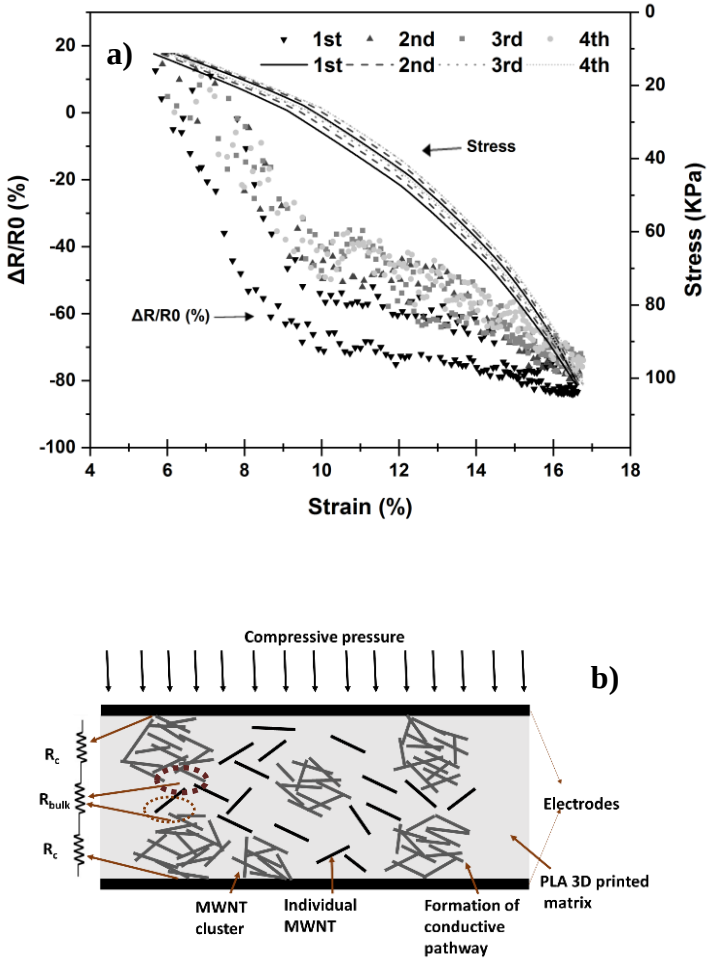

Figure 48 Piezoresistive behavior of 3D printed PLA/1 wt.% MWNT nanocomposite (a) Synchronism of A_r with stress versus deformation. (b) Schematic diagram of the transduction mechanism of PLA/1 wt.% MWNT nanocomposite sandwiched between two metal electrodes towards compressive pressure. The electrical model of the FSR comprises a series connection between the bulk (tunneling) resistance (R_{bulk}) and the contact resistance (R_c).

When the sample is subjected to external stress (σ), the inter-particle distance is reduced. According to the proposed model by Paredes-Madrid *et al.* [173], the total resistance across the Force Sensing Resistor (FSR) can be decomposed from Equation 5:

$$R_{FSR} = R_{bulk} + 2R_c \quad (5)$$

where R_{bulk} is the resistance of the CPC caused by the quantum tunneling phenomenon and R_c is the contact resistance between the metal electrodes and the conductive particles. An FSR is created by the series connection between R_{bulk} and $2R_c$ as shown in Figure 48b. However, three

phenomena occur when an incremental stress applied on an FSR [170]: (1) the contact resistance of the existing paths is reduced following power laws, (2) new contact paths are formed further contributing to reducing the contact resistance, and (3) the average inter-particle distance is reduced thus decreasing the tunneling resistance, R_{bulk}. It seems that for 1 wt.% MWNT 3D printed layer, the contact resistance is decreased by forming new contact paths and decreasing the contact resistance of the existing paths under 30 KPa and 10% strain. But, over that, the resistance decrease is because of the diminishing of inter-particle distance and consequently decreasing the tunneling resistance. The piezoresistive coefficient (also named gauge factor, G) can be graphically determined from the slope of the curve in Figure 48 and calculated with Equation 6 [141]:

$$G = \frac{A_r}{\varepsilon} \qquad (6)$$

where $A_r = \frac{\Delta R}{R_0}$ (Equation 4) is the amplitude of piezoresistive response or relative change in resistance, and $\varepsilon = \frac{\Delta T}{T_0}$ is the deformation of the sensor. For 3D printed PLA/1wt.% MWNT layers the value of G = 7.6 obtained with the amplitude of the piezoresistive response of about A_r = -0.8 (-80%).

4.2.2 Effect of force rate

To further investigate the limits of sensitivity of the 3D printed layers, i.e., the stress rate and related strain, the piezoresistive response of 3D printed composite layers has been monitored under cyclic compressive stress profile from 10 up to 100 kPa with the high speed of 18 N/min.

Figure 49 shows the piezoresistive responses of PLA/1 wt.% MWNT and PLA/4 wt.% KB samples, exposed to ten cycles of 100 kPa compressive stress.

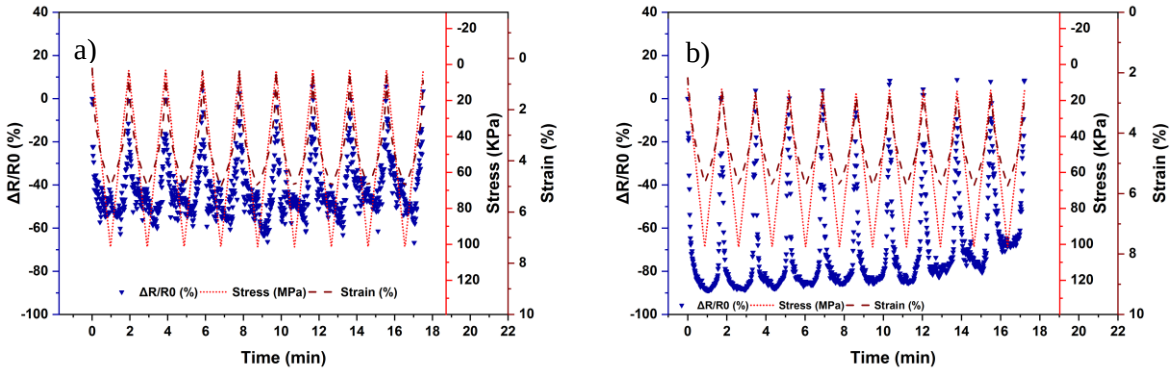

Figure 49 Comparison of 3D printed nanocomposites piezoresistive responses in high force rate of 18 N/min (a) PLA/1 wt.% MWNT (b) PLA/ 4 wt.% KB

Figure 49a shows that the piezoresistive response of PLA/ 1 wt.% MWNT with applied force rate of 18 N/min has a smaller amplitude (A_r = -0.60) and more noisy signals than a piezoresistive response with low force rate of 1 N/min in Figure 46a. Simultaneously, the value of G = 9.3 obtained which imply that the high force rate does not decrease the piezoresistive effect of PLA/ 1 wt.% MWNT 3D printed layers, even though it is increased. According to Figure 50, when the high force rates were applied then the related strain is much smaller than applying low force rates. At high strain rate, there is insufficient time for the material to respond to stress with large-scale viscoelastic deformation or yielding [174]. Therefore, with lower strain quantities in figure 49a, the resistance decrease is because of more contact resistance decrease than diminishing of tunneling distance and consequently causes the smaller amplitude of the piezoresistive response. Interestingly, in Figure 49b, it is clear that PLA/4 wt.% KB 3D printed layers under high force rates is leading to responses of large sensitivity (A_r = -0.90) and exempt of noise. Nevertheless, after almost 7 cycles, the maximum sensitivity is not stable and starts to decrease. So, if the cyclic functionality of the PLA/4 wt.% KB 3D printed layers is not needed, the value of G = 47.6 is obtained in the first cycle of applied stress which shows the high piezoresistive effect of these 3D printed layers. By the way, the gauge factor decreases to G = 28 in the 10^{th} cycle of stress. Therefore, PLA/KB nanocomposites 3D printed layers do not show stable piezoresistive behavior in a cyclic mode in low and high force rates.

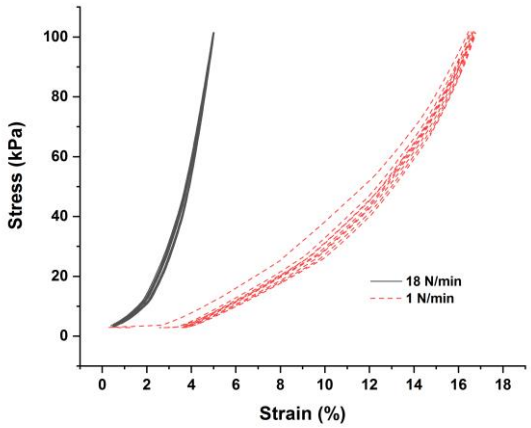

Figure 50 Stress-strain diagrams of 3D printed PLA/ 1 wt.% MWNT with different force rates in a cyclic mode

4.3 Conclusion

A force-sensing resistor (FSR) or a pressure sensor is a material whose resistance changes when a force, pressure or mechanical stress is applied. Conductive polymer nanocomposites (CPC) can be part of FSRs as their resistance changes with the application of force to their surface. In percolation threshold of CPCs and lower filler contents, the variations in a few numbers of contact points within the network upon pressure application impact more significantly the effective changes in electrical resistance than for the case when the network is densely packed. Therefore, in such contents, FSR is more efficient. In this part of the thesis, the PLA/MWNT and PLA/KB 3D printed layers were created using fused deposition modeling and their piezoresistive behavior were investigated. It has been shown that it was possible to FDM 3D print piezoresistive PLA nanocomposite layers from the MWNT and KB fillers and PLA matrix. For PLA/1 wt.% MWNT 3D printed layers with 1 mm thickness, there is no significant change in resistance with tensile stress as the maximum strain up to 18N load is about 0.2%. But, in compression mode, it exhibits a negative pressure coefficient (NPC) characterized by a decrease of piezoresistive responses with increasing compressive loadings up to 18 N with the maximum strain up to about 16%. In the cyclic mode with the 1 N/min force rate, PLA/1 wt.% MWNT 3D printed layers showed good performance with the value of G = 7.6 obtained with the amplitude of the piezoresistive response of about A_r = -0.8 (-80%). The response was linear in the range of pressure 10-100 kPa, with low noise and hysteresis which is come from the layer by layer architecture of the component and tunneling effect of MWNT nanofillers in lower contents than the percolation threshold. The pressure sensor with the sensitivity in medium range from 10 to 100 kPa can be applied, for example, to fabricate sensor gloves to monitor hand stress during manual activity and object manipulation [164][165]. The pressure produced by the foot due to the body weight and the force applied by athletes using tools such as tennis racket with repetitive motions are other examples of the medium pressure ranges [164].

In high force rate 18N/min, the piezoresistive response of PLA/ 1 wt.% MWNT has a smaller amplitude (A_r = -0.60) and more noisy signals but the value of G = 9.3 obtained which imply that the high force rate does not decrease the piezoresistive effect of PLA/ 1 wt.% MWNT 3D printed layers, even though it is increased. Therefore, the decrease in sensitivity is because of lower strain rates in high force rates. KB composites could not show stable piezoresistive responses in a cyclic mode. However, in high force rate, PLA/4 wt.% KB 3D printed layers is leading to responses of large sensitivity (with an amplitude: A_r = -0.90) and exempt of noise with the value of G = 47.6 obtained in the first cycle of applied stress which is highly efficient piezoresistive behavior, however decreases to G = 28 in 10^{th} cycle of stress. The results demonstrate PLA/MWNT and PLA/KB as a good piezoresistive feedstock for 3D printing with

potential applications in wearable electronics, soft robotics, and prosthetics, where complex design, multi-directionality, and customizability are demanded.

5 Deposition of polymers and nanocomposites on textiles: adhesion properties

This section focuses on direct 3D printing of different polymers and nanocomposites on textiles, the technology which can provide new opportunities for development of functional and smart textiles. Adhesion which is one of the most important parameters in deposition of polymers on textiles was studied systematically with the aid of statistical design of experiments. The 3D printer filaments and fabrics were chosen from well-known polymers like PLA and PA. The combination of deposited polymers and fabrics was mostly selected from similar types for example PLA on PLA as well as PA on PA to investigate more pure and less mix approaches for development of functional and smart textiles. The effect of 3D printing process parameters such as extruder temperature, construction platform temperature and printing speed on the adhesion of mentioned polymers and nanocomposites onto fabric was investigated with the aid of statistical design.

Figure 51 represents the adhesion force of deposited PA6.6/6 and PLA onto PA6.6 fabric via 3D printing. The treatment combination and adhesion force for each sample coded from 1 to 26 can be found in detail in Table 2. Apparently, different treatment combinations in the 3D printing process affect the adhesion force of deposited polymers onto fabrics providing different results.

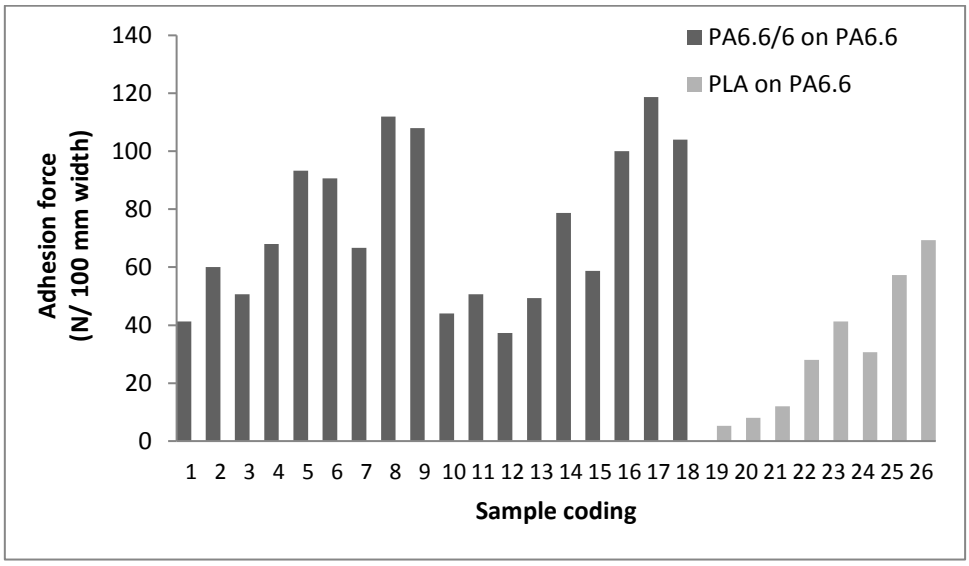

Figure 51 Average of adhesion force of deposited PA6.6/6 and PLA 3D printed layers on PA6.6 fabric [3]

5.1 PA6.6/6 onto PA6.6 fabric

Experiment 1 was done for adhesion of PA6.6/6 on PA6.6 with three different factors and levels of extruder temperature (235, 250 and 260 °C), platform temperature (23, 50°C) and printing

speed (18, 50 and 83 mm/min) which is in total 18 treatment combinations with three replications. The detailed treatment combinations for samples 1 to 18 and the results of related adhesion force can be found in Table 2. Minitab software was used to do regression analysis, specify the model, interpret the adhesion results and determine how well the model fits. The regression analysis is a set of statistical processes for estimating the relationship between variables. The analysis shows how the typical value of the dependent variable changes when any of the independent variables is changed [175].

As it is shown in Figure 52a, adhesion force versus extruder temperature has a linear regression model and P-value is less than 0.05 which means there is a significant linear effect of the factor extruder temperature on adhesion. In 3D printing of PA6.6/6 filament onto PA6.6 fabric, when the extruder temperature is close to the melting point of the PA6.6 fabric (268 °C), diffusion of polymers in interfaces has happened resulting in higher adhesion forces [176].

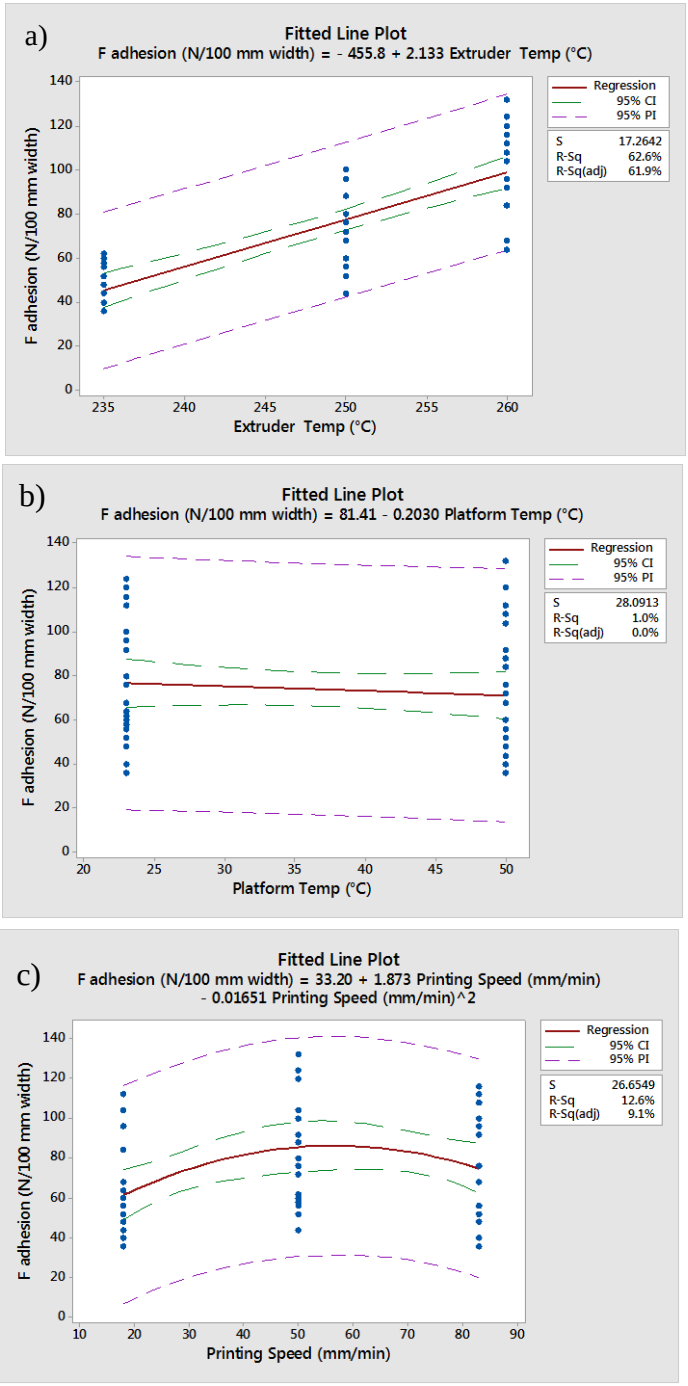

Figure 52 Effect of different variables of 3D printing process including (a) extruder temperature, (b) platform temperature, and (c) printing speed on adhesion force of PA6.6/6 deposited onto PA6.6 fabric [3]

Deposition of polymers directly on fabrics can be considered as a thermal welding method in which joining of the polymer as an adhesive and fabric as an adherent take place during the printing process. Different theories have been applied to explain polymer-to-polymer adhesion [177]. According to the adsorption theory of McLaren, the bonding formation is divided into

two steps. In first step, micro Brownian motion causes the migration of large polymer molecules from adhesive to the surface of adherent, subsequently, polar groups of the adhesive macromolecules approach the polar groups of the adherent. Applying pressure and lowering viscosity while heating can facilitate this step. Sorption process is the second step which starts when the distance between molecules of adhesive and adherent become less than 5Å and intermolecular forces begin to have an effect. This theory cannot explain the high adhesion between non-polar polymers and the low adhesion of the too high polar polymer to the very polar adherent.

Diffusion is a more reasonable theory that explains the adhesion of polymers to each other by the diffusion of chainlike molecules that leads to the formation of a strong bond between adhesive and adherent. Polymer diffusion has a major effect on properties of the layers of polymers across the interface and is the function of temperature, composition, compatibility, molecular weight, orientation and molecular structure of polymers [23]. Diffusion improves the adhesion between the two layers of the polymer and makes the interface stable.

In fact, the diffusion theory can easily explain the increase of adhesion force by the rise of extruder temperature for deposited 3D printed polymers on fabric. Extruder temperature increase causes the rise of thermal motion of macromolecules of polymer or their segments, and consequently diffusive penetration into the fabric increases. Hence, the higher increase in the adhesion with increasing extruder temperature (consequently contact temperature) would be explained from a purely kinetic viewpoint by the greater intensity of micro-Brownian motion of their chains and by the fact that the increase of flexibility of molecular chains and the destruction of intermolecular links take place with increasing temperature more rapidly [177].

Furthermore, deposited polymer (PA6.6/6) and applied fabric (PA6.6) are both polyamides which Van der Waals dispersion forces are involved in the bonding mechanisms. Depositing polymer with higher extruder temperature soften the fabric to make a stronger interface by making good contact. Increasing the extruder temperature to the melting point of the fabric enhance the joint interface stability by improving good contact and Van der Waals forces. It is worth mentioning that although PAs include polar amide groups which can hydrogen bond with each other but used copolymer PA6.6/6 for extruding which offer the most favorable combination of price, properties, and processability is designed for high adhesion of 3D printed layers together which means the cohesive forces are high.

So extruder and platform temperatures can have an important role in interface stability. Since the platform temperature (23 and 50°C) was chosen not higher than the glass transition temperature of PA6.6 fabric (T_g=55°C), there is no significant linear effect of platform

temperature on adhesion force (Figure 52b). Proceeding from the above discussion about the nature of adhesion, it is obvious that the value of adhesion at the interface of polymer-polymer is dependent upon the phase state of the polymers [177]. Figure 52b shows that platform temperatures not higher than glass transition does not show significant effect on adhesion force. In fact, at the glassy point of the polymer when there is no mobility of the molecule chains, diffusion and consequently adhesion is nothing. The middle segments and macromolecule ends start to have thermal motion in the rubberlike region. At the end in a flow state, all of the macromolecules participate in the diffusion. Thus, the phase state of the polymer of the fabric which is determined by the platform temperature of the 3D printer can play a pivotal role in adhesion when it is higher than the glass transition temperature of the polymer.

According to Figure 52c, the quadratic regression coefficient is significantly different from 0. So there is a significant quadratic effect of printing speed on adhesion force. Adhesion force increases with increasing the printing speed from 18 to 50 mm/min, printing speed in middle ranges (50 mm/min) causes the highest adhesion results and after that with increasing the printing speed to 83 mm/min, adhesion forces decreases.

In connection with the influence of thickness layer on adhesion strength and in order to find out why printing speed causes a quadratic effect on adhesion force, an analysis was done on the effect of printing speed on the thickness of 3D printed layers. The thickness of the 3D printed layers versus printing speed has a linear regression model and P-value is less than 0.05 and as it is shown in Figure 53 the thickness of the layers decrease by increasing print speed.

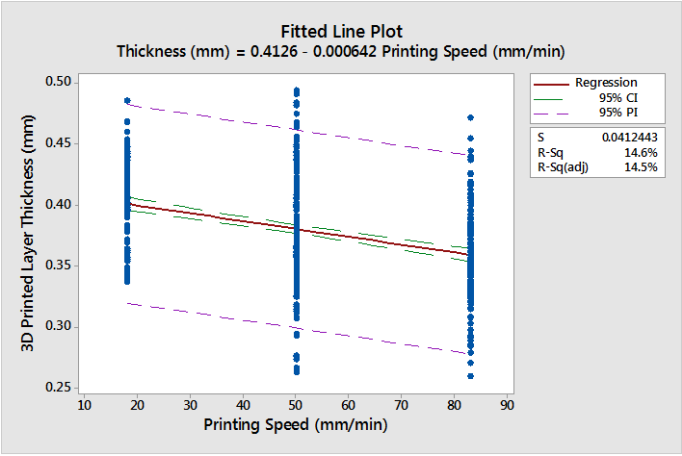

Figure 53 Effect of printing speed on PA6.6/6 3D printed layers thickness [3]

It has been shown that the adhesion force is dependent on the thickness of the adhesive layer for composite interfaces [178]. As the thickness of the adhesive layer is reduced, interfacial bonding strength increases because stress is able to dissipate through the interface easier. Although the highest printing speed (83 mm/min) causes the lowest layer thicknesses (Figure 53), a decrease is observed in adhesion strength in comparison to middle ranges (50 mm/min) (Figure 52c). Adhesion is the tendency of different surfaces to join to each other and cohesion is relevant to the tendency of similar surfaces to adhere to one another (Figure 54). Since the penetration of the macromolecules of polymers into the fabric is slow at high printing speed, adhesive forces are less than cohesive forces and subsequently adhesion strength decreases.

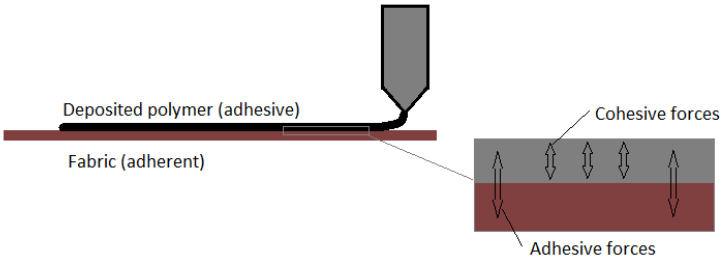

Figure 54 Adhesive and cohesive forces while deposition of the polymer as an adhesive to the fabric as an adherent [3]

According to different considered models in the analysis of variance (ANOVA) test and related P-values, the best model which fits the effect of processing parameters on adhesion force of PA6.6/6 deposited onto the PA6.6 fabric is shown in Equation 7 (β_i is constant):

$$y = \beta_1 + \beta_1 x_1 + \beta_2 x_2 + \beta_3 x_2^2 \quad (7)$$

Which

$$y\ is\ adhesion\ force$$
$$x_1\ is\ extruder\ temperature$$
$$x_2\ is\ printing\ speed$$

As long as the platform temperature is not higher than the glass transition temperature of the applied fabric, the model is fitted. Interaction plot of different discussed processing parameters is shown in Figure 55 which help to see the variation of the response to one factor in different levels of another factor. The interaction plot clearly can represent the linear effect of extruder temperature, no effect of platform temperature and quadratic effect of printing speed on adhesion force. Interaction of the parameters is not effective in this experiment.

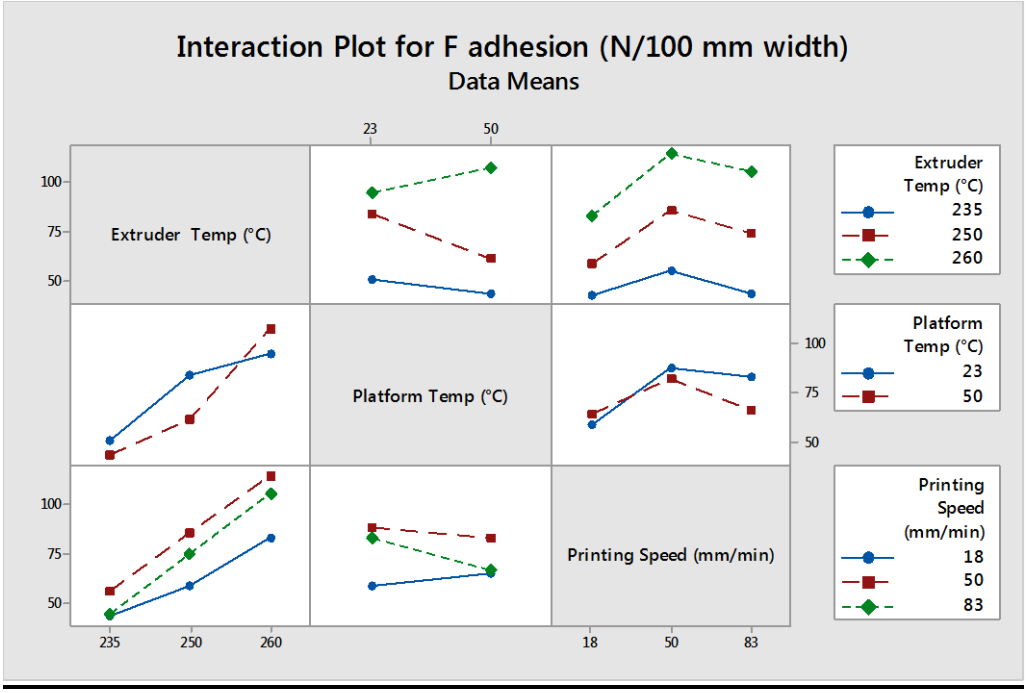

Figure 55 Interaction plot for adhesion force versus different processing parameters of the 3D printing for PA6.6/6 deposited on PA6.6 fabric [3]

5.2 PLA onto PA6.6 fabric

Deposition of PLA on PA6.6 was done in two steps according to Table 2: a single factor experiment (No. 2) with extruder temperature as a variable factor (190, 210, 230°C) and then a factorial experiment (No. 3) with platform temperature (23, 50, 70°C) and fabric type (1,2) variables. Minitab analysis of the results showed that there is the significant linear effect of the factor extruder temperature on adhesion and the highest temperature applied for extruding PLA (230°C) on PA causes the highest adhesion force (12 N/100mm) (Figure 56a) which is in agreement with previous results for PA6.6/6 on PA. When the platform temperature increases to 70°C which is higher than the glass transition temperature of PA6.6 which is 55°C, it has a significant linear effect on adhesion as it is discussed above (Figure 56b). Fabric type also shows a significant linear effect (Figure 56c). PA fabric type 2 with higher yarn count in warp per centimeter (warp 39 × weft 27 / 180 ×180 dtex) in comparison with fabric type 1 (warp 50× weft 30 / 78×180 dtex) shows higher adhesion properties. The closeness of yarns increases fabric covering properties and decrease fabric surface roughness [179]. Mechanical interlocking states that decrease in adherent surface roughness will cause decrease in the adhesion of adhesive to adherent because if a surface is rough the adhesive can penetrate into the pores and then lock mechanically to the surface [24]. However, mechanical interlocking is a controversial theory since there are some experiments such as above results showing that decrease in

roughness can increase the adhesion. In adhesion studies of 3D printed layers to fabrics, it is assumed that the dominant theory is diffusion. Therefore, it seems the segments of long polymer chains above their T_g can diffuse more into the fabric with higher covering factor. Therefore, the surface structure of the fabric also affects the adhesion force.

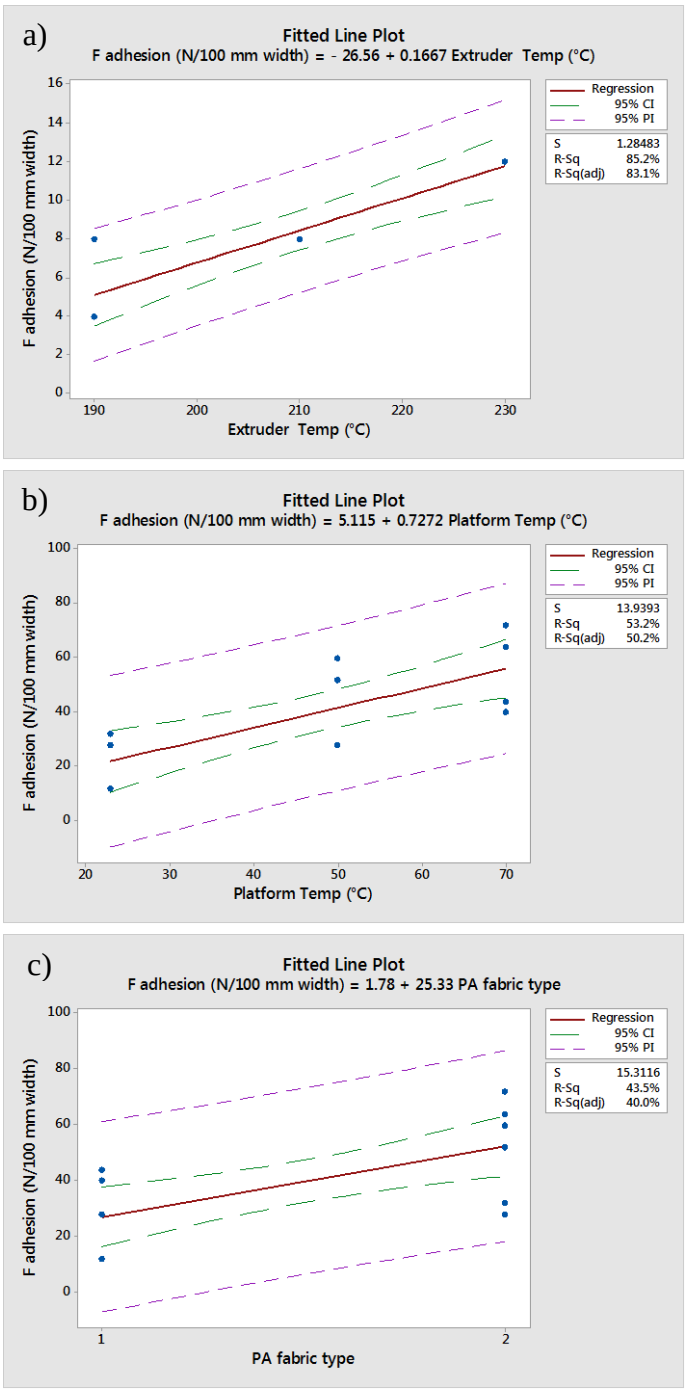

Figure 56 Effect of different variables of the 3D printing process on adhesion force of PLA deposited on PA6.6 fabric (a) extruder temperature (b) platform temperature (c) PA6.6 fabric type [3]

5.3 PLA on PLA fabric

Samples number 27 to 44 in Table 3 are related to different treatments of experiment number 4 which the applied factors and levels and the adhesion results also are presented in details. When the deposited polymer is being debonded from fabric, there are three possible modes of failure including adhesive failure with debonding of deposited polymer from fabric, cohesive failure or breaking the deposited polymer itself and fabric tear or failure itself. While peeling test for PLA deposited on PLA fabrics, two of mentioned modes happened: (1) fabric tear or failure and (2) breaking the 3D printed polymer layer (cohesive failure) (Figure 57) which shows high peeling strength and proves high adhesion of PLA deposited on PLA.

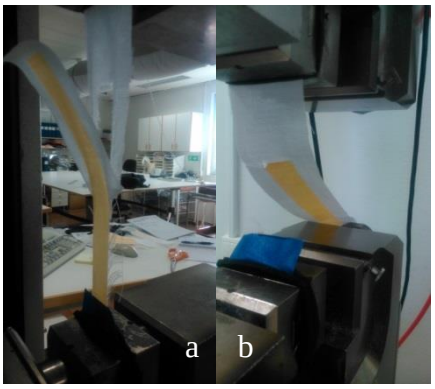

Figure 57 (a) fabric tearing (b) deposited layer breakage during adhesion test [3]

PLA is an aliphatic biopolyester which has vicinal and regularly distributed polar ester groups [180]. The high adhesion between deposited PLA on PLA also can be described by high-efficiency diffusion of extruded PLA filament into PLA fabric and their low interfacial tension due to the similar chemical nature of both and interpolymer polar interactions (Van der Waals dipole-dipole interactions) across phase boundaries.

As it is shown in Figure 58, 3D printed polymer layer failure during peeling test has happened in samples 29, 33, 34, 38, 42 and 43. According to Table 3, it is obvious that low extruder temperature with a high printing speed of 3D printing has been applied in samples 29 and 38. In this case, feeding of the polymer could not be done properly to deposit layers uniformly. Applying high extruder temperature with low printing speeds also cause failure of deposited layers during the peeling test in samples 33, 34, 42 and 43. Breakage of the deposited layers can be used to denote the brittleness which means a lack of ductility or stretchability and poor flexibility [181]. Brittleness of the samples prepared in low 3D printing speeds like 18 mm/min

with high processing temperatures like 230°C can be attributed to the formation of more polar interchain interactions when PLA remains for more time span in high temperature. Therefore, polar groups can affect the physicochemical interactions between polymer chains and reduce more the possibility of chain shear throughout physical deformation. This phenomenon can explain the high brittleness of the mentioned samples. In such samples deposited layer break strength is lower than the adhesion force of the deposited polymer on fabric. In other samples according to Figure 58, the fabric was torn during the peeling test which means that the tearing strength of the fabric was lower than the adhesion force of PLA deposited on fabric.

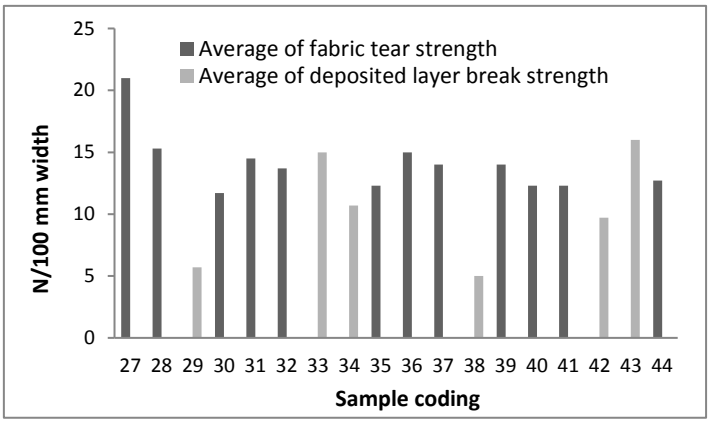

Figure 58 Average of fabric tear strength and deposited layer break strength during adhesion test of PLA deposited on PLA fabric [3]

5.4 CPCs on PLA fabric

In this section, the adhesion properties of two types of CPC including PLA/ 2 wt.% MWNT and PLA/ 5 wt.% KB deposited on PLA fabrics are reported. The selected 3D printer filament has almost the same conductivity of 0.04 S/cm to investigate the difference in properties of the printed layers with two different types of filler with the same conductivity in their 3D printer filament.

In the experiment No. 5, the considered factors were extruder temperature (240, 260°C), platform temperature (23, 50°C), PLA fabric type (Panama (1), Twill (2)) and filler type (2% MWNT (1), 5% KB (2)) which the treatment combination and adhesion results for samples 46 to 60 are shown in detail in Table 3. The chosen weaves were panama 2/2 and twill 2/1. In panama weave 2/2, groups of two warp and two weft threads are interlaced so they form a simple crisscross pattern like plain weave. The reason the panama and twill was weaved instead

of the plain was that mentioned weave structures are stronger than plain weave with the same yarn for doing successful peeling test.

As it is shown in figure 59, while peeling test of deposited PLA nanocomposites on PLA fabrics, separated from treatment combination selection, two modes of failure happened including 3D printed layer break (cohesive failure) and fabric tear or failure which proves again, as discussed above, high adhesion force of PLA nanocomposites deposited on PLA.

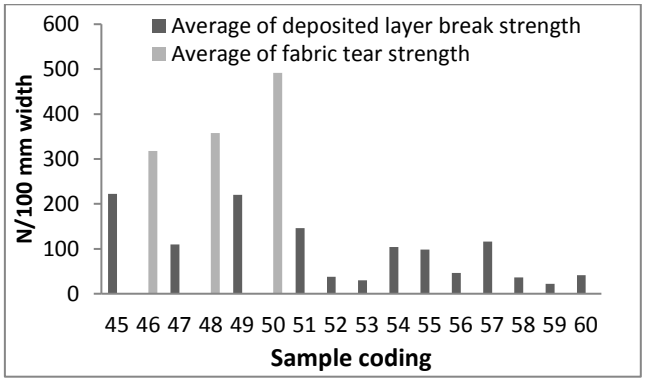

Figure 59 Average of fabric tear strength and deposited layer break strength during adhesion test of PLA nanocomposites deposited on PLA fabric

Incorporation of MWNTs and KB make PLA more polar. ANOVA test showed that deposited layers including 5% KB in comparison with 2% MWNT layers have lower break strength which means they are more brittle (Figure 60a). Fillers like carbon black which is spherical and has a low aspect ratio in comparison with CNTs with high aspect ratio, require higher filler contents to get conductive polymer-based composite which makes the polymer more brittle. In addition, higher extruder temperature causes lower deposited layer break strength which is compatible with the above results on the effect of extruder temperature on brittleness of the deposited PLA (Figure 60b).

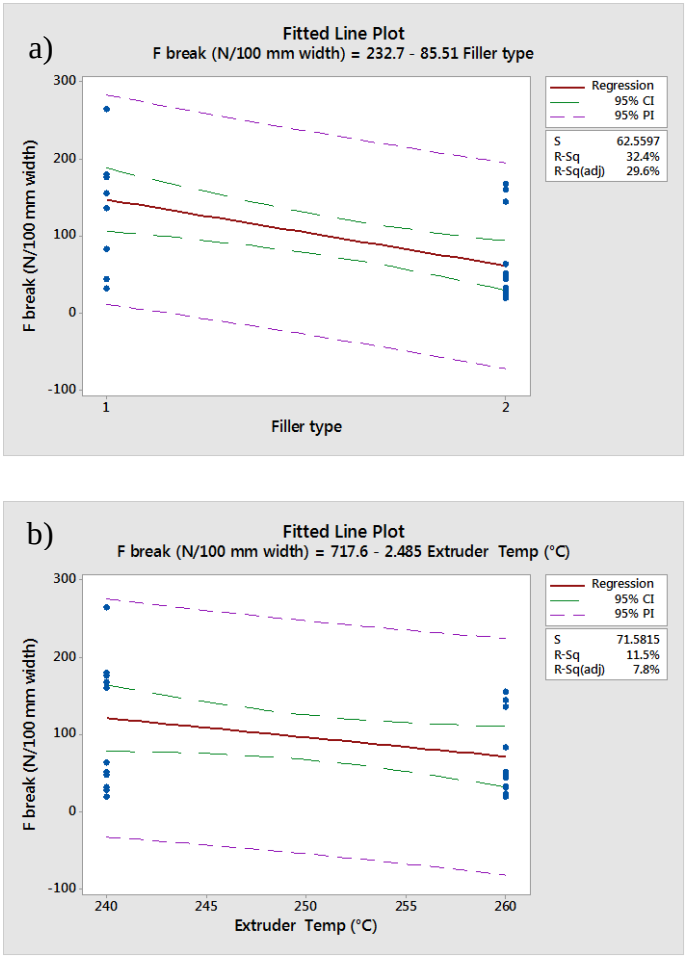

Figure 60 Effect of (a) filler type (b) extruder temperature on break strength of nanocomposite 3D printed layers [3]

5.5 Conclusion

Polymer deposition onto textiles depends strongly on the polymer-textile combination which covers different aspects of material/polymer science, material/polymer compatibility, polymer-textile adhesion, and polymer deposition technology. This chapter of the thesis has contributed to new knowledge by using direct 3D printing with FDM technology on fabrics to provide a better understanding of textile-polymer adhesion phenomena. This method is proposed to the possibility of developing innovative smart textiles by integrating functional polymers with textiles without compromising on quality and flexibility of the fabric. Different variables which may affect the adhesion properties including 3D printing process parameters, fabric type and filler type in composites were considered. The polymers were printed in different series of experimental design: PA6.6/6 on PA6.6 fabric, PLA on PA6.6 fabric, PLA on PLA fabric, and finally PLA/KB and PLA/MWNT nanocomposites on PLA fabrics.

It is concluded that different 3D printing processing parameters can have a significant effect on the adhesion of polymers to fabrics. According to the best-fitted model, there is a significant linear effect of extruder temperature and significant quadratic effect of printing speed on the adhesion force of PA6.6/6 on PA6.6 fabric. Platform temperature does not have a significant effect on adhesion force if the temperature is lower than the glass transition temperature of the applied fabric. These phenomena can be explained by diffusion theory which explains the adhesion of polymers to each other by the diffusion of chainlike molecules which leads to the formation of a strong bond between adhesive and adherent. PLA deposited on PA fabric does not show high adhesion force since two polymers are not compatible; yet, it confirms our former results regarding the effect of extruder and platform temperature on adhesion force and shows that fabric surface structure as well can be effective.

The adhesion force of deposited PLA and PLA nanocomposites on PLA fabrics are completely high which in all samples according to the strength of the deposited layer and fabric, tearing of the fabric or breaking of the deposited layers happened which polar ester groups in both adhesive and adherent with the help of diffusion theory can explain this phenomenon.

5% KB PLA nanocomposites in comparison with 2% MWNT 3D printed layers showed lower break strength which expresses it is more brittle. In addition, higher extruder temperatures cause lower 3D printed layer break strength which denotes using high extruder temperatures can be the cause of higher brittleness.

6 Conclusions and future work

Textile industry needs to introduce more effective processes avoiding unnecessary use of water, energy, chemicals and minimization of waste materials. However, there are lots of challenges to achieve the goal for example the technologies are not ready yet to respond to the needs of industry, and the awareness and education is needed to apply resource-effective processes in textiles. This thesis focused on applying a novel technology for development of functional and smart textiles. The most challenging problem in smart textile market is that the existing technologies can not respond to the customized needs, therefore the economy and production scale challenges still exist. 3D printing was applied in this thesis as a flexible technology to enable customized production with less water, chemical and energy for different possible applications such as integrating sensors and interconnections directly on fabric where they are needed, water and solvent-free as well as patterned functionalization processes.

The thesis has been able to answer to the below research questions were set as guidelines to fulfill the goals.

1) What are the characteristics of conductive polymer nanocomposites before and after FDM 3D printing?

To answer the first research question, conductive polymer nanocomposite 3D printer filaments containing two types of nanofillers including MWNT and KB were created using a melt mixing process. The focus was on the morphological, electrical, thermal and mechanical properties of CPCs in different forms before and after 3D printing. The results showed that there was no dependence of developed rod diameter on the MWNT loading, instead, the diameter was dependent on the KB loading and increased with increasing the filler amount.

Electrical properties were measured using two different systems including two-point measurement (2w) and four-point measurement (4w). A 4w method in comparison with 2w showed lower percolation thresholds and higher conductivity especially in the case of anisotropic nanocomposite filament containing nanotubes, therefore 4w method is proposed to apply if precise results are needed. Presenting the lower percolation thresholds and more precise results can be attributed to eliminating the effect of contact resistance by 4W measuring system.

KBs as spherical particles showed the higher percolation threshold in comparison with MWNTs, as the percolation threshold is proportional to the ratio of the average particle diameter over its mean length. However, the percolation threshold of 1.7 wt.% for KB in comparison with other types of CBs showed the effectiveness as the promising filler to enhance the conductivity of PLA filaments.

The conductivity of the extruded filaments from 3D printer decreases up to several orders of magnitude in comparison with loaded filaments in both conductivity curves of MWNT and KB composites. The effect of extruder temperature on the conductivity of monofilaments extruded from the 3D printer was investigated. The conductivity of filaments in low filler contents decreases with increasing extruder temperature, yet in higher filler contents there is no effect of extruder temperature on conductivity. More, two CPC including 2% MWNT and 5% KB were applied to 3D print tracks with different cross-sectional areas. Results show that the resistance decreases exponentially with the increase of the cross-sectional area of 3D printed tracks. In 3D printed layers, the sudden transition from insulator to conductor which is the indication of percolation threshold happened in PLA/4 wt.% KB and PLA/1 wt.% MWNT.

In manufactured 3D printer PLA filaments, the addition of KB and MWNT significantly lowered the crystallization temperature values (up to about 20 for KB and to 35 ˚C for MWNT) which signify that both fillers have the positive effect on crystallization and acted as a nucleating agent and accelerated overall crystallization. However, crystallinity percent of 3D printed layers remarkably decreased in comparison with the 3D printer filaments. The annealing process could affect the 3D printed samples by increasing the crystallinity percent.

DMTA curves showed that there is no significant difference in storage modulus of various composites of PLA 3D printer filaments at 40°C (below Tg), but the stiffening effect of the fillers especially nanotubes is specifically significant at higher temperatures like 90°C. The storage modulus of the 3D printed nanocomposites of KB (below and over T_g) was found to substantially increase with the KB content in the PLA matrix. By adding 0.5 wt.% MWNT to PLA matrix, the storage modulus of 3D printed layers increased. However, with increasing the filler content to 5 wt. %, the storage modulus at 40°C decreased significantly. The stiffening effect of the MWNT is specifically significant at higher temperatures like 90°C, therefore, the presence of fillers enables the 3D printer filaments and 3D printed layers to sustain a higher modulus value to higher temperature.

Finally, the 3D printed layers on fabric showed lower storage modulus at 40˚C in comparison with the 3D printed layers which means more flexibility. However, the 3D printed layers on the fabric have the higher storage modulus at 90˚C in comparison with 3D printed layers which again shows the positive effect of printing on fabric as the storage modulus of the 3D printed layers of PLA nanocomposites is too low in high temperatures like 90˚C. Accordingly, 3D printing of nanocomposites on fabrics gives rise to the flexibility of these nanocomposites for different applications in smart and functional textiles.

2) What is the functionality of the CPC FDM 3D printed layers?

To answer the second research question, the CPCs were 3D printed and the piezoresistivity of 3D printed layers in tension and compression mode was investigated. Results showed it is possible to FDM 3D print piezoresistive PLA nanocomposite layers from the MWNT and KB fillers and PLA matrix. For PLA/1 wt.% MWNT 3D printed layers with 1mm thickness, there is no significant change in resistance with tensile stress but, in compression mode, it exhibits a negative pressure coefficient (NPC) characterized by a decrease of about one decade in resistance with increasing compressive loadings up to 18 N with the maximum strain up to about 16%. In the cyclic mode with the1N/min force rate, PLA/1 wt.% MWNT 3D printed layers showed good performance with the value of G = 7.6 obtained with the amplitude of the piezoresistive response of about A_r = -0.8 (-80%). The response was linear in the range of pressure 10-100 kPa, with low noise and hysteresis which is come from the layer by layer architecture of the component and tunneling effect of MWNT nanofillers in lower contents than the percolation threshold. In high force rate 18N/min, the piezoresistive response of PLA/ 1 wt.% MWNT has a smaller amplitude (A_r = -0.60) and more noisy signals but the value of G = 9.3 obtained which imply that the high force rate does not decrease the piezoresistive effect of PLA/ 1 wt.% MWNT 3D printed layers, even though it is increased. Therefore, the decrease in sensitivity is because of lower strain rates in high force rates. KB composites could not show stable piezoresistive responses in a cyclic mode. However, in high force rate, PLA/4 wt.% KB 3D printed layers is leading to responses of large sensitivity (A_r = -0.90) and exempt of noise with the value of G = 47.6 obtained in the first cycle of applied stress which is highly efficient piezoresistive behavior, however decreases to G = 28 in 10^{th} cycle of stress. The results demonstrate PLA/MWNT and PLA/KB as a piezoresistive feedstock for 3D printing with the possible applications in wearable electronics, soft robotics, and prosthetics, where complex design, multi-directionality, and customizability are demanded.

3) What is the effect of different variables of FDM 3D printing process on the adhesion properties of deposited polymer and nanocomposites on textile fabric?

To answer the third research question, different polymers and nanocomposites were printed on some different fabrics. Effect of different variables of FDM printing process was investigated on the adhesion which is one of the most important factors of polymer deposition on fabrics and a best-fitted model was proposed. The results showed that different 3D printing processing parameters can have a significant effect on the adhesion of polymers to fabrics. According to the best-fitted model, there is a significant linear effect of extruder temperature and significant quadratic effect of printing speed on the adhesion force of PA6.6/6 on PA6.6 fabric. Platform temperature does not have a significant effect on adhesion force if the temperature is lower than

the glass transition temperature of the applied fabric. These phenomena can be explained by diffusion theory which explains the adhesion of polymers to each other by the diffusion of chainlike molecules which leads to the formation of a strong bond between adhesive and adherent. PLA deposited on PA fabric does not show high adhesion force since two polymers are not compatible; yet, it confirms our former results regarding the effect of extruder and platform temperature on adhesion force and shows that fabric surface structure as well can be effective.

The adhesion force of deposited PLA and PLA nanocomposites on PLA fabrics are completely high which in all samples according to the strength of the deposited layer and fabric, tearing of the fabric or breaking of the deposited layers happened which polar ester groups in both adhesive and adherent with the help of diffusion theory can explain this phenomenon.

The outcomes of this thesis can motivate future research in several directions. Some suggestions are given below.

- Applying more flexible polymers such as thermoplastic elastomers (TPE), soft PLA and polyurethane (TPU) as the matrix of the nanocomposite and different fillers like graphene
- Modification of the 3D printer head to print flexible polymers
- Proposing a combined model for adhesion of polymers onto fabrics considering both 3D printing process variables and fabric structure parameters
- Investigation of the effect of temperature, stress area and layer thickness on the piezoresistivity of PLA nanocomposites
- Investigation the functionality of 3D printed composites (with desired pattern and composition) as chemical, humidity and temperature sensors
- Investigation the performance of the proposed technology for other functionalization processes other than making smart textiles

References

[1] A. Schwarz, L. Van Langenhove, D. Deguillemont, and P. Guermonprez, "A roadmap on smart textiles," *Text. Prog.*, vol. 42, no. 2, pp. 99–180, 2010.

[2] L. A. Verhoef, B. W. Budde, C. Chockalingam, B. García Nodar, and A. J. M. van Wijk, "The effect of additive manufacturing on global energy demand: An assessment using a bottom-up approach," *Energy Policy*, vol. 112, pp. 349–360, 2018.

[3] R. Hashemi Sanatgar, C. Campagne, and V. Nierstrasz, "Investigation of the adhesion properties of direct 3D printing of polymers and nanocomposites on textiles: Effect of FDM printing process parameters," *Appl. Surf. Sci.*, vol. 403, pp. 551–563, 2017.

[4] European Committee for Standardization, "CEN/TR 16298:2011 Textiles and textile products – smart textiles – definitions, categorizations, applications and standardization needs," 2011.

[5] X. Tao, "1 - Smart technology for textiles and clothing – introduction and overview," in *Smart Fibres, Fabrics and Clothing*, X. Tao, Ed. Woodhead Publishing, 2001, pp. 1–6.

[6] T. Kirstein, "1 - The future of smart-textiles development: new enabling technologies, commercialization and market trends," in *Multidisciplinary Know-How for Smart-Textiles Developers*, Woodhead Publishing, 2013, pp. 1–25.

[7] J. W. Stansbury and M. J. Idacavage, "3D printing with polymers: Challenges among expanding options and opportunities," in *Dental Materials*, 2016, vol. 32, no. 1, pp. 54–64.

[8] T. A. Campbell and O. S. Ivanova, "3D printing of multifunctional nanocomposites," *Nano Today*, vol. 8, no. 2, pp. 119–120, 2013.

[9] P. Dudek, "FDM 3D Printing Technology in Manufacturing Composite Elements," *Arch. Metall. Mater.*, vol. 58, no. 4, pp. 10–13, 2013.

[10] M. Lukic, J. Clarke, C. Tuck, W. Whittow, and G. Wells, "Printability of elastomer latex for additive manufacturing or 3D printing," *J. Appl. Polym. Sci.*, vol. 133, no. 4, 2016.

[11] D. Espalin, D. W. Muse, E. MacDonald, and R. B. Wicker, "3D Printing multifunctionality: Structures with electronics," *Int. J. Adv. Manuf. Technol.*, vol. 72, no. 5–8, pp. 963–978, 2014.

[12] Y. Xu *et al.*, "The Boom in 3D-Printed Sensor Technology," *Sensors (Basel).*, vol. 17, no. 5, May 2017.

[13] R. Melnikova, A. Ehrmann, and K. Finsterbusch, "3D printing of textile-based structures by Fused Deposition Modelling (FDM) with different polymer materials," *IOP Conf. Ser. Mater. Sci. Eng.*, vol. 62, no. 1, p. 12018, 2014.

[14] C. K. Chua, K. F. Leong, and C. S. Lim, *Rapid Prototyping*. WORLD SCIENTIFIC,

2010.

[15] J. Mueller, J. R. Raney, K. Shea, and J. A. Lewis, "Architected Lattices with High Stiffness and Toughness via Multicore–Shell 3D Printing," *Adv. Mater.*, vol. 30, no. 12, pp. 1–8, 2018.

[16] Y. Chen, T. Li, Z. Jia, F. Scarpa, C. W. Yao, and L. Wang, "3D printed hierarchical honeycombs with shape integrity under large compressive deformations," *Mater. Des.*, vol. 137, pp. 226–234, 2018.

[17] R. H. Sanatgar, A. Cayla, C. Campagne, and V. Nierstrasz, "Morphological and electrical characterization of conductive polylactic acid based nanocomposite before and after FDM 3D printing," *J. Appl. Polym. Sci.*, vol. 136, no. 6, p. 47040, 2019.

[18] M. Fahad, P. Dickens, and M. Gilbert, "Novel polymeric support materials for jetting based additive manufacturing processes," *Rapid Prototyp. J.*, vol. 19, no. 4, pp. 230–239, 2013.

[19] M. Hofmann, "3D printing gets a boost and opportunities with polymer materials," *ACS Macro Lett.*, vol. 3, pp. 382–386, 2014.

[20] P. K. Jain, P. M. Pandey, and P. V. M. Rao, "Effect of delay time on part strength in selective laser sintering," *Int. J. Adv. Manuf. Technol.*, vol. 43, pp. 117–126, 2009.

[21] S. Shaffer, K. Yang, J. Vargas, M. A. Di Prima, and W. Voit, "On reducing anisotropy in 3D printed polymers via ionizing radiation," *Polymer (Guildf).*, vol. 55, pp. 5969–5979, 2014.

[22] J. A. Von Fraunhofer, "Adhesion and cohesion," *Int. J. Dent.*, vol. ID 951324, 2012.

[23] J. K. Kim, S. Thomas, and P. Saha, Eds., *Multicomponent Polymeric Materials*, vol. 223. Dordrecht: Springer Netherlands, 2016.

[24] M. Björkman, "Improved Adhesion of Polyolefin Laminates to Textiles Using New Plasma Technology," Chalmers University of Technology, 2012.

[25] E. P. Scilingo, F. Lorussi, A. Mazzoldi, and D. De Rossi, "Strain-sensing fabrics for wearable kinaesthetic-like systems," *IEEE Sens. J.*, vol. 3, no. 4, pp. 460–467, 2003.

[26] F. Lorussi, W. Rocchia, E. P. Scilingo, A. Tognetti, and D. De Rossi, "Wearable, redundant fabric-based sensor arrays for reconstruction of body segment posture," *IEEE Sens. J.*, vol. 4, no. 6, pp. 807–818, 2004.

[27] Y. Li, X. Y. Cheng, M. Y. Leung, J. Tsang, X. M. Tao, and M. C. W. Yuen, "A flexible strain sensor from polypyrrole-coated fabrics," *Synth. Met.*, vol. 155, pp. 89–94, 2005.

[28] C. Cochrane, V. Koncar, M. Lewandowski, and C. Dufour, "Design and development of a flexible strain sensor for textile structures based on a conductive polymer composite," *Sensors*, vol. 7, no. 4, pp. 473–492, 2007.

[29] W. Yi, Y. Wang, G. Wang, and X. Tao, "Investigation of carbon black/silicone elastomer/dimethylsilicone oil composites for flexible strain sensors," *Polym. Test.*, vol. 31, pp. 677–684, 2012.

[30] K. Yang, R. Torah, Y. Wei, S. Beeby, and J. Tudor, "Waterproof and durable screen printed silver conductive tracks on textiles," *Text. Res. J.*, vol. 83, no. 19, pp. 2023–2031, 2013.

[31] I. Kazani, C. Hertleer, G. De Mey, G. Guxho, and L. Van Langenhove, "Dry cleaning of electroconductive layers screen printed on flexible substrates," *Text. Res. J.*, vol. 83, no. 14, pp. 1541–1548, 2013.

[32] G. Paul, R. Torah, S. Beeby, and J. Tudor, "The development of screen printed conductive networks on textiles for biopotential monitoring applications," *Sensors Actuators, A Phys.*, vol. 206, pp. 35–41, 2014.

[33] S. Merilampi, T. Laine-Ma, and P. Ruuskanen, "The characterization of electrically conductive silver ink patterns on flexible substrates," *Microelectron. Reliab.*, vol. 49, no. 7, pp. 782–790, 2009.

[34] I. Kazani, C. Hertleer, G. de Mey, A. Schwarz, G. Guxho, and L. van Langenhove, "Electrical conductive textiles obtained by screen printing," *Fibres Text. East. Eur.*, vol. 90, no. 1, pp. 57–63, 2012.

[35] G. Paul, R. Torah, K. Yang, S. Beeby, and J. Tudor, "An investigation into the durability of screen-printed conductive tracks on textiles," *Meas. Sci. Technol.*, vol. 25, no. 2, p. 025006, 2014.

[36] W. Zeng, L. Shu, Q. Li, S. Chen, F. Wang, and X. Tao, "Fiber-Based Wearable Electronics: A Review of Materials, Fabrication, Devices, and Applications," *Adv. Mater.*, vol. 26, no. 31, pp. 5310–5336, 2014.

[37] B. H. Nguyen and V. H. Nguyen, "Promising applications of graphene and graphene-based nanostructures," *Adv. Nat. Sci. Nanosci. Nanotechnol.*, vol. 7, no. 2, p. 023002, 2016.

[38] Z. Stempien, E. Rybicki, T. Rybicki, and J. Lesnikowski, "Inkjet-printing deposition of silver electro-conductive layers on textile substrates at low sintering temperature by using an aqueous silver ions-containing ink for textronic applications," *Sensors Actuators, B Chem.*, vol. 224, pp. 714–725, 2015.

[39] J. Kastner *et al.*, "Silver-based reactive ink for inkjet-printing of conductive lines on textiles," *Microelectron. Eng.*, vol. 176, pp. 84–88, 2017.

[40] C. Paragua, K. Frigui, S. Bila, and D. Baillargeat, "Study and characterization of CNT Inkjet printed patterns for paper-based RF components," 2015, pp. 861–864.

[41] J. Tudor *et al.*, "Inkjet printed dipole antennas on textiles for wearable communications," *IET Microwaves, Antennas Propag.*, vol. 7, no. 9, pp. 760–767, Jun. 2013.

[42] X. Tao, Ed., *Handbook of Smart Textiles*. Singapore: Springer Singapore, 2015.

[43] A. Chauraya *et al.*, "Inkjet printed dipole antennas on textiles for wearable communications," *IET Microwaves, Antennas Propag.*, vol. 7, no. April, pp. 760–767, 2013.

[44] W. G. Whittow *et al.*, "Inkjet-Printed Microstrip Patch Antennas Realized on Textile for Wearable Applications," *IEEE Antennas Wirel. Propag. Lett.*, vol. 13, pp. 71–74, 2014.

[45] Y. L. Tai, Z. G. Yang, and Z. D. Li, "A promising approach to conductive patterns with high efficiency for flexible electronics," *Appl. Surf. Sci.*, vol. 257, no. 16, pp. 7096–7100, 2011.

[46] G. J. Brinks, M. M. C. . Warmoeskerken, R. Akkerman, and W. Zweers, "the Added Value of 3D Polymer Deposition on Textiles," in *13th AUTEX World Textile Conference*, 2013, pp. 1–6.

[47] E. Pei, J. Shen, and J. Watling, "Direct 3D printing of polymers onto textiles: experimental studies and applications," *Rapid Prototyp. J.*, vol. 21, no. 5, pp. 556–571, 2015.

[48] I. Holme, "Adhesion to textile "bres and fabrics," *J. Adhes.*, vol. 19, no. June, 1999.

[49] E. P. T. Spahiu1, N. Grimmelsmann, A. Ehrmann and E. Shehi, "Effect of 3D printing on textile fabric," in *Engineering and Entrepreneurship*, 2017.

[50] L. Sabantina, F. Kinzel, A. Ehrmann, and K. Finsterbusch, "Combining 3D printed forms with textile structures - mechanical and geometrical properties of multi-material systems," *IOP Conf. Ser. Mater. Sci. Eng.*, vol. 87, no. October, p. 012005, 2015.

[51] C. Döpke, N. Grimmelsmann, and A. Ehrmann, "3D printing on knitted fabrics," *Melliand Int.*, vol. 97, pp. 97–98, 2017.

[52] N. Grimmelsmann, M. Lutz, M. Korger, H. Meissner, and A. Ehrmann, "Adhesion of 3D printed material on textile substrates," *Rapid Prototyp. J.*, vol. 24, pp. 166–170, 2018.

[53] T. Spahiu, M. Al-Arabiyat, Y. Martens, A. Ehrmann, E. Piperi, and E. Shehi, "Adhesion of 3D printing polymers on textile fabrics for garment production," *IOP Conf. Ser. Mater. Sci. Eng.*, vol. 459, p. 12065, 2018.

[54] N. Grimmelsmann, H. Meissner, and A. Ehrmann, "3D printed auxetic forms on knitted fabrics for adjustable permeability and mechanical properties," in *IOP Conference Series: Materials Science and Engineering*, 2016.

[55] J. N. Grima, D. Attard, R. Gaff, and R. N. Cassar, "A novel process for the manufacture of auxetic foams and for their re-conversion to conventional form," *Adv. Eng. Mater.*, vol. 11, no. 7, pp. 533–535, 2009.

[56] J. Neuß, M. Kreuziger, N. Grimmelsmann, M. Korger, and A. Ehrmann, "Interaction between 3D deformation of textile fabrics and imprinted lamellae," 2016.

[57] E. Kreikebaum, M. Kreuziger, M. Doerfel, K. Finsterbusch, and A. Ehrmann, "3D printing of Braille on textiles," *Tech. Text. Int.*, vol. 59, pp. E187–E188, 2016.

[58] R. V. Subramanian, "Chemistry of Adhesion," in *The Chemistry of Solid Wood*, American Chemical Society, 1984, pp. 323–348.

[59] M. Korger, J. Bergschneider, M. Lutz, B. Mahltig, K. Finsterbusch, and M. Rabe, "Possible applications of 3D printing technology on textile substrates," in *IOP Conference Series: Materials Science and Engineering*, 2016.

[60] T. Kozior, C. Döpke, N. Grimmelsmann, I. Juhász Junger, and A. Ehrmann, "Influence of fabric pretreatment on adhesion of three-dimensional printed material on textile substrates," *Adv. Mech. Eng.*, vol. 10, no. 8, pp. 1–8, 2018.

[61] A. Gorzen *et al.*, "Increasing adhesion of 3D printing on textile fabrics by polymer coating," *TEKSTILEC*, vol. 61, no. 4, pp. 265–271, 2018.

[62] P. A. Eutionnat-Diffo *et al.*, "Correlation between heat transfer of polyester textiles and its adhesion with 3D-printed extruded thermoplastic filaments," *18th AUTEX World Text. Conf.*, pp. 20–23, 2018.

[63] T. M. Tenhunen *et al.*, "Surface tailoring and design-driven prototyping of fabrics with 3D-printing: An all-cellulose approach," *Mater. Des.*, vol. 140, pp. 409–419, 2018.

[64] T. Spahiu, S. Fafenrot, N. Grimmelsmann, E. Piperi, E. Shehi, and A. Ehrmann, "Varying fabric drape by 3D-imprinted patterns for garment design," *IOP Conf. Ser. Mater. Sci. Eng.*, vol. 254, no. 172023, 2017.

[65] N. Grimmelsmann, Y. Martens, P. Schäl, H. Meissner, and A. Ehrmann, "Mechanical and Electrical Contacting of Electronic Components on Textiles by 3D Printing," *Procedia Technol.*, vol. 26, pp. 66–71, 2016.

[66] M. G. Tadesse, D. Dumitrescu, C. Loghin, Y. Chen, L. Wang, and V. Nierstrasz, "3D Printing of NinjaFlex Filament onto PEDOT:PSS-Coated Textile Fabrics for Electroluminescence Applications," *J. Electron. Mater.*, vol. 47, no. 3, pp. 2082–2092, 2018.

[67] D. Vollath, *Nanoparticles, nanocomposites, nanomaterials : an introduction for beginners*, 1st ed. Wiley, 2013.

[68] B. Wessling, "Electrical conductivity in heterogeneous polymer systems. V (1): Further experimental evidence for a phase transition at the critical volume concentration," *Polym. Eng. Sci.*, vol. 31, no. 16, pp. 1200–1206, Aug. 1991.

[69] A. B. Makar, K. E. McMartin, M. Palese, and T. R. Tephly, "Formate assay in body fluids: application in methanol poisoning.," *Biochem. Med.*, vol. 13, no. 2, pp. 117–26, Jun. 1975.

[70] S. A. Mirmohammadi, S. Sadjadi, and N. Bahri-laleh, "10 - Electrical and Electromagnetic Properties of CNT/Polymer Composites," in *Carbon Nanotube-*

Reinforced Polymers, Elsevier Inc., 2018, pp. 233–258.

[71] H. Oxfall, G. Ariu, T. Gkourmpis, R. W. Rychwalski, and M. Rigdahl, "Effect of carbon black on electrical and rheological properties of graphite nanoplatelets/poly(ethylene-butyl acrylate) composites," *EXPRESS Polym. Lett.*, vol. 9, no. 1, pp. 66–76, 2015.

[72] A. Celzard, J. F. Marêché, F. Payot, and G. Furdin, "Electrical conductivity of carbonaceous powders," *Carbon N. Y.*, vol. 40, no. 15, pp. 2801–2815, 2002.

[73] J.-B. Donnet, R. C. Bansal, and M.-J. Wang, *Carbon black : science and technology*. Dekker, 1993.

[74] D. Fitz-Gerald and J. Boothe, "Manufacturing and Characterization of Poly (Lactic Acid)/Carbon Black Conductive Composites for FDM Feedstock: An Exploratory Study," California Polytechnic State University, 2016.

[75] V. Kumar, S. Kalia, and H. C. Swart, *Conducting Polymer Hybrids*. Springer International Publishing, 2017.

[76] A. Dorigato, V. Moretti, S. Dul, S. H. Unterberger, and A. Pegoretti, "Electrically conductive nanocomposites for fused deposition modelling," *Synth. Met.*, vol. 226, pp. 7–14, 2017.

[77] S. M. Lebedev, O. S. Gefle, E. T. Amitov, D. Y. Berchuk, and D. V. Zhuravlev, "Poly(lactic acid)-based polymer composites with high electric and thermal conductivity and their characterization," *Polym. Test.*, vol. 58, pp. 241–248, 2017.

[78] B. Sitharaman *et al.*, "In vivo biocompatibility of ultra-short single-walled carbon nanotube/biodegradable polymer nanocomposites for bone tissue engineering," *Bone*, vol. 43, no. 2, pp. 362–370, 2008.

[79] K. Gnanasekaran *et al.*, "3D printing of CNT- and graphene-based conductive polymer nanocomposites by fused deposition modeling," *Appl. Mater. Today*, vol. 9, pp. 21–28, 2017.

[80] K. Prashantha and F. Roger, "Multifunctional properties of 3D printed poly(lactic acid)/graphene nanocomposites by fused deposition modeling," *J. Macromol. Sci. Part A*, vol. 54, no. 1, pp. 24–29, Jan. 2017.

[81] E. MacDonald and R. Wicker, "Multiprocess 3D printing for increasing component functionality," *Science*, vol. 353, no. 6307. 2016.

[82] Y. S. Rim, S. H. Bae, H. Chen, N. De Marco, and Y. Yang, "Recent Progress in Materials and Devices toward Printable and Flexible Sensors," *Adv. Mater.*, vol. 28, pp. 4415–4440, 2016.

[83] S. B. Kesner and R. D. Howe, "Design principles for rapid prototyping forces sensors using 3-D printing," *IEEE/ASME Trans. Mechatronics*, vol. 16, no. 5, pp. 866–870, 2011.

[84] J. T. Muth *et al.*, "Embedded 3D printing of strain sensors within highly stretchable elastomers," *Adv. Mater.*, vol. 26, no. 36, pp. 6307–6312, 2014.

[85] B. Igrec, M. Bosiljevac, Z. Sipus, D. Babic, and S. Rudan, "Fiber optic vibration sensor for high-power electric machines realized using 3D printing technology," in *Photonic Instrumentation Engineering III*, 2016, vol. 9754.

[86] R. I. Haque, E. Ogam, C. Loussert, P. Benaben, and X. Boddaert, "Fabrication of capacitive acoustic resonators combining 3D printing and 2D inkjet printing techniques," *Sensors (Switzerland)*, vol. 15, no. 10, pp. 26018–26038, 2015.

[87] M. Saari, B. Xia, B. Cox, P. S. Krueger, A. L. Cohen, and E. Richer, "Fabrication and Analysis of a Composite 3D Printed Capacitive Force Sensor," *3D Print. Addit. Manuf.*, vol. 3, no. 3, pp. 137–141, 2016.

[88] E. Suaste-Gómez, G. Rodríguez-Roldán, H. Reyes-Cruz, and O. Terán-Jiménez, "Developing an ear prosthesis fabricated in polyvinylidene fluoride by a 3D printer with sensory intrinsic properties of pressure and temperature," *Sensors (Switzerland)*, vol. 16, no. 3, pp. 1–11, 2016.

[89] S. Krachunov and A. J. Casson, "3D Printed Dry EEG Electrodes," *Sensors (Basel).*, vol. 16, no. 10, 2016.

[90] P. Pötschke *et al.*, "Liquid sensing properties of fibres prepared by melt spinning from poly(lactic acid) containing multi-walled carbon nanotubes," *Compos. Sci. Technol.*, vol. 70, no. 2, pp. 343–349, 2010.

[91] C. Cochrane, M. Lewandowski, and V. Koncar, "A Flexible Strain Sensor Based on a Conductive Polymer Composite for in situ Measurement of Parachute Canopy Deformation," *Sensors*, vol. 10, no. 9, pp. 8291–8303, 2010.

[92] V. Koncar, C. Cochrane, M. Lewandowski, F. Boussu, and C. Dufour, "Electro-conductive sensors and heating elements based on conductive polymer composites," *Int. J. Cloth. Sci. Technol.*, vol. 21, no. 2/3, pp. 82–92, 2009.

[93] I. Krucińska, B. Surma, M. Chrzanowski, E. Skrzetuska, and M. Puchalski, "Application of melt-blown technology in the manufacturing of a solvent vapor-sensitive, non-woven fabric composed of poly(lactic acid) loaded with multi-walled carbon nanotubes," *Text. Res. J.*, vol. 83, no. 8, pp. 859–870, 2013.

[94] F. Mai *et al.*, "Poly(lactic acid)/carbon nanotube nanocomposites with integrated degradation sensing," *Polymer (Guildf).*, vol. 54, no. 25, pp. 6818–6823, 2013.

[95] B. Kumar, M. Castro, and J. F. Feller, "Poly(lactic acid)-multi-wall carbon nanotube conductive biopolymer nanocomposite vapour sensors," *Sensors Actuators, B Chem.*, vol. 161, no. 1, pp. 621–628, 2012.

[96] P. Poetschke *et al.*, "Liquid sensing properties of fibers prepared by melt spinning from poly (lactic acid) containing multiwalled carbon nanotubes.," *Annu. Tech. Conf. - Soc. Plast. Eng.*, vol. 67, pp. 561–566, 2009.

[97] S. J. Leigh, R. J. Bradley, C. P. Purssell, D. R. Billson, and D. A. Hutchins, "A simple, low-cost conductive composite material for 3D printing of electronic sensors," *PLoS One*, vol. 7, no. 11, p. e49365, 2012.

[98] J. F. Christ, N. Aliheidari, A. Ameli, and P. Pötschke, "3D printed highly elastic strain sensors of multiwalled carbon nanotube/thermoplastic polyurethane nanocomposites," *Mater. Des.*, vol. 131, pp. 394–401, 2017.

[99] K. Kim, J. Park, J. hoon Suh, M. Kim, Y. Jeong, and I. Park, "3D printing of multiaxial force sensors using carbon nanotube (CNT)/thermoplastic polyurethane (TPU) filaments," *Sensors Actuators, A Phys.*, vol. 263, pp. 493–500, 2017.

[100] Z. C. Kennedy *et al.*, "3D-printed poly(vinylidene fluoride)/carbon nanotube composites as a tunable, low-cost chemical vapour sensing platform," *Nanoscale*, vol. 9, no. 17, pp. 5458–5466, 2017.

[101] M. Stoppa and A. Chiolerio, "Wearable electronics and smart textiles: A critical review," *Sensors (Switzerland)*, vol. 14, pp. 11957–11992, 2014.

[102] K. Cherenack, C. Zysset, T. Kinkeldei, N. Münzenrieder, and G. Tröster, "Woven electronic fibers with sensing and display functions for smart textiles," *Adv. Mater.*, vol. 22, pp. 5178–5182, 2010.

[103] C. Zhang, C. A. Ma, P. Wang, and M. Sumita, "Temperature dependence of electrical resistivity for carbon black filled ultra-high molecular weight polyethylene composites prepared by hot compaction," *Carbon N. Y.*, vol. 43, pp. 2544–2553, 2005.

[104] R. C. Zhuang, T. T. L. Doan, J. W. Liu, J. Zhang, S. L. Gao, and E. Mäder, "Multi-functional multi-walled carbon nanotube-jute fibres and composites," *Carbon N. Y.*, vol. 49, pp. 2683–2692, 2011.

[105] M. Sibinski, M. Jakubowska, and M. Sloma, "Flexible temperature sensors on fibers," *Sensors*, vol. 10, pp. 7934–7946, 2010.

[106] J. Yun, H. Il Kim, and Y. S. Lee, "A hybrid gas-sensing material based on porous carbon fibers and a TiO2 photocatalyst," *J. Mater. Sci.*, vol. 48, pp. 8320–8328, 2013.

[107] J. Kim, S. H. Lee, S. J. Park, and Y. S. Lee, "Preparation and gas-sensing properties of pitch-based carbon fiber prepared using a melt-electrospinning method," *Res. Chem. Intermed.*, vol. 40, pp. 2571–2581, 2014.

[108] W. Zhang, Y. Y. Tan, C. Wu, and S. R. P. Silva, "Self-assembly of single walled carbon nanotubes onto cotton to make conductive yarn," *Particuology*, vol. 10, pp. 517–521, 2012.

[109] G. E. Collins and L. J. Buckley, "Conductive polymer-coated fabrics for chemical sensing," *Synth. Met.*, vol. 78, pp. 93–101, 1996.

[110] W. Weng, P. Chen, S. He, X. Sun, and H. Peng, "Smart electronic textiles," *Angew. Chemie - Int. Ed.*, vol. 55, no. 21, pp. 6140–6169, 2016.

[111] B. S. Shim, W. Chen, C. Doty, C. Xu, and N. A. Kotov, "Smart electronic yarns and wearable fabrics for human biomonitoring made by carbon nanotube coating with polyelectrolytes," *Nano Lett.*, vol. 8, no. 12, pp. 4151–4157, 2008.

[112] S. Gao, R.-C. Zhuang, J. Zhang, J.-W. Liu, and E. Mäder, "Glass Fibers with Carbon Nanotube Networks as Multifunctional Sensors," *Adv. Funct. Mater.*, vol. 20, no. 12, pp. 1885–1893, 2010.

[113] M. L. Hammock, A. Chortos, B. C.-K. Tee, J. B.-H. Tok, and Z. Bao, "25th Anniversary Article: The Evolution of Electronic Skin (E-Skin): A Brief History, Design Considerations, and Recent Progress," *Adv. Mater.*, vol. 25, no. 42, pp. 5997–6038, 2013.

[114] O. Atalay, "Development and Investigation of Weft Knitted Strain Sensor," The University of Manchester, 2014.

[115] A. Ehrmann, F. Heimlich, A. Brücken, M. Weber, and R. Haug, "Suitability of knitted fabrics as elongation sensors subject to structure, stitch dimension and elongation direction," *Text. Res. J.*, vol. 84, no. 18, pp. 2006–2012, 2014.

[116] T. W. Shyr, J. W. Shie, and Y. E. Jhuang, "The effect of tensile hysteresis and contact resistance on the performance of strain-resistant elastic-conductive webbing," *Sensors*, vol. 11, pp. 1693–1705, 2011.

[117] T. Yamashita, S. Takamatsu, K. Miyake, and T. Itoh, "Fabrication and evaluation of a conductive polymer coated elastomer contact structure for woven electronic textile," *Sensors Actuators, A Phys.*, vol. 195, pp. 213–218, 2013.

[118] O. Atalay and W. R. Kennon, "Knitted strain sensors: Impact of design parameters on sensing properties," *Sensors (Switzerland)*, vol. 14, pp. 4712–4730, 2014.

[119] T. W. Shyr, J. W. Shie, C. H. Jiang, and J. J. Li, "A textile-based wearable sensing device designed for monitoring the flexion angle of elbow and knee movements," *Sensors (Switzerland)*, vol. 14, pp. 4050–4059, 2014.

[120] T. E. Campbell, B. J. Munro, G. G. Wallace, and J. R. Steele, "Can fabric sensors monitor breast motion?," *J. Biomech.*, vol. 40, pp. 3056–3059, 2007.

[121] J. Wu, D. Zhou, C. O. Too, and G. G. Wallace, "Conducting polymer coated lycra," *Synth. Met.*, vol. 155, pp. 698–701, 2005.

[122] P. Xue, X. M. Tao, and H. Y. Tsang, "In situ SEM studies on strain sensing mechanisms of PPy-coated electrically conducting fabrics," *Appl. Surf. Sci.*, vol. 253, no. 7, pp. 3387–3392, 2007.

[123] P. Xue, J. Wang, and X. Tao, "Flexible textile strain sensors from polypyrrole-coated XLA™ elastic fibers," *High Perform. Polym.*, vol. 26, no. 3, pp. 364–370, 2014.

[124] M. Z. Seyedin, J. M. Razal, P. C. Innis, and G. G. Wallace, "Strain-Responsive Polyurethane/PEDOT:PSS Elastomeric Composite Fibers with High Electrical

Conductivity," *Adv. Funct. Mater.*, vol. 24, no. 20, pp. 2957–2966, 2014.

[125] S. Lee *et al.*, "Ag Nanowire Reinforced Highly Stretchable Conductive Fibers for Wearable Electronics," *Adv. Funct. Mater.*, vol. 25, no. 21, pp. 3114–3121, 2015.

[126] C. Yan *et al.*, "Highly Stretchable Piezoresistive Graphene–Nanocellulose Nanopaper for Strain Sensors," *Adv. Mater.*, vol. 26, no. 13, pp. 2022–2027, 2014.

[127] K. Koziol *et al.*, "High-performance carbon nanotube fiber," *Science (80-.).*, vol. 318, no. 5858, pp. 1892–1895, 2007.

[128] W. Lu, M. Zu, J.-H. Byun, B.-S. Kim, and T.-W. Chou, "State of the Art of Carbon Nanotube Fibers: Opportunities and Challenges," *Adv. Mater.*, vol. 24, no. 14, pp. 1805–1833, 2012.

[129] J. T. Han *et al.*, "Rearrangement of 1D Conducting Nanomaterials towards Highly Electrically Conducting Nanocomposite Fibres for Electronic Textiles," *Sci. Rep.*, vol. 5, no. 9300, 2015.

[130] W. P. Eaton and J. H. Smith, "Micromachined pressure sensors: Review and recent developments," *Smart Mater. Struct.*, vol. 6, pp. 530–539, 1997.

[131] S. Takamatsu, T. Kobayashi, N. Shibayama, K. Miyake, and T. Itoh, "Fabric pressure sensor array fabricated with die-coating and weaving techniques," *Sensors Actuators, A Phys.*, vol. 184, pp. 57–63, 2012.

[132] H. B. Muhammad *et al.*, "A capacitive tactile sensor array for surface texture discrimination," *Microelectron. Eng.*, vol. 88, pp. 1811–1813, 2011.

[133] M. Catrysse, R. Puers, C. Hertleer, L. Van Langenhove, H. Van Egmond, and D. Matthys, "Towards the integration of textile sensors in a wireless monitoring suit," *Sensors Actuators, A Phys.*, vol. 114, pp. 302–311, 2004.

[134] R. Wijesiriwardana, "Inductive fiber-meshed strain and displacement transducers for respiratory measuring systems and motion capturing systems," *IEEE Sens. J.*, vol. 6, no. 3, pp. 571–579, 2006.

[135] J. Fang, X. Wang, and T. Lin, "Electrical power generator from randomly oriented electrospun poly(vinylidene fluoride) nanofibre membranes," *J. Mater. Chem.*, no. 30, 2011.

[136] L. T. Beringer, X. Xu, W. Shih, W. H. Shih, R. Habas, and C. L. Schauer, "An electrospun PVDF-TrFe fiber sensor platform for biological applications," *Sensors Actuators, A Phys.*, vol. 222, pp. 293–300, 2015.

[137] L. Persano *et al.*, "High performance piezoelectric devices based on aligned arrays of nanofibers of poly(vinylidenefluoride-co-trifluoroethylene)," *Nat. Commun.*, vol. 4, no. 1633, 2013.

[138] B. Baghaei, M. Skrifvars, and L. Berglin, "Manufacture and characterisation of

thermoplastic composites made from PLA/hemp co-wrapped hybrid yarn prepregs," *Compos. Part A Appl. Sci. Manuf.*, vol. 50, pp. 93–101, 2013.

[139] J. Janesch, "Two-wire vs. four-wire resistance measurements: which configuration makes sense for your application?," no. May. pp. 1–3, 2013.

[140] T. Bashir, L. Fast, M. Skrifvars, and N.-K. Persson, "Electrical resistance measurement methods and electrical characterization of poly(3,4-ethylenedioxythiophene)-coated conductive fibers," *J. Appl. Polym. Sci.*, vol. 124, no. 4, pp. 2954–2961, May 2012.

[141] T. T. Tung, C. Robert, M. Castro, J. F. Feller, T. Y. Kim, and K. S. Suh, "Enhancing the sensitivity of graphene/polyurethane nanocomposite flexible piezo-resistive pressure sensors with magnetite nano-spacers," *Carbon N. Y.*, vol. 108, pp. 450–460, Nov. 2016.

[142] A. Dean and D. Voss, *Design and analysis of experiments*. 2008.

[143] J. T. Yoon, G. Jeong, S. C. Lee, and B. G. Min, "Influences of poly(lactic acid)-grafted carbon nanotube on thermal, mechanical, and electrical properties of poly(lactic acid)," *Polym. Adv. Technol.*, vol. 20, no. 7, pp. 631–638, 2009.

[144] R. Rizvi, L. Tong, and H. Naguib, "Processing and properties of melt spun polylactide-multiwall carbon nanotube fiber composites," *J. Polym. Sci. Part B Polym. Phys.*, vol. 52, no. 6, pp. 477–484, Mar. 2014.

[145] J. C. Li, Y. Wang, and D. C. Ba, "Characterization of Semiconductor Surface Conductivity by Using Microscopic Four-Point Probe Technique," *Phys. Procedia*, vol. 32, pp. 347–355, 2012.

[146] J. Yu, N. Wang, and X. Ma, "Fabrication and Characterization of Poly (lactic acid)/ Acetyl Tributyl Citrate / Carbon Black as Conductive Polymer Composites," vol. 9, pp. 1050–1057, 2008.

[147] S. Gong, Z. H. Zhu, and S. A. Meguid, "Anisotropic electrical conductivity of polymer composites with aligned carbon nanotubes," *Polymer (Guildf).*, vol. 56, pp. 498–506, Jan. 2015.

[148] I. Alig *et al.*, "Establishment, morphology and properties of carbon nanotube networks in polymer melts," *Polymer (Guildf).*, vol. 53, no. 1, pp. 4–28, Jan. 2012.

[149] H. Zois, L. Apekis, and M. Omastová, "Electrical properties of carbon black-filled polymer composites," *Macromol. Symp.*, vol. 170, no. 1, pp. 249–256, Jun. 2001.

[150] C. Li, E. T. Thostenson, and T. W. Chou, "Dominant role of tunneling resistance in the electrical conductivity of carbon nanotube-based composites," *Appl. Phys. Lett.*, vol. 91, no. 22, 2007.

[151] H. Tsuji, Y. Kawashima, H. Takikawa, and S. Tanaka, "Poly(l-lactide)/nano-structured carbon composites: Conductivity, thermal properties, crystallization, and biodegradation," *Polymer (Guildf).*, vol. 48, no. 14, pp. 4213–4225, 2007.

[152] S. R. Broadbent and J. M. Hammersley, "Percolation processes," *Math. Proc. Cambridge Philos. Soc.*, vol. 53, no. 03, p. 629, Jul. 1957.

[153] L. Yu, H. Liu, F. Xie, L. Chen, and X. Li, "Effect of annealing and orientation on microstructures and mechanical properties of polylactic acid," *Polym. Eng. Sci.*, vol. 48, no. 4, pp. 634–641, 2008.

[154] A. R. Bhattacharyya *et al.*, "Crystallization and orientation studies in polypropylene/single wall carbon nanotube composite," *Polymer (Guildf).*, vol. 44, pp. 2373–2377, 2003.

[155] Hevin P. Menard, "Dynamic Mechanical Analysis," *CRC Press*. pp. 97–120, 2008.

[156] K. Gnanasekaran *et al.*, "3D printing of CNT- and graphene-based conductive polymer nanocomposites by fused deposition modeling," *Appl. Mater. Today*, vol. 9, pp. 21–28, 2017.

[157] F. Samperi, C. Puglisi, R. Alicata, and G. Montaudo, "Thermal degradation of poly(butylene terephthalate) at the processing temperature," *Polym. Degrad. Stab.*, vol. 83, no. 1, pp. 11–17, Jan. 2004.

[158] Z. Weng, J. Wang, T. Senthil, and L. Wu, "Mechanical and thermal properties of ABS/montmorillonite nanocomposites for fused deposition modeling 3D printing," *Mater. Des.*, vol. 102, pp. 276–283, 2016.

[159] C. Gonçalves, I. C. Gonçalves, F. D. Magalhães, and A. M. Pinto, "Poly(lactic acid) composites containing carbon-based nanomaterials: A review," *Polymers (Basel).*, vol. 9, no. 7, pp. 1–37, 2017.

[160] J. Ramontja, S. S. Ray, S. K. Pillai, and A. S. Luyt, "High-performance carbon nanotube-reinforced bioplastic," *Macromol. Mater. Eng.*, vol. 294, no. 12, pp. 839–846, 2009.

[161] R. Mohan, J. Subha, and J. Alam, "Influence of Multiwalled Carbon Nanotubes on Biodegradable Poly(lactic acid) Nanocomposites for Electroactive Shape Memory Actuator," *Adv. Polym. Technol.*, vol. 37, no. 1, 2016.

[162] J. Bai, R. D. Goodridge, R. J. M. M. Hague, M. Song, and M. Okamoto, "Influence of carbon nanotubes on the rheology and dynamic mechanical properties of polyamide-12 for laser sintering," *Polym. Test.*, vol. 36, pp. 95–100, 2014.

[163] H. A. K. Toprakci, "Piezoresistive Properties of Polyvinyl Chloride Composites," North Carolina State University, 2012.

[164] M. Tessarolo *et al.*, "Adaptable pressure textile sensors based on a conductive polymer," *Flex. Print. Electron.*, vol. 3, no. 3, 2018.

[165] S. C. B. Mannsfeld *et al.*, "Highly sensitive flexible pressure sensors with microstructured rubber dielectric layers," *Nat. Mater.*, vol. 9, no. 10, pp. 859–864, 2010.

[166] S. Chen, B. Zhuo, and X. Guo, "Large Area One-Step Facile Processing of

Microstructured Elastomeric Dielectric Film for High Sensitivity and Durable Sensing over Wide Pressure Range," *ACS Appl. Mater. Interfaces*, vol. 8, no. 31, pp. 20364–20370, 2016.

[167] T. Q. Trung and N. E. Lee, "Flexible and Stretchable Physical Sensor Integrated Platforms for Wearable Human-Activity Monitoringand Personal Healthcare," *Adv. Mater.*, vol. 28, no. 22, pp. 4338–4372, 2016.

[168] H. So, J. Woo, J. Kwon, J. Yun, S. Baik, and W. Seok, "Carbon nanotube based pressure sensor for flexible electronics," *Mater. Res. Bull.*, vol. 48, no. 12, pp. 5036–5039, 2013.

[169] P. Slobodian, P. Riha, A. Lengalova, and P. Saha, "Compressive stress-electrical conductivity characteristics of multiwall carbon nanotube networks," *J Mater Sci*, vol. 46, pp. 3186–3190, 2011.

[170] L. Paredes-Madrid, A. Matute, J. O. Bareño, C. A. P. Vargas, and E. I. G. Velásquez, "Underlying physics of conductive polymer composites and Force Sensing Resistors (FSRs). A study on creep response and dynamic loading," *Materials (Basel).*, vol. 10, no. 11, 2017.

[171] W. Luheng, D. Tianhuai, and W. Peng, "Influence of carbon black concentration on piezoresistivity for carbon-black-filled silicone rubber composite," *Carbon N. Y.*, vol. 47, pp. 3151–3157, 2009.

[172] P. Slobodian and P. Saha, "Stress-strain Hysteresis of a Carbon Nanotube Network as Polymer Nanocomposite Filler under Cyclic Deformation," vol. 231, no. 2011, pp. 224–231.

[173] L. Paredes-Madrid, A. Matute, J. O. Bareño, C. A. P. Vargas, and E. I. G. Velásquez, "Underlying physics of conductive polymer composites and Force Sensing Resistors (FSRs). A study on creep response and dynamic loading," *Materials (Basel).*, vol. 10, no. 11, 2017.

[174] M. Hussein, "Effects of strain rate and temperature on the mechanical behavior of carbon black reinforced elastomers based on butyl rubber and high molecular weight polyethylene," *Results Phys.*, vol. 9, pp. 511–517, 2018.

[175] E. T. Koh and W. L. Owen, "Relationships Among Variables," in *Introduction to Nutrition and Health Research*, Boston, MA: Springer US, 2000, pp. 103–126.

[176] H. R. Brown, "Polymer adhesion," *Mater. Forum*, vol. 24, pp. 49–58, 2000.

[177] S. S. Voyutskii and V. L. Vakula, "The role of diffusion phenomena in polymer-to-polymer adhesion," *J. Appl. Polym. Sci.*, vol. 7, no. 2, pp. 475–491, Mar. 1963.

[178] F. Awaja, M. Gilbert, G. Kelly, B. Fox, and P. J. Pigram, "Adhesion of polymers," *Prog. Polym. Sci.*, vol. 34, no. 9, pp. 948–968, 2009.

[179] M. Akgun, "Effect of Yarn Filament Fineness on the Surface Roughness of Polyester Woven Fabrics," *J. Eng. Fiber. Fabr.*, vol. 10, no. 2, pp. 121–128, 2015.

[180] R. Auras, H. Tsuji, R. A. Auras, and S. E. M. Selke, *Poly(lactic acid) : synthesis, structures, properties, processing, and applications*. Wiley, 2010.

[181] L. E. Amborski and T. D. Mecca, “A study of polymer film brittleness,” *J. Appl. Polym. Sci.*, vol. 4, no. 12, pp. 332–342, Nov. 1960.